Development of new therapeutic strategies targeting cancer associated fibroblasts (CAFs) in pancreatic ductal adenocarcinoma

PhD thesis

Magdolna Djurec

Pathological Sciences Doctoral School

Semmelweis University

Consultant: László Kopper, MD, D.Sc,

Official reviewers: Krisztina Buzás, PhD

Zoltán Wiener, PhD

Head of the Final Examination Committee: Zsuzsa Schaff, MD, D.Sc,
Full Member of the Hungarian Academy of Science

Members of the Final Examination Committee: Erika Tóth, MD, PhD

Attila Patócs, MD, PhD

Budapest

2018

TABLE OF CONTENTS

Abbreviations

A2m: Alpha-2-macroglobulin

ADEX: Aberrantly Differentiated Endocrine exocrine tumor

ADM: Acinar to Ductal Metaplasia

Aldh2: Aldehyde dehydrogenese 2

ApoA-1: Apolipoprotein A1

Apo-SAA: Serum Amyloid A Apolipoprotein

Arg1: Arginase 1

αSMA: alpha-Smooth Muscle Actin

ATP: Adenosine Tri-Phosphate

BRCA: Breast Cancer susceptibility protein

BSA: Bovine Serum Albumin

CAFs: Cancer Associated Fibroblasts

CCL: Chemokine (C-C motif) ligand

CDK: Cyclin-Dependent Kinase

CDKN2A: Cyclin-Dependent Kinase Inhibitor 2A

cDNA: Complementary DNA

Cfh: Complement Factor H

Chi3l: Chitinase 3 like 1

Clec3b: C-type Lectin Domain Family 3 Member B

Col11a1: Collagen type 11 Alpha 1 chain

Cre: Cre recombinase

CRISPR: Clustered Regularly Interspaced Short Palindromic Repeats

Ct: Comparative cycle Threshold

CTGF: Connective Tissue Growth Factor

CTLA-4: cytotoxic T-lymphocyte-associated protein 4

CXCL: Chemokine (C-X-C motif) ligand

Dcn: Decorin

DMEM: Dulbecco´s Modified Eagle´s Medium

DMSO: Dimethyl Sulfoxide

DNA: Deoxyribonucleic acid

DNase: Deoxyribonuclease

dNTP: Deoxynucleotide

DRS: Dual Recombinase System

DTT: Dithiothrietol

ECM: Extracellular Matrix

EDTA: Ethylene Diamine Tetraacetic Acid

EGFR: Epidermal Growth Factor Receptor

ERK: Extracellular signal Regulated Kinases

EYFP: Enhanced Yellow Fluorescent Protein

FAP: Fibroblast activation protein

FBS: Fetal Bovine Serum

FDA: Food and Drug Administration

FDR: False Discovery Rate

FGF: Fibroblast growth factor

Flp: Flipase

FPR2: formyl peptide receptor 2

FSP: Fibroblast specific protein

Fzd1: Frizzled class receptor 1

GAG: Glycosamino Glycans

GAPDH: Glyceraldehyde 3-Phosphate Dehydrogenase

GEMM: Genetically Engineered Mouse Model

GFAP: Glial Fibrillary Acidic Protein

GFP: Green Fluorescent Protein

GLI: Glioma – associated oncogene

GM-CSF: Granulocyte-macrophage colony stimulating factor

GPCR: G-Protein Coupled Receptors

GSEA: Gene Set Enrichment Analysis

GTP: Guanosine Triphosphate

HA: Hyaluronic acid

HAS1: Hyaluronic Acid Synthase

HABP: Hyaluronic acid binding protein

HBSS: Hank´s Balanced Salt Solution

H&E: Hematoxylin and Eosin

HDL: High Density Lipoprotein

HP: Haptoglobin

Hpse: Heparanase

HRP: Horseradish Peroxidase

HSC: Hepatic Stellate Cell

hUBC: Human Ubiquitin C

iCAFs: inflammatory CAFs

IGF: Insulin Growth Factor

IGFBP: Insulin Growth Factor Binding Protein

IGFR: Insulin Growth Factor Receptor

IHC: Immunohistochemistry

IL: Interleukin

IPMN: Intraductal Papillary Mucinous Neoplasms

ITGA11: Integrin Subunit Alpha 11

JAK: Janus Kinase

JNK: c-Jun N-terminal kinases

KPC: K-Ras; P53; Cre

KPeCY: K-Ras; P53; Elastase-Cre; EYFP

Lgals1: Galectin 1

LSL: Lox-STOP-Lox

Lrg1: Leucine Rich Alpha-2-Glycoprotein1

Lum: Lumican

Lyz2: Lysozime 2

MAPK: Mitogen Activated Protein Kinase

MAGUK: Membrane-Associated Guanylate Kinases

MDM2: Mouse double minute 2 homologue

MDSC: Myeloid Derived Suppressor Cells

MEK: Mitogen Activating Protein Kinase

MMP: Matrix Metalloproteinase

MPO: Myeloperoxidase

MPP6: Membrane Palmitoylated Protein 6

MSC: Mesenchymal Stem Cells

Msln: Mesothelin

MyCAFs: Myofibroblast CAFs

nAb-Paclitaxel: nanoparticle albumin-bound Paclitaxel

Neo: Neomycin

NF-κB: Nuclear Factor Kappa B

NK cells: Natural Killer Cells

NPFs: Normal Pancreatic Fibroblasts

OCT: Optimum Cutting Temperature compound

OS: overall survival

PanIN: Pancreatic Intraepithelial Neoplasia

PBS: Phosphate Buffered Saline

PCR: Polymerase Chain Reaction

PD-1: Programmed Death Receptor 1

PD-1L: Programmed Death Receptor 1 Ligand

PDAC: Pancreatic Ductal Adenocarcinoma

PDGF: Platelet Derived Growth Factor

PDGFR: Platelet Derived Growth Factor Receptor

PDX: Patient-Derived Xenografts

PDX1: Pancreatic and Duodenal Homeobox 1

PI3K: Phosphoinositol-3-kinase

PIK3CA: Phosphatidylinositol-4,5-Bisphosphate 3-Kinase Catalytic Subunit Alpha

PSCs: Pancreatic Stellate Cells

Ptger3: Prostaglandin E Receptor 3

PTEN: Phosphatase and Tensin homolog

qRT-PCR: Quantitative Reverse Transcription Polymerase Chain Reaction

RAF: Rapidly Accelerated Fibrosarcoma

RAGE: Receptor for Advanced Glycation End Products

RIN: RNA Integrity Number

ROS: Reactive Oxygen Species

RNA: Ribonucleic acid

RT: Room Temperature

RT-PCR: Reverse Transcription Polymerase Chain Reaction

SAA: Serum Amyloid A

SDS: Sodium Dodecyl Sulfate

Sfrp: Secreted Frizzled Protein 1

sgRNA: single guide RNA

Shh: Sonic hedgehog

shRNA: short hairpin RNA

SMO: Smoothened

SPARC: Secreted Protein Acidic and Rich in Cysteine

Spon1 Spondin 1:

SR-BI: scavenger receptor class B type I

STAT: Signal Transducer and Activator of Transcription

TAE: Tris Acetate EDTA

TAMs: Tumor Associated Macrophages

Taq-Polymerase: *Thermus aquaticus* DNA Polymerase

TBS: Tris Buffered Saline

TBST: Tris Buffered Saline with Tween

TGF-ß: Transforming Growth Factor β

Thbd: Trombomodulin

TNF-α: Tumor Necrosis Factor α

Tnfsf8: TNF Superfamily Member 8

TLR: Toll-like receptors

TKI: Tyrosine Kinase Inhibitors

Trp53/P53: Transformation Related Protein 53

TME: Tumor Microenvironment

VEGF: Vascular Endothelial Growth Factor

VEGFR: Vascular Endothelial Growth Factor Receptor

WT: Wild Type

1 Introduction

1.1 Pancreatic Ductal Adenocarcinoma

Pancreatic ductal adenocarcinoma (PDAC) is the most frequent type of pancreatic tumors. It is an extremely aggressive disease with diagnosis at advanced stages and highly refractory to most treatments. By 2030 it will become the second leading cause of cancer death in developed countries (1).

1.1.1 Epidemiology and biological features

Pancreatic cancer is a disease of the elderly, the median age at diagnosis is 71 years and it is more frequent in men (1). PDAC is associated with a very poor prognosis, with a 5-year survival rate of only 6% and a median survival of less than 6 months (2). This low survival rate is the result of its aggressive features and its late diagnosis due to the lack of early symptoms and early biomarkers. Therefore, at the time of detection 80% of patients have locally advanced or metastatic PDAC and less than 20% of the patients are eligible for resection. Moreover, PDAC biology contributes to early recurrence, distant metastasis and resistance to chemotherapy and radiotherapy (3). A very important player in this poor prognosis is the extensive stromal reaction (desmoplasia) resulting in a hypovascular and hypoxic microenvironment and evasion of tumor immunity (4).

1.1.2 Histopathology and molecular characterization of PDAC

1.1.2.1 Histopathology

PDAC commonly arises and progresses through a multistep process of well-defined and non-invasive precursor lesions that gradually accumulate mutations in oncogenes and tumor suppressors (5) (Fig 1). Histological and clinical studies identified distinct types of precursor lesions, being the most frequent, the pancreatic intraepithelial neoplasia (PanIN) (6). PanIN lesions can be classified into four grades based on the degree of dysplasia: PanIN1A (flat) and PanIN1B (papillary type) are low-grade lesions with minimal cytological and architectural atypia; PanIN2, a high-grade lesion with frequent papillary structure and nuclear pleomorphia, crowding, and hyperchromasia; and PanIN3 (or *in situ* carcinoma) characterized by severe cytological and architectural atypia with papillary morphology. All grade PanINs are non-invasive lesions that do not invade the basement membrane (5, 7).

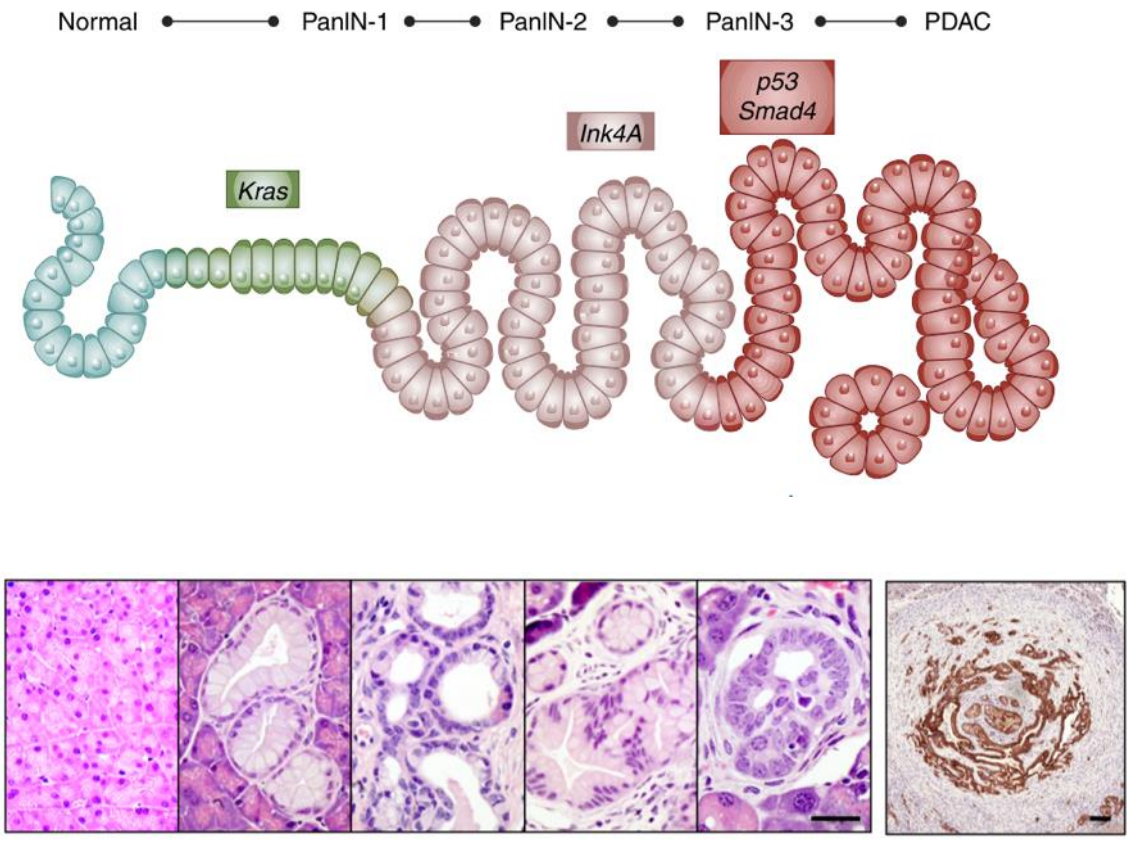

Figure 1. Multistep pancreatic carcinogenesis. *(Upper)* Scheme of step-wise genetic alterations followed by histological transformation. Mutation in the K-Ras oncogene initiating ductal reprogramming and transformation into PanIN1A/B low grade lesions. Accumulation of subsequent mutations in tumor suppressors, such as INK4A (PanIN2); and P53 and SMAD4 (PanIN3) results in high grade lesions and finally to PDAC formation. *(Lower)* H&E staining of histological alterations during pancreatic tumor development and CK19 IHC of PDAC (adapted from Neesse et al., 2015; and Barbacid, 2013).

PanIN lesions develop through a reprogramming process (transdifferentiation), known as acinar-to-ductal metaplasia (ADM), which is frequently associated with atrophy of acinar parenchyma and activation of the K-RAS oncogene as initiating steps (6). Molecular analyses have demonstrated that PanINs harbor many of the genetic alterations found in PDACs (8). Early events include mutations in *K-RAS* and *CDKN2A* as well as telomere shortening providing an environment that is permissive to acquisition of chromosomal rearrangements and preceding mutations in *P53* and *SMAD4*, tumor suppressors that are found lost in high grade lesions (PanIN3) (Fig 1) (8).

1.1.2.2 Molecular genetics of pancreatic ductal adenocarcinoma

More than 90% of PDACs harbor mutations in the *K-RAS* oncogene, detected already in early PanIN lesions (8, 9). Therefore, it is considered the initial driver mutation.

The K-RAS oncogene: K-RAS is a member of the RAS family of GTP-binding proteins that mediate different cellular functions: proliferation, differentiation, and survival (10). In pancreatic cancer, oncogenic mutations in the *K-RAS* locus cluster in hot spots, more frequently in codon 12 (11, 12). This results in inhibition of GTP hydrolysis activity that leads to constant activation of the protein and finally aberrant cell proliferation (13). The most common mutations are G12D (44%), followed by G12V (30%) and G12R (20%), respectively. The latter was present with high prevalence in samples with multiple *K-RAS* mutations suggesting distinct signaling properties of this allele (9). In addition, PDACs with wild-type *K-RAS* have activating mutations in members of the MAPK pathway (9). Oncogenic mutations in BRAF, such as V600E, can be found in 3% of PDAC samples (14) and are mutually exclusive with *K-RAS* mutations (15). Interestingly, a subset of *K-RAS* wild-type PDACs display elevated activation of MTOR pathway, converting it into a therapeutic target for these patients (9).

CDKN2A: The most frequent allelic losses in PDAC affects the locus that encodes the cyclin-dependent kinase *CDKN2A/p16* tumor suppressor that inhibits cell cycle progression (16). Deletion, mutation or promoter hypermethylation of 9q21 locus occurs in 80–95% of low-grade PanINs (17, 18). This locus encodes two overlapping tumor suppressors - INK4A and ARF, and their respective protein products $P16^{INK4A}$ and $P14^{ARF}$ (19). INK4A inhibits CDK4/6-mediated phosphorylation of RB, thereby blocking the cell cycle; ARF stabilizes P53 by inhibiting its MDM2-dependent proteolysis. Cooperation of K-RAS and *INK4A* mutation was postulated in several studies (20) given their mutual genetic alteration during early steps of pancreatic carcinogenesis.

P53: Inactivating missense mutations in the DNA binding domain of *P53* are frequently found in PDAC patients (50-70%) (17). These genetic alterations appear in later stages of PanIN formation, in an established environment of genomic instability and ROS induced DNA damage response (20). Interestingly, loss of function of ARF and P53 coexist in 40% of human PDAC (18).

SMAD4: sporadic loss of function of SMAD4/DPC transcriptional regulator by deletion or intragenic point mutations takes place in 50% of human PDACs (21). As a central component of TGF-ß signaling, SMAD4 mutations appear at late stages of pancreatic tumorigenesis (22).

1.1.2.3 Signaling pathways activated in PDAC

1.1.2.3.1 RAS – MAPK

In addition to the role of K-RAS mutations in PDAC initiation, constitutive RAS signaling has been described to be required for PDAC maintenance (2, 23). Three *RAS* genes encode four RAS isoforms (H-RAS, N-RAS and K-RAS4A and K-RAS4B), with the splice variant K-RAS4B being the main isoform expressed in human cells (24) and tumors (25). Upon extracellular stimuli RAS proteins activate numerous downstream signaling pathways including the MAPK signaling, a key pathway that controls essential cellular processes, such as proliferation, survival and differentiation (10). This pathway includes a family of serine/threonine kinases (RAF/MEK/ERK), that through phosphorylation events result in a proliferative phenotype in many cells (26). RAS-GTP binds to RAF proteins (A-RAF, B-RAF, C-RAF), initiating a signaling cascade and activates MEK1/2, which phosphorylates ERK1/2 kinases. The latter has more than 150 substrates in the cytosol and in the nucleus, most of them involved in cell proliferation (27).

RAS can also activate the PI3K signaling pathway, which is an essential regulator of cell survival (28) via AKT, p70-S6K, and PDK-1 downstream effectors (29). This pathway is constitutively active in most pancreatic cancers. Moreover, mutations in the catalytic subunit of PI3K (p110α, encoded by *PI3KCA*) and amplification of AKT are commonly found in human PDACs, however mutations in its endogenous inhibitor, PTEN, are uncommon (15). The importance of this pathway in pancreatic tumorigenesis was shown by activating the p110α subunit of PI3K in K-*Ras* driven mouse model resulting in PDAC promotion (30, 31), whilst PDK-1 ablation abrogated tumor development (31).

1.1.2.3.2 Growth factor signaling

PDAC shows increased expression of Epidermal Growth Factor Receptors (EGFR and ERBB2) and their ligands (TGF and EGF), consistent with the presence of an autocrine loop (32). Importantly, EGFR inhibitors decrease PDAC cell growth and tumorigenesis *in vitro* (33), as well as inhibit growth of orthotopic tumors in combination with cytotoxic chemotherapy (34). In 2007, a clinical trial in phase III showed a limited benefit in survival of PDAC patients with the combination of gemcitabine and the EGFR inhibitor Erlotinib, compared with the treatment with gemcitabine only (35).

Other important growth factors, such as the Insulin Growth Factor (IGF), regulate survival, invasion, and angiogenesis of many human cancers. PDACs show elevated expression of IGF-I in both the tumor and stromal compartment, as well as aberrant activation of the IGF-I receptor (IGF-IR) in tumor cells (36). In PDAC patients, IGF1R overexpression was associated with decreased survival (37). Increased levels of IGF binding proteins (IGFBPs) are found in PDAC (38), however, low expression of IGFBP3 and IGFBP7 has been correlated with poor clinical outcome (39). IGFBP-s are reservoirs of circulating IGFs but also regulate cell growth and survival (40), although their complete function is not well understood.

Fibroblast Growth Factor (FGF) and Vascular Endothelial Growth Factor (VEGF) signaling appears to contribute to mitogenesis and angiogenesis of PDAC (41). Overexpression of FGF receptors has been detected in pancreatic tumors (42), where elevated bFGF levels contributed to the PDAC desmoplasia (43). VEGF promotes endothelial cell proliferation and survival by binding to the VEGFR-1 and VEGFR-2 transmembrane receptors (44). VEGF is overexpressed by PDAC cells (45), whereas disruption of VEGF signaling strongly suppresses tumor growth of pancreatic cancer xenografts (46).

1.1.2.4 Stroma modulating pathways in PDAC

1.1.2.4.1 Hedgehog signaling

The Sonic Hedgehog family is comprised of secreted signaling proteins that regulate the growth of many organs, including the pancreas during embryogenesis (47). Hedgehog ligands, such as SHH, disrupt inhibition of SMO and activate the GLI transcription factor. SHH is activated in PanINs and neoplastic cells (48), yet, the activity of GLI in PDAC is restricted to the stromal compartment (49). Pharmacological inhibition of Shh signaling in PDAC GEMMs resulted in reduced stroma, increased vessel density and enhanced drug delivery (50). However, genetic deletion of Shh in mouse tumor cells recapitulated stroma reduction but resulted in aggressive, undifferentiated tumors (51). This is in line with another study demonstrating that Shh activation provokes stromal hyperplasia and reduced growth of epithelial compartment (52).

1.1.2.4.2 TGF-ß signaling

TGF-ß belongs to a superfamily of secreted proteins, whose other members include growth factors (BMPs, Activins) that activate SMAD proteins and regulate proliferation,

differentiation, as well as migration. More importantly, TGF-ß promotes transformation and proliferation of fibroblasts and controls the process of epithelial mesenchymal transition (EMT) in tumors (53).

In pancreatic cancer, more than 50% of the tumors show inactivation of SMAD4 (6). In tumor cells TGFß regulates EMT process downregulating the activity of Snail and Zeb-1 transcription factors (54). Moreover, TGFß regulates PDAC stroma as a major factor of fibrosis via the secretion of several pro-tumorigenic growth factors including VEGF and CTGF, as well as MMP2 and MMP9 (55). In addition, it suppresses inflammatory processes through inhibition of cytotoxic T-cells, macrophages and NK cells (56).

1.1.2.4.3 IL – 6/JAK-STAT pathway

The Signal Transducer and Activator of Transcription (STAT) family of transcription factors are phosphorylated by Janus Kinases (JAK) tyrosine kinases (57, 58). They regulate numerous cellular processes including self-renewal, proliferation and inflammatory pathways (59).

In human PDAC, frequency of STAT3 alteration ranges between 30-100% (60) and correlates with decreased survival (61). Moreover, STAT3 is not essential for normal pancreatic homeostasis (62) but is involved in all stages of pancreatic tumorigenesis (63, 64) Recent studies have demonstrated that IL6 cytokine-induced activation of STAT3 is responsible for remodeling the desmoplastic PDAC stroma and for immune surveillance (61, 65). In addition, IL6 secreted by stromal cells also induced Stat3/Socs3 expression via IL6 trans-signaling and accelerated PDAC progression in mouse models (66).

1.1.2.4.4 NF-κB pathway

Nuclear factor kappa B (NF-κB) signaling might be another downstream mediator of the mutated RAS pathway in pancreatic cancer. Its activation occurs in response to cellular stress through pro-inflammatory cytokines and growth factors resulting in regulation of immune response and apoptosis (67, 68). A link between K-RAS and NF-κB signaling through pP62 was reported to drive tumor initiation and progression in PDAC (69). Moreover, NF-κB connects inflammation and cancer by recruitment of inflammatory cells and activation of cytokines. Cross activation of TGF-ß and IL-1ß signaling via NFκB further contributes to the generation of complex inflammatory PDAC stroma (70).

1.1.2.5 Molecular subtypes of PDAC

In 2011, an analysis based on gene expression data of primary tumors and tumor cell lines correlated with clinical outcome and response treatment identified three molecular subtypes of PDAC: classical, quasimesenchymal (*QM*) and exocrine-like tumors. *Classical subtype* was characterized by overexpression of adhesion-related and epithelial genes, such as GATA6. *QM tumors* had high expression of mesenchymal-associated genes and these patients showed the worst median survival. *Exocrine-like PDAC* genes were enriched in digestive enzyme genes (71). Interestingly, *QM PDAC* cells were more sensitive to gemcitabine than the *Classical subtype*. Conversely, the latter responded better to Erlotinib suggesting treatment specificity.

In 2015, virtual microdissection of gene expression in PDAC samples by non-negative matrix factorization identified two tumor-specific subtypes: *classical* (more differentiated tumors associated with GATA6 expression and characterized by significantly higher SMAD4 expression) and *basal* [tumors with significantly worse median survival and faster growth rate in PDX (Patient Derived Xenografts) (72)].

In 2016, a study based on integrated genomic analysis of 456 PDACs defined 4 molecular subtypes: *squamous, pancreatic progenitor, aberrantly differentiated endocrine exocrine (ADEX) and immunogenic* (73). *Squamous tumors*, presented poor prognosis and were associated with mutations in *P53*. EGF signaling and upregulated *TP63DN* transcriptional network were found activated, whereas genes involved in pancreatic cell differentiation (ie: *Pancreatic and Duodenal Homeobox* 1 (*PDX1*), *GATA6*) were downregulated (73). *Pancreatic progenitor tumors* overexpressed genes involved in early pancreatic development like *FOXA2, FOXA 3 and PDX1* among others (73). *Immunogenic tumors* appeared similar to the pancreatic progenitor subtype, but with a significant increase in immune cell infiltrates. These tumors exhibited overexpression of immune network pathways, including CD4+ and CD8+ T cell and Toll-like receptor signaling (73). *ADEX tumors* showed deregulation of pathways involved in late stages of pancreatic development. They were characterized by upregulating genes associated with *K-RAS* activation and transcriptional networks related to acinar and endocrine differentiation (73).

Finally, recent findings showed integrated molecular analysis and classification of 150 primary tumor samples from the TCGA database. Whole exome sequencing, mRNA and protein profiling provided a complex molecular landscape of PDACs. The above classifications were applied on the TCGA PDAC data set and the analysis found an

overlapping between *basal – like* (Moffitt et al.) and *squamous* tumor (Bailey et al.) subtypes, enriched in *P53* mutations. Likewise, *classical* and *pancreatic progenitor* subtypes of PDAC were confirmed across platforms and were associated with increased GNAS mutations (9).

1.1.2.6 Molecular subtypes of PDAC stroma

Interestingly, the study of Moffitt et al. described PDACs with two distinct stroma subtypes: '*activated* and *normal*' (Fig 2). Additionally, this study identified a cluster of samples with low or missing stroma ('*low stroma'*). Patients with '*activated*' stroma had significantly worse median survival than patients with '*normal*' stroma (Fig 2) (72). *Normal stroma* was characterized by high expression of the well-established myofibroblast marker αSMA (alpha-smooth muscle actin), Vimentin and Desmin. *Activated stroma* was characterized by a diverse inflammatory signature of macrophage related chemokines (CCLs) and integrins, as well as other tumor promoting factors like SPARC, members of the Wnt pathway, collagens and matrix metalloproteinases (MMPs) (72).

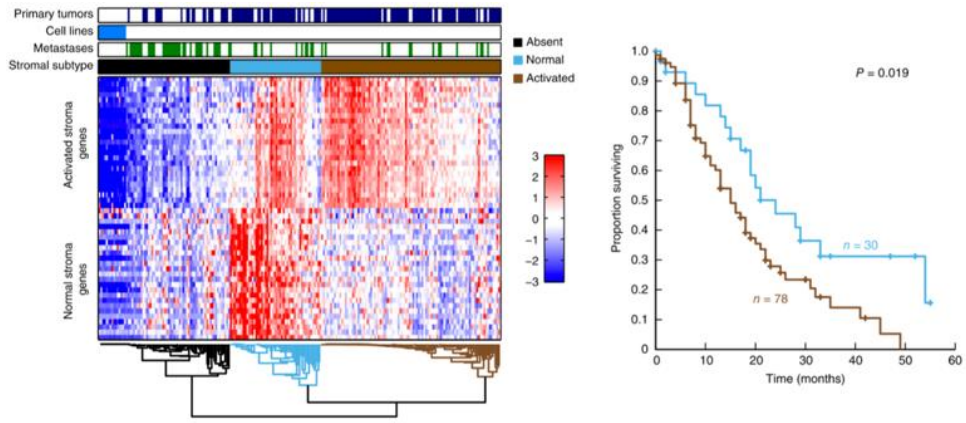

Figure 2. Stroma subtypes of PDAC in the virtual microdissection study of Moffitt et al. *(Left)* Heat map of primary tumor samples separated based on transcriptome profiles and matrix factorization. Samples clustered into three groups, describing samples with activated stroma, samples with normal stroma and samples with low or absent stromal gene expression. *(Right)* Kaplan-Meier survival analysis of patients with resected PDAC from the activated and normal stromal clusters shows that samples in the activated stroma group have worse prognosis (P = 0.019) (adapted from Moffitt et al., 2015).

Taken together, identification of tumor and stroma specific molecular signatures suggests an important interaction between tumor compartments to be considered in the future for tumor characterization and for stroma and immune modulating therapies.

1.1.3 Therapeutic approaches to treat pancreatic cancer

1.1.3.1 Conventional chemotherapies and standard of care treatments

One of the reasons of the poor overall survival (OS) rates of pancreatic cancer is the lack of efficient therapies. Despite of the progress already achieved among gastrointestinal malignancies, there have been modest advances in the treatment of pancreatic ductal adenocarcinoma (74, 75). In 1996, Gemcitabine was approved by the FDA for treatment of pancreatic cancer. This was further confirmed by a randomized clinical trial showing a significant improvement in the OS of gemcitabine versus 5-fluorouracil (76). A decade later Erlotinib (EGFR inhibitor) in combination with Gemcitabine was approved for treating metastastic PDAC. However, the survival improvement was marginal (0.4 month) (35). Other combinations of cytotoxic agents or targeted therapies failed to achieve survival benefit or presented increased toxicity. Indeed, first-line therapy FOLFIRINOX, a combination of leucovorin, 5-fluorouracil, irinotecan and oxaliplatin, showed significant advantage versus Gemcitabine (11.1 vs. 6.8 months), but only for patients with good performance (77). The other important advance was a clinical trial in 2013 with the combination of gemcitabine plus nab-paclitaxel (the nanoparticle albumin-bound formulation of paclitaxel) and since then, it became the standard of care treatment. Yet, the improvement in survival remains low compared to Gemcitabine alone (8.5 months vs. 6.7 months, respectively) (76), which highlights the urgency for developing new and more effective therapeutic strategies.

1.1.3.2 Molecular targeted therapies – clinical trials

In addition to the aforementioned novel front-line treatments, many others possibilities are under investigation. It is expected that molecular targeted therapies, monoclonal antibodies and immunologic activation will add survival benefit and will increase life quality of PDAC patients.

Direct pharmacologic inhibition of K-RAS has been unsuccessful in the past decades due to its high binding affinity to GTP and the inability to identify an easily accessible active site. Studies are ongoing to find alternative approaches, still with limited success (78). Targeting of the downstream RAF/MEK/ERK signaling pathway by MEK inhibition resulted in PI3K mediated reactivation of EGFR (79). PDAC cells also

overexpress IGF-1R, although its inhibition with ganitumab combined with gemcitabine in a Phase III randomized controlled trial did not show improvement and the study finished earlier (80).

Targeting JAK/STAT signaling by ruxolitinib in combination with capecitabine (precursor of the 5-fluorouracil) showed improved OS in patients with high C reactive protein levels in a Phase II trial (81). Phase II trial is currently ongoing to evaluate ruxolitinib in metastatic PDAC (ClinicalTrials.gov identifiers: NCT02119663 and NCT02117479). In addition, inhibitors of TGF-ß, WNT and NOTCH signaling pathways based on preclinical studies are under clinical testing (82).

1.1.3.3 Immune therapies – clinical trials

Different strategies have been addressed to harness the host's immune system against PDAC (82). For instance, by using vaccines such as the Mesothelin specific CD8+ T cell that improved overall survival (83). Immunotherapy by immune checkpoint inhibitors (i.e., CTLA-4, PD-1, PD-L1 and others) inhibitors offers encouraging results in preclinical models but often fails to show clear benefits in clinical trials for PDAC. The monoclonal antibody anti-CTLA4 Ipilimumab was ineffective in PDAC (84). However, its combination with a GM-CSF secreting PDA vaccine (GVAX) resulted in synergistic effects and raised OS (85). Clinical trial of PD-L1 inhibition with the monoclonal antibody BMS-936559 was sadly unsuccessful in PDAC (86). Yet, in preclinical studies combination with the CXCR4 inhibitor, AMD3100, the treatment induced tumor regression (87, 88). Currently, combination of Ulocuplumab (anti-CXCR4) and Nivolumab (anti-PD1) is in a phase Ⅰ study (NCT02472977) (82).

1.1.4 Mouse models to study pancreatic cancer

Genetically engineered mouse models (GEMMs) that recapitulate the human disease are important tools to understand PDAC biology and to design novel therapeutic approaches (89). Homologous recombinant technology on ES cells and the use of Cre and Flp recombinases allows a fine-tuned control of genetic alterations in a time- and tissue-specific manner.

1.1.4.1 K-Ras induced mouse models

Remarkable efforts have been made to generate GEMMs that recapitulate the full spectrum of histological alterations found in human patients. Since transformation of K-

RAS is considered to be the initiating genetic event in PDAC tumorigenesis, most of the models involve endogenous expression the K-RAS oncogene. The first model that fulfilled the above criteria included the conditional expression of a mutant *K-Ras*^{LSLG12D} allele controlled by the expression of the Cre recombinase in early embryonic development under the Pdx1 or P48 pancreatic lineage specific promoters (*Pdx1*-**C**re; ***K***-*Ras*^{LSLG12D}, referred as "KC") (90).

Our laboratory generated a bitransgenic strain (Elas-tTA/tetO-Cre) that allows the control of the K-Ras oncogene expression by a tet-off strategy: the expression of the Cre recombinase is controlled by the acinar cell specific *Elastase* promoter that controls the expression of a tetracycline trans-activator and the expression of the Cre recombinase is under the control of a Tet operon. These mice were crossed with the K-*Ras*^{LSLG12Vgeo} conditional knock-in mice (91). In the absence of doxycycline, this compound strain (K-*Ras*^{LSLG12Vgeo}; Elas-tTA/tetO-Cre) expresses the K-Ras oncogene and the β-Galactosidase reporter in a 20-30% of acinar cells from E16.5 of embryo development (92). These mice recapitulate the human disease, develop the full spectrum of PanIN lesions and a small proportion develop PDAC. Surprisingly, when mice are treated with doxycycline until the age of 8 weeks and the K-*Ras* oncogene is expressed in adult acinar cells no neoplastic growth occurs in the pancreas unless these mice undergo chronic pancreatitis (92).

The low frequency of malignant transformation suggested the need of additional genetic events that occur in later stages of PDAC development, such as mutations in tumor suppressors (*p16Ink4a/p19Arf* and *p53*) (6, 93). p53 inactivation, either by a conditional knock-in mutant (*p53*^{R172H}) (**K**-*Ras*^{LSLG12D};**p**53^{R172H}**;** Pdx1-**C**re, referred as "KPC") or by *p53* conditional *null* alleles (**K**-*Ras*^{LSLG12Vgeo};**p**53$^{lox/lox}$;**E**las-tTA/tetO-**C**re, in this study referred as "KPeC") results in accelerated tumor progression and generation of invasive lesions with complete penetrance (94). In addition, a percentage of these mice also develop metastatic tumors (89). Inactivation of *p16Ink4a/p19Arf* results in 100% penetrance of PDAC and decreases tumor latency in mice.

Numerous mouse models were generated and characterized with additional genetic alterations known to play a role in PDAC development. Modifications in *Smad4*, *Ink4/Arf*, or elimination of *Lkb1* and *Tgfbr2, Notch1* acted as tumor suppressors and accelerated PDAC formation. On the other hand, *Egfr* was shown to be essential for pancreatic tumor development by two independent groups including our laboratory (95,

96). Many of them target all cell types of the pancreas (acinar, ductal and endocrine), and are expressed at early embryonic stages. Therefore, these studies only represent preventive strategies.

To perform real therapeutic trials new mouse models have been developed that allow the elimination of the target in established lesions. These models utilize a dual recombinase system (DRS) (Cre-LoxP, Flp-FRT), where tumors are induced by K-Ras in cells expressing Flp recombinase driven by *Pdx1*, along with the ablation of the p53 tumor suppressor gene ($p53^{Frt}$) during embryonic development. When the tumor is developed, secondary modifications can be obtained in targets flanked by loxP sites by tamoxifen induced Cre recombination. On the other hand, expression of the Cre recombinase, can be also controlled by a stromal lineage specific promoter (i.e. fibroblasts) (97).

In parallel, our laboratory has generated a "therapeutic strain" using the same approach. These animals express the Flp recombinase in Elastase positive cells during late embryonic development leading to the expression of the resident $K\text{-}Ras^{G12V}$ oncogene and to the ablation of the p53 tumor suppressor gene. When the tumor is developed, tamoxifen induced elimination of Egfr or C-Raf targets occur ubiquitously in cells expressing the Cre-recombinase driven by the human Ubiquitin C promoter (Blasco et al. unpublished).

These new models will help not only to target tumor cells, but also other cell types in the tumor microenvironment. This will greatly contribute to better understanding of tumor – stroma interactions and to develop novel combinatory therapeutic approaches.

1.2 Tumor microenvironment

Cancers are heterogeneous cellular entities, whose growth not only depends on tumor cells that harbor driver mutations of oncogenes and loss of tumor suppressors, but also on interactions with the dynamic microenvironment (stroma) co-evolved during tumor development (98).

1.2.1 Distinct cell types of the tumor microenvironment

The tumor microenvironment (TME) is constituted by a diverse population of activated and/or recruited cell types by cancer cell and cancer stem cells (CSCs), such as cancer associated fibroblasts (CAFs), innate and adaptive immune cells, endothelial and other cell types that form blood and lymphatic vessels. Interaction between cancer cells and the closed normal tissue, as well as the components of the stroma regulates and define the aspect of tumorigenesis (Fig 3) (99).

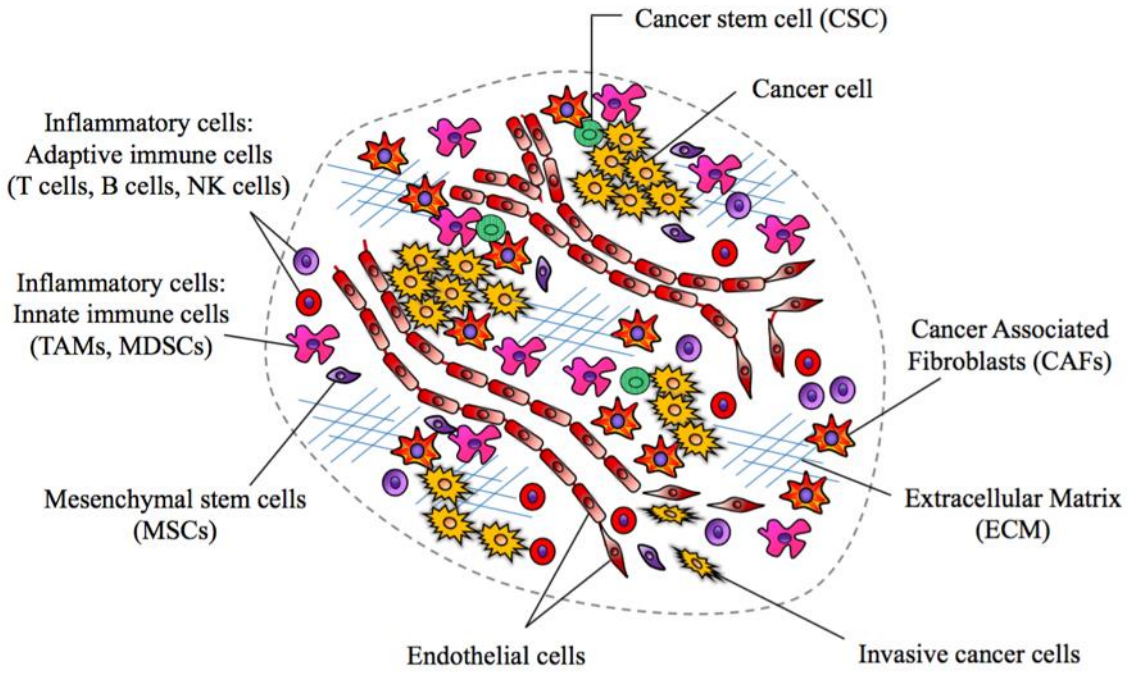

Figure 3. Distinct cells types of the tumor microenvironment (TME) in solid tumors. Subtypes of the stromal cells, such as inflammatory cells can include both tumor-promoting as well as tumor-killing subclasses either they belong to adaptive (T cells, B cells, natural killer (NK) cells) or innate immune (tumor associated macrophages (TAMs), myeloid derived suppressor cells (MDSCs)) response. Cell types including cancer associated fibroblasts (CAFs), endothelial cells, mesenchymal stem cells (MSCs)

are depicted. Cancer cells and cancer stem cells (CSCs) orchestrating the recruitment of the TME, while invasive cancer cells break away from primary tumor sites.

1.2.1.1 Immune cells - immunosurveillance

A functional link between inflammation and cancer is well accepted. Patients suffering from chronic inflammation are more prone to develop tumors due to the pro-growth environment of the inflammatory cells (98). However, the immune system plays dual role in tumor development by either tumor inhibition or support (100).

1.2.1.1.1 Innate immune cells

Components of the innate immunity, including macrophages, dendritic cells, mast cells, granulocytes or myeloid-derived suppressor cells (MDSCs) are recruited by growth factors, such as TGF-ß, VEGF or colony-stimulating factor-1 (CSF-1) and chemokines (CCL2, CCL5, etc.). These inflammatory cells release mediators that contribute to tumor growth, invasion and metastasis (101).

Tumor associated macrophages (TAMs), with similar characteristics as of M2 polarized (anti-inflammatory) macrophages, produce factors (101), that can directly affect cancer growth and metastatic dissemination by establishing pre-metastatic niches (102, 103). Furthermore, TAMs are also responsible for therapeutic resistance by antagonizing antitumor activity of treatments or by regulating T-cell activation (104).

MDSCs are a heterogeneous population of immature myeloid cells recruited from bone-marrow (105), and have strong immunosuppressive activities such as the regulation of T and NK cells anti-tumor activity and stimulation of regulatory T cells (106).

1.2.1.1.2 Adaptive immune cells

A typical solid tumor will contain all adaptive immune cell-types (natural killer (NK) cells, B and T cells), mainly located in the surrounding layer. Mature T cells are divided into two major groups based on the T cell receptors (TCRs) and are further classified according to the effector functions as CD8+ cytotoxic T cells (CTLs) and CD4+ helper T (Th) cells, which include Th1, Th2, Th17, and T regulatory (Treg) cells, as well as natural killer T (NKT) cells (107). The process of activating cytotoxic CD8+ T cells and/or DC4+ T helper cells can be skewed in different ways, e.g. by cancer cells reprogramming the protective immune response, termed immunosurveillance (108).

Increased numbers of T cells usually are correlated with better prognosis in several cancer types, including melanoma, colon and pancreatic cancer (108). The ratio of CD8+

CTLs and Treg cells indicates the balance between host defense or tumor promotion (109). Treg cells mostly suppress antitumor immune responses (110), whilst NK cells and CTLs perform cytotoxic immunity (111). Recently, programmed death-ligand 1 (PD-L1) overexpressed by various tumor cell types, and its receptor (PD-1) on T cells became an important target. In several tumors refractory to conventional chemotherapy anti-PD-1/PD-L1 succeeded, such as in melanoma (112). Yet, a group of solid cancers remain unresponsive (86).

1.2.1.2 Endothelial cells – angiogenesis

For the rapid expansion of a primary tumor, oxygen and nutrition supplies are needed. This requires the generation of new blood vasculature by activation of quiescent vessels (angiogenesis) (113). However, tumors develop irregular and dysfunctional new vessels (114), very often via overexpression of VEGF growth factor.

Endothelial cells can be activated by cytokines (bFGF, TNF-α, TGF-ß, PDGFs, PIGF and Neuropilin-1), chemokines (CXCL12, IL8/CXCL8), matrix metalloproteinases (MMPs), ROS and bioactive mediators, such as nitric oxide (NO) (115). Angiogenesis can be regulated by tumor associated macrophages (TAMs) through direct VEGF-A production (116) or via MMP9 secretion, which releases VEGF-A from the extracellular matrix (ECM) (117). Blockade of TAM secreted CSF-1 resulted in vascular normalization and improved therapeutic response (118). In addition, neutrophils were also reported to promote angiogenesis by MMP9 production (119), as well as cancer associated fibroblasts (CAFs) through pro-angiogenic signaling factors (120).

1.2.1.3 Extracellular Matrix

The tridimensional organization of the TME is highly dynamic and is dependent of the extracellular matrix (ECM) surrounding the cells. The ECM contains a mixture of fibrillar proteins, glycoproteins, proteoglycans, cytokines and growth factors (121), which supports cell adhesion via binding cell surface adhesion receptors and integrin signaling (122). Physical features of the ECM include its porosity and rigidity, spatial arrangement and orientation of insoluble components, as well as other features that together determine its role supporting tissue architecture.

Abnormal ECM and increase in collagen deposition can result in tumor stiffness and upregulation of integrin signaling, thus promoting cell survival and proliferation (123). Additional components, such as Hyaluronic acid also defines the structure and physical properties of the stroma (124). In addition, aberrant regulation of the ECM may

convert a normal stem cell niche into a cancer stem cell niche, disrupt tissue polarity and integrity to promote invasion (125). Importantly, in the periphery of benign tumors, enhanced collagen synthesis results in tight encapsulation of the tumor (126), suggesting that initial stromal responses may retain neoplastic expansion. However, reprogramming of the stroma by cancer cell directs them towards malignant progression (98).

1.2.1.4 Cancer Associated Fibroblasts (CAFs)

Fibroblasts are important and abundant cells in any context. They survive severe stress that is usually lethal to all other cells and are essential in tissue homeostasis, wound healing and repair processes in response to exposure to chemicals or carcinogens (127). Indeed, there is an increasing body of evidence of their role in tumor development, in agreement with the hypothesis of Dvorak stating "cancer is a wound that never heals" (128).

1.2.1.4.1 Origins of CAFs

In tissue repair, fibroblasts proliferate and differentiate into myofibroblasts, along with the expression alpha-smooth muscle actin (α-SMA), collagen, fibronectin, and other fibrillar proteins resulting in a reactive desmoplastic stroma (129). Aberrant regulation of the constitutive wound healing process leads to the generation of malignant stromal tissue and diverse fibroblast populations. In the process of tumorigenesis, they are collectively designated as cancer associated fibroblasts (CAFs).

CAFs are a heterogeneous cell population (Fig 4) derived from multiple origins, such as bone marrow, adipose tissue, mesenchymal stem cells (MSCs), epithelial and cancer cells through EMT process, endothelial cells via endothelial mesenchymal transition (EndMT) or mainly from adjacent normal tissue fibroblasts (130). They are defined by elongated, spindle-like morphology and by expression of distinct markers, characterizing each subtype (127). They are found in many solid cancers, however, abundance of CAFs is a typical feature of prostate, breast and pancreatic cancer (131).

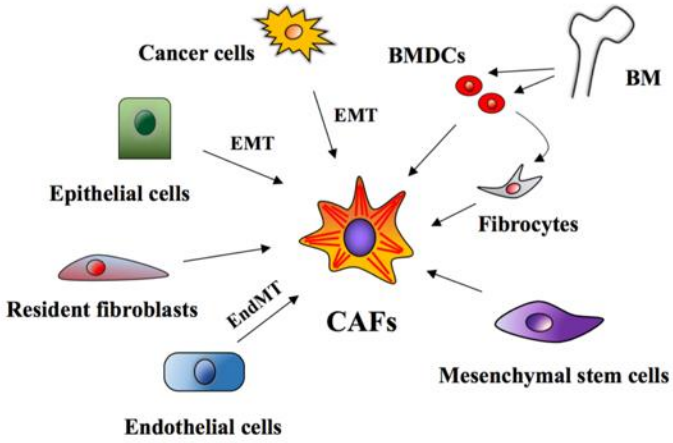

Figure 4. Origins of CAFs. Bone marrow derived cells (BMDCs) including fibrocyte precursors and mesenchymal stem cells (MSCs) contribute to the diverse CAF population, as well as epithelial, cancer and endothelial cells via EMT or EndMT process. The majority of CAFs is derived from tissue resident fibroblasts.

1.2.1.4.2 Molecular markers

The molecular characterization of CAFs has illustrated that there is no unique marker to label all CAFs and that most markers are not even specific to CAFs or fibroblasts. While αSMA is used as a robust CAF marker, which usually identifies CAFs with myofibroblast morphology (132), it is also expressed by normal fibroblasts (133) and in some cases at comparable or even higher level (134, 135). FSP1 or S1004A is another marker of CAFs, even though it seems to have a differing role in cancer (136). Another well described marker is the cell surface serine protease fibroblast activation protein (FAP) (137). Further overexpression among cell surface proteins include the neural marker, NG2 and PDGFRß, that is also found on vascular cells (138). Interestingly, PDGFRß activation was also reported in invasive pancreatic tumor cells (139).

Finally, it was reported in different cancer types, such as skin and pancreatic tumors that PDGFRα is a marker of a CAF population characterized by pro-inflammatory gene signature (140). However, it also labels immune, adipose and mesenchymal stem cells; and drives adipose tissue derived fibrosis (141, 142). Of note, PDGFRα could be considered as EMT marker in tumor cells (143).

1.2.1.4.1 Functional properties of CAFs

Each of CAF subtypes can contribute to a variety of tumor-promoting functions in different organ-specific TMEs (Fig 5). For example, CAFs are a source of paracrine

signaling molecules that include mitogenic epithelial growth factors, hepatocyte growth factor (HGF), EGF family members, insulin-like growth factor-1 (IGF-1), stromal cell-derived factor-1 (SDF-1/CXCL12), and a variety of FGFs and VEGFs, with the capability to stimulate cancer cell proliferation, angiogenesis, invasion and metastasis (88, 127, 144, 145). CAFs can also orchestrate functional attributes associated with EMT via secretion of TGF-ß (146). In addition, they can express a wide range of ‘‘proinflammatory’’ cytokines (140, 147), thereby recruiting and activating inflammatory cells, that in turn provide proliferative signals. Importantly, CAFs also undergo metabolic reprogramming by switching from oxidative phosphorylation to glycolysis via IDH3 downregulation, resembling a Warburg-like effect that leads to tumor growth support (148).

Nevertheless, evidence suggests that normal connective tissue fibroblasts (but not CAFs) from various organs can inhibit tumor growth through a process that requires contact of the normal fibroblasts with cancer cells, in governing epithelial homeostasis and proliferative quiescence (149, 150). Therefore, normal fibroblasts could act as tumor suppressors, a function that is lost upon reprogramming to become CAFs.

1.2.2 Tumor microenvironment in PDAC

Among many epithelial tumors, pancreatic cancer displays the most extensive stromal reaction accounting for up to 90% of the tumor volume. This profuse desmoplastic stroma is characterized by CAFs and inflammatory infiltrates, as well as huge amount of ECM generating a rigid, impenetrable tumor tissue with high interstitial fluid pressure and compression of vessels (124). This reactive environment acts as a physical and a chemical barrier against treatments (151, 152).

CAFs are the most abundant cell type in PDAC stroma that produce ECM components, such as collagens, fibronectin, laminins and hyaluronic acid, glycosamino glycans (GAGs) (Fig 5) (124). They also stimulate tumor cell growth by paracrine signaling, support migration and invasion, as well as acquired resistance mechanisms.

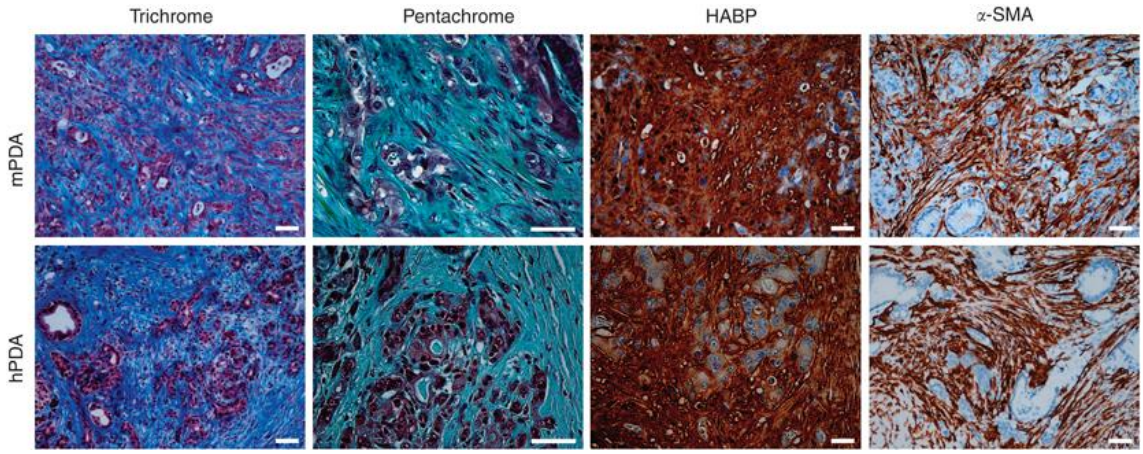

Figure 5. Histology of human and mouse PDAC. Masson's trichrome histochemistry shows robust collagen deposition (blue). Pentachrome staining reveals collagen, (GAGs) and mucins (turquoise/green). Hyaluronic acid binding protein hybridization probe displayes intense HA content. αSMA immunohistochamistry shows abundant expression in the stroma but not in tumor cells. (Adapted from Provenzano et al. 2012.)

The reactive fibrotic environment contributes to hypoxia and immune cell infiltrates. While immune cells are also plentiful within the stroma, they mostly belong to immunosuppressive subsets, such as regulatory T cells (Tregs), T-helper (Th cells) cells, TAMs and multiple subsets of immature MDSCs. TAMs support tumor progression and invasion by producing pro-tumorigenic factors and induce resistance to gemcitabine treatment by upregulating the levels of the drug metabolism related enzyme, cytidine deaminase, in PDAC cells (153). In a recent study, Zhu et al. identified TAMs of distinct origins in PDAC: tissue resident macrophages display pro-tumorigenic functions and pro-fibrotic transcriptional signature, whilst monocyte-derived TAMs appear to play a role in antigen presenting (154). In contrast, CD8+ T cells are not frequent in the tumor stroma and when present they are located in the surrounding tumor tissue (152).

Therefore, these findings suggest that stroma elimination could deplete the physical barrier and enhance drug delivery to the cancer cells located inside of the tumor mass, while also disrupting deleterious stroma – cancer cell interactions. Studying tumor – stroma interactions by GEMMs can shed light on important cellular processes and therapeutically targetable pathways.

1.2.3 Cancer Associated Fibroblasts (CAFs) in PDAC

In pancreatic cancer, a specific cell type, pancreatic stellate cells (PSC) are the major source of CAFs. PSCs is a specific cell type (155), that can be found in pancreas,

liver, kidney, lung and intestine (156) and that share many characteristics of fibroblasts. In normal pancreas, PSCs are in a quiescent state with a specific stellate morphology located in the peri-acinar space and contain lipid droplets that serve as Vitamin A storage (Fig 6). Various markers have been described to identify quiescent PSCs, including desmin, nestin, GFAP, vimentin (155, 157, 158). Upon activation, they start to express αSMA, change their cytoskeleton, and acquire elongated shape and myofibroblast phenotype. They control the ECM turnover by producing MMPs and collagens. They can be activated by PDGFs TGF-ß, TNF-α, and interleukins, such as IL1, IL6 and IL10. Indeed, PSCs associated to PDAC express receptors of these cytokines (159). This activation could be reversed *in vitro* by retinoic acid (Fig 6) (160).

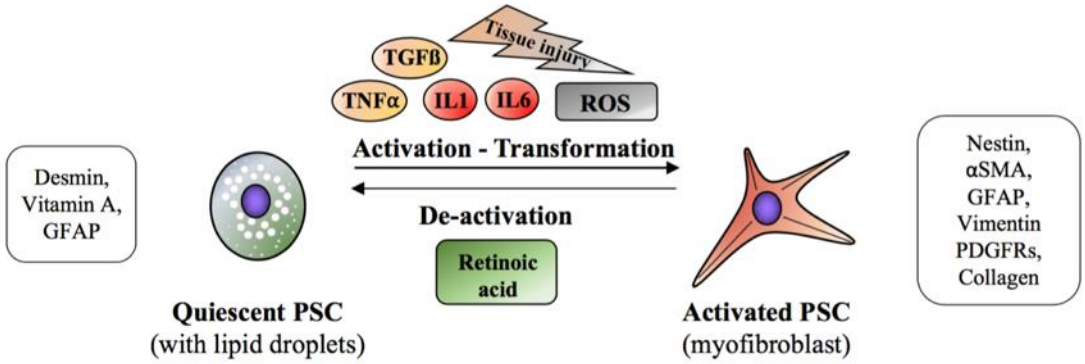

Figure 6. Activation of Pancreatic Stellate Cells (PSCs). Quiescent PSCs express Desmin, Vitamin A and GFAP; and contain lipid droplets. Upon activation by inflammatory cytokines, tissue injury or oxidative stress (ROS) they transform into myfibroblasts, change their morphology and start to express markers, such as αSMA, Vimentin, PDGFRs, etc. Activated PSCs can be reverted by retinoic acid.

As described above, CAFs are key players in the TME of pancreatic cancer. Being the most frequent cell type in PDAC stroma (80%) they are also responsible for the extreme stiffness of the tumor tissue by producing insoluble fibrillary matrix components. This results in hypoxia and a reactive microenvironment, rich in infiltrating, suppressive immune cell populations, ideal for tumor progression and therapy resistance (124). Subpopulations of CAFs in PDAC

CAF subpopulations can be defined by their origins or/and molecular profile (127, 130). CAF subtypes are not well characterized, indeed, there is only minor description of these subpopulations in PDAC. For instance, a CD10-positive subpopulation of CAFs was identified in human PDAC specimens. These cells were localized juxtatumorally, in

the vicinity of tumor cells in patients with shorter survival (161). In a recent study, Öhlund at el. defined two distinct populations of CAFs showing molecular divergence. MyCAFs (myofibroblast CAFs), with increased expression of the well-known myofibroblast marker αSMA, located in close proximity of neoplastic cells. iCAFs (inflammatory CAFs), on the other hand were localized more distant from tumor cells and displayed inflammatory-secretory expression profile with elevated expression levels of IL-6 but lacking αSMA in a mutually exclusive but reversible fashion (162).

1.2.3.1 Preclinical studies targeting CAFs in PDAC

Targeting the pro-tumorigenic effects of CAFs in pancreatic cancer offers many possibilities due to their functional diversity. Indeed, several strategies have been suggested to obtain therapeutic benefits in PDAC (Fig 7).

Targeting the stroma and ECM as physical or chemical barrier. The desmoplatic stroma in PDAC has been considered a barrier to drug delivery. Targeting the production of the ECM or its degradation are both feasible strategies to loosen the stroma and to induce expansion of blood vessels. In 2009, inhibition of the Hedgehog pathway by the Smo inhibitor IPI-926, was shown to be efficient to reduce stromal content, induce angiogenesis and improve intratumoral Gemcitabine content (151). In contrast, when Hh was genetically deleted in a pancreatic cancer mouse model, despite the attenuated stroma and an increased vascularization, these tumors appeared undifferentiated and more aggressive leading to reduced survival in mice (51, 52).

High interstitial fluid pressure can be reduced by enzymatic digestion of hyaluronic acid, a major component of the ECM (124). Degradation of hyaluronan by the peglylated form of hyaluronidase (PEGPH20) normalized the hydrostatic pressure, lead to increased delivery of chemotherapy and prolonged survival in KPC mice (124, 163). The matrix protein SPARC is overexpressed in the ECM of many tumor types. nAb-Paclitaxel, an albumin-bound Paclitaxel, was postulated to bind to SPARC and thereby induce stromal depletion. This hypothesis was supported by the analysis of PDAC samples and patient-derived xenografts (PDX) (164). However, in KPC mice stromal loss occurred rather due to implicated drug–drug interactions via reduction of cytidine deaminase levels (165). Moreover, tumor-bearing KPC mice lacking SPARC did not respond differently to nAb-paclitaxel compared to control mice, showing the mechanism of action is independent of SPARC expression (166).

It was recently illustrated in KPC mice that CAFs can act as a chemical barrier by retaining gemcitabine metabolites through reduced levels of key inactivating metabolic enzymes compared to tumor cells. By this mechanism, CAFs limited the drug uptake of cancer cells (167).

Targeting secreted factors of CAF-tumor cell interactions. Blocking the CAF-secreted connective tissue growth factor (CTGF) resulted in a synergistic effect with gemcitabine without increasing the intratumoral gemcitabine concentration via deregulation of the apoptosis modulating protein XIAP (168).

On the other hand, Cxcl12 secreted from FAP-positive cells was shown to be important for immune suppression, explaining why immune checkpoint inhibitors, such as anti-PD-L1, have failed in pancreatic cancer (84). Notably, in KPC mice, inhibition of Cxcr4, the Cxcl12 receptor, promoted the intratumoral T cell recruitment and strongly cooperated with anti-PD-1L (137). Likewise, inhibition of Cxcr2, a receptor activated by CAF produced ligand Cxcl1/2 in KPC mice prolonged survival and improved T cell entry. Interestingly, germline elimination of Cxcr2 completely abrogated metastasis but had no effect on tumor development suggesting cellular context and tumor stage dependent action of this receptor (169).

Targeting CAFs by reprogramming. Depletion of CAFs in a pancreatic cancer model led to more aggressive and less differentiated tumors (170). Thus, the protective role of certain stromal elements should be taken into consideration and reprogramming, rather than eliminating CAFs, should be considered. Reprogramming of CAF behavior to change their properties to a more “normal” phenotype can be achieved by multiple mechanisms. Since CAFs undergo metabolic changes, normalization of the metabolic phenotype and inhibition of metabolic pathways have also been suggested as a possible way to target tumors (171).

Another approach postulated to dedifferentiate them into a quiescent state is based on Vitamin D since Vitamin D Receptor (VDR) ligands promoted the dedifferentiation of liver stellate cells and abrogated fibrosis (172). In PDAC, Vitamin-D mediated stromal reprogramming markedly reduced inflammation and returned PSCs into a quiescent state, thereby decreasing tumor volume and increasing chemotherapy efficacy (173).

Finally, inhibition of PDGF signaling, an important pathway in the activation of CAFs, can reverse CAFs into normal fibroblasts (174). In PDAC, metastatic potential was significantly reduced upon Imatinib treatment of tumor-bearing KPC mice, while showing no effect on primary tumor development (139).

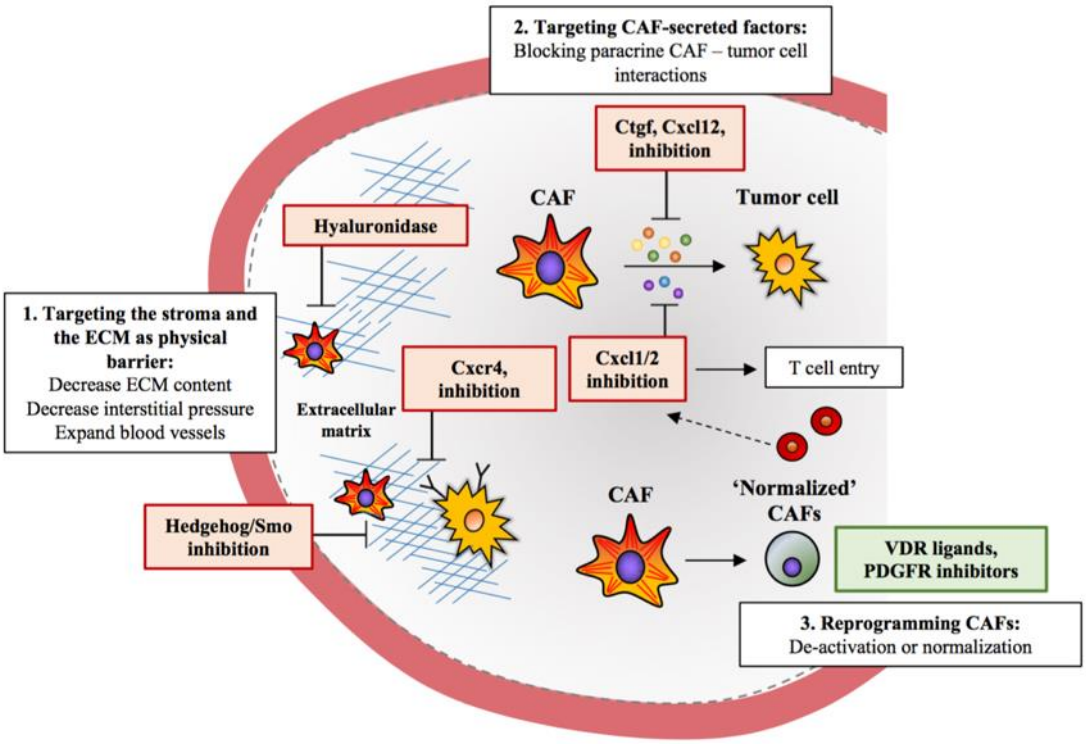

Figure 7. CAF targeting approaches. *1. Targeting the stroma as a physycal barrier* :by Hyaluronidase and Hedgehog inhibitors to decrease ECM and to improve drug delivery. *2. Targeting CAF secreted factors:* by inhibitors of Ctgf, Cxcl12 to block interactions with tumor cells. Targeting CAFs – secreted ECM mediated pro-tumorigenic effect by Cxcr4 inhibition. Blocking Cxcl1/2 improves intratumoral T cell entry. *3. Reprogramming CAFs* into "normal" fibroblasts by deactivation using PDGFR inhibitors or VDR ligands.

In conclusion, there is emerging evidence from preclinical studies that pro-tumorigenic properties of CAFs represent an attractive and promising therapeutic target in PDAC that deserve further studies.

1.3 Serum Amyloid A protein family

Serum Amyloid A (SAA) is an acute phase high-density apolipoprotein family, whose levels are highly increased upon inflammatory stimuli, tissue injury, trauma or cancer (175). Although, different pro- and anti-inflammatory properties have been recently connected to distinct isoforms of SAAs, their role in defense mechanisms and cancer development is not entirely understood.

1.3.1 SAA functions in normal homeostasis

SAA is a highly conserved protein family (176) suggesting evolutionary significance and physiological importance (177). They are considered apolipoproteins (proteins that bind lipids and transport them through the circulatory systems) since in the circulation they associate with high-density lipoproteins (HDL), such as cholesterol, thereby playing an important role in lipid metabolism (178). During inflammatory events, acute phase response is initiated to eliminate pathogens and restore normal homeostasis. This involves HDL remodeling, where SAA1 and SAA2 displace ApoA-1 and become apolipoprotein of HDL (179). It is unknown if the role of SAAs during acute inflammation is to raise cholesterol removal from tissue damage sites or to deliver cholesterol esters to cells involved in tissue repair (180). In addition, it was recently reported that SAAs could have functional role in retinol (Vitamin A) binding and transport during infection and inflammatory response (181).

1.3.1.1 SAA family members

In humans, four SAA encoding genes are clustered on chromosome 11 in a segment of 150 Kb (182). SAA1 and SAA2 are located in close proximity and contain several allelic variants. The third gene, SAA3 is situated further downstream of SAA4 and was identified as pseudogene in humans (hSAA3P) with a defective promoter generating a translational stop signal (183). However, mRNA transcripts were reported in mammary gland epithelial cells (184) and in cancer. SAA1 and SAA2 are designated as ‘acute phase SAA’ (A-SAA) since their serum concentration could strike to 1000-fold during inflammatory response, whilst SAA4 is referred as ‘constitutive SAA’ (C-SAA) secreted into the blood circulation constitutively by hepatocytes in ‘normal’ physiological conditions (185).

In mice, as well as in humans, Saa1 and Saa2 are major acute phase proteins along with constitutive expression of Saa4 in liver. Nevertheless, Saa3 is secreted

predominantly by extrahepatic tissues, including macrophages, adipocytes and fibroblasts (186) associated with a wide range of inflammation related cellular functions.

1.3.2 SAAs in disease and cancer

1.3.2.1 SAAs as major acute phase protein and inflammatory cytokine

Chronic inflammatory diseases, such as obesity, diabetes, rheumatoid arthritis, atherosclerosis and Alzheimer's disease are associated with SAA overexpression. Increased levels of SAA are found in serum and synovial fluid of rheumatoid arthritis (RA) patients (187), as well as in synovial fibroblast, macrophages and endothelial cells (188). SAA is upregulated in smooth muscle cells of obese patients (189). Moreover, the same type of cells stimulated with recombinant Apo-SAA exhibited increased proliferation and migration via induction of chemokines, such as CCL2 and CXCL8, chemotactic agents for monocytes and neutrophils in atherosclerosis (190). Finally, SAA overexpression was associated with pulmonary diseases including cigarette smoke induced chronic lung inflammation (191), as well as with systemic inflammatory response upon brain injury (192).

1.3.2.2 Regulation, receptors and signaling

SAA transcription can be induced by cytokines, chemokines, both in autocrine or paracrine fashion. The strongest activators of SAA are pro-inflammatory cytokines via NFKB signaling, where Il-ß is the most potent SAA inducer followed by IL6 and TNF-α, although cooperation of at least two of them is often necessary (193). On the other hand, SAA induces the production of these cytokines and chemokines in different cell types including CCL2, CXCL8 and CXCL1 in monocytes, neutrophils and fibroblasts (193).

Functional receptors of SAA identified until now include the formyl peptide receptor 2 (FPR2), the scavenger receptor class B type I (SR-BI), the receptor for advanced glycation end products (RAGE), the Toll-like receptors 2 (TLR2) and 4 (TLR4) (180). *FPR2* is the main receptor of SAA induced cytokine synthesis via NFKB and MMP transcription (188). In addition, chemoattractant activity of SAA via FPR2 have been described in monocytes, neutrophils, and T-cells (193). *SR-BI*, is the primary receptor for native HDL through binding its apolipoprotein, SAA. Native HDL promoted cellular cholesterol efflux was induced by SAA via SR-BI (175). *RAGE* activated by SAA leads to the stimulation of NF-κB and MAPK in rheumatoid synovial fibroblasts. *TLR2/4* are involved in SAA induced inflammatory signaling and activation of cytokine/chemokine

production. Indeed, IL-6, TNF-α and IL-10 in synovial fibroblasts was stimulated through TLR2 (194).

1.3.2.3 Dual role of SAA in cancer

Increased SAA levels were reported in several type of cancers, such as gastric and ovarian cancer, myeloma and osteosarcoma (180) with a gradual increment between early and late stages suggesting involvement in tumor pathogenesis, and a potential to be a prognostic marker (195).

Several studies have shown pro- and anti-tumorigenic properties. These include inhibition of tumor invasion by binding to ECM components, or on the contrary, induction of ECM degrading enzymes allowing tumor cell migration (180). Interestingly, such dual role of SAA was recently reported in nasopharingeal carcinoma, where opposite effects were associated to SAA1 SNP variants. Out of the five SAA1 polymorphic allele, SAA1.1 and SAA1.3 possessed anti-angiogenic properties, whereas SAA1.5 lacked tumor suppressive effect (196). Of note, these polymorphic variants in mice were not identified (197). In fibroblasts, such as hepatic stellate cells (HSCs), SAA activated IκB kinase, c-Jun N-terminal kinase (JNK), Erk and Akt and enhanced NF-κB. In the liver, SAA induced cell death upon NFKB treatment in rat HSCs, while in hepatocytes the same conditions promoted phosphorylation of ERK/MAPK signaling (198).

In pancreatic cancer SAA was among the 183 overexpressed genes in tumor tissue compared to normal samples (199). Moreover, its plasma levels correlated with clinical stage in PDAC patients (200), thus it was proposed to be used as a biomarker combined with *Haptoglobin* (201).

1.3.2.4 Functional studies of Saa3 in mice

SAA is a family of highly homologous proteins. This similarity is even conserved between species. For example, the murine Saa3 and human SAA1 share 74% of their amino acid sequence, and 73% with the mouse Saa1 (194).

Adipose tissue damage augmented Saa3 and hyaluronic acid levels which induced monocyte recruitment and retention, as well as cell adhesion leading to local inflammation (202). However, Saa3 is not amyloidogenic and does not contribute to plasma Saa levels during acute phase response (203) In MDSCs, Saa3 overexpression resulted in limited antitumor activity, thereby exacerbating tumor growth (204). Moreover, Saa3 activates p38 – MAPK and NF-κB via Tlr4 (205), while it stimulates growth of regulatory T cells in a process involving Il-1β and Il-6 induction in monocytes

(206). In endothelial cells and macrophages Saa3 contributes to establishing pre-metastatic niche (207). Indeed, involvement of Saa3 in metastatic processes was further confirmed by several groups (191, 208). For instance, S100A4 stimulated transcription of Saa1 and Saa3 through TLR4/NFKB pathway, which in turn, enhanced cell adhesion to fibronectin and increased tumor cell migration linking inflammation to metastasis promotion.

Mice deficient in Saa3 has been generated (209). When fed with high fat diet, Saa3 knockout mice reduced weight gain and adipose tissue inflammation. Female Saa3 *null* mice also improved plasma cholesterol, triglycerides and lipoproteins profiles compared to controls implicating an a significant role of Saa3 in cholestherol regulation (209).

Taken altogether, in this thesis, I have characterized a CAF subpopulation with protumorigenic properties defined by the expression of the platelet-derived growth factor receptor alpha (PDGFRα). The comparative transcriptome analysis of fibroblasts present in normal pancreata showed that the most differentially overexpressed gene in CAFs was *Saa3*, a member of the acute-phase Serum Amyloid A (SAA) apolipoprotein family found associated with high density lipoproteins in plasma (176). Expression of SAA members is induced in injured tissues and cells including atherosclerotic plaques, rheumatoid synovitis and in certain tumor cells (180). Moreover, they are considered as biomarkers whose expression is associated with tumor progression and reduced survival in many human cancers, including PDAC (180, 210).

We describe that Saa3 plays a key role in inducing the pro-tumorigenic properties of PDGFRα+ CAFs. In addition, we also specify that the pro-tumorigenic activity of Saa3 is regulated by the Membrane Palmitoylated Protein 6 (Mpp6), a member of the peripheral membrane-associated guanylate kinases (MAGUK). In addition, we identified and functionally validated further targets differentially overexpressed in CAFs and generated GEMMs by CRISPR/Cas9 gene editing technology in order to study their role and their potential therapeutic value in PDAC development.

2 Objectives

The following objectives were set for this thesis work:

1. Comparison of the gene expression profiles of cancer associated fibroblasts (CAFs) in PDAC to normal pancreatic fibroblasts (NPFs) to find specific targets that can help to reprogram the CAFs to counteract their pro-tumorigenic properties.

2. Functional validation of the pro-tumorigenic properties of the selected targets.

3. Generation of germline knock-out alleles in PDAC mouse model to study the role of the selected targets *in vivo* in pancreatic cancer development.

3 Materials and Methods

3.1 Mouse models

3.1.1 KPeCY mouse model

The K-*Ras*$^{+/LSLG12Vgeo}$;*Trp53*$^{lox/lox}$;*Elas*-tTA/*tetO*-Cre PDAC mouse strain was generated by crossing K-*Ras*$^{+/LSLG12Vgeo}$ (91) with the bitransgenic *Elas*-tTA/*tetO*-Cre strain (provided by Dr. Grippo, Northwestern University, Chicago, IL, USA and Dr. J.I Gordon, Washington University, St. Louis, MO, USA). The Cre recombinase expression is driven by the acinar cell specific *Elastase* promoter and is under the negative control of the doxycycline inducible Tet operon (Tet-off system). *Trp53*$^{Lox/Lox}$ mice were obtained from Anton Berns´ laboratory (The Netherlands Cancer Institute, Amsterdam, The Netherlands). *Rosa26*$^{+/LSLEYFP}$ mice were obtained from The Jackson Laboratory, (generated by Dr. Soriano). Mice were maintained in a mixed C57BL/6 - 129/Sv background.

3.1.2 Saa3 germline KO

Saa3 null sperm (Saa3$^{tm1(KOMP)Vlcg}$) was obtained from the KOMP Repository and used to generate *Saa3 null* mice by *in vitro* fertilization of KPeCY females at the CNIO Transgenic Unit. *Tm1* modification was designed to replace the entire protein with a reporter tagged selection cassette utilizing BAC-VEC system (211).

3.1.3 Therapeutic strain

The K-*Ras*$^{+/FSFG12V}$;*Trp53*$^{frt/frt}$;Elas-tTA/tetO-FLp(o);*Egfr*$^{lox/lox}$;*c-Raf*$^{lox/lox}$;Ub-CreERT2 strain was generated by intercrossing. The *K-Ras*$^{+/FSFG12V}$ was developed in Mariano Barbacid's laboratory in CNIO (Drosten unpublished). In collaboration with the CNIO Transgenic Mice Unit, we generated the *Elas-tTA/tetO-Flp* bitransgenic strain. The *Trp53*$^{Frt/Frt}$ was generated in David Kirsch´s laboratory (Duke University Medical Center, Durham, NC, USA). The *Tg.hUBC-CreERT2*$^{+/T}$ (212) was generated in Eric. J. Brown´s laboratory (University of Pennsylvania, School of Medicine, Philadelphia, PA, USA). The *Egfr*$^{Lox/Lox}$ allele (213) was obtained from Maria Sibilia´s laboratory (Institute for Cancer Research, Vienna, Austria). The *c-Raf*$^{Lox/Lox}$ (214) was generated in Manuela Baccarini´s laboratory (Institute of Microbiology and Genetics, Vienna, Austria).

3.1.4 Maintenance of mice

All mice used in these projects were housed in the Animal Facility of the Spanish National Cancer Research (CNIO) in accordance with Federation of European Laboratory Animal Science Association (FELASA) recommendations and following European Union legislation. All experiments described in this thesis have been approved by the Bioethics and Animal Welfare Committee of the Institute for Health Care Carlos III. Mice were subjected to light and dark cycles of 12 hours each with temperature and humidity regulated. Animals were fed *ad libitum* with a standardized diet (28018S, Tekland).

3.1.5 Generation of mouse models by CRISPR

3.1.5.1 sgRNA design and validation

For each target gene, six sgRNA sequence were designed by CRISPRScan (215) based on their disposition in the locus and the off-target effects. Sequences were validated in CAF cell line by a dual lentiviral system. SgRNA sequences were cloned into a pLKVU6 lentiviral backbone and constitutive Cas9 expressing CAFs were infected as described above (see 3.2.5). Validation of mutations (indels) was performed by T7 endonuclease assay and sequencing (see 3.3.4.3). When antibodies were available protein expression was validated by western blot. Most efficient sgRNA knock-down sequence was selected to proceed with *in vivo* microinjection. The following sgRNA sequences were used:

Has1:

sgRNA 5': CACCGCGTTGGGGCGGCAAACGTGGT

sgRNA 3': TAAAACCACGTTTGCCGCCCCAACGC

Lumican:

sgRNA 5': CACCGACACTACCGACTAATGCCAGT

sgRNA 3': TAAAACTGGCATTAGTCGGTAGTGTC

Haptoglobin:

sgRNA 5': CACCGAGATTGCAAACGGCTATGTGT

sgRNA 3': TAAAACACATAGCCGTTTGCAATCTC

Mesothelin:

sgRNA 5': CACCGCCAACAGCTCGACCCCTGCGT

sgRNA3': TAAAACGCAGGGGTCGAGCTGTTGGC

3.1.5.2 sgRNA preparation and Microinjection

To prepare sgRNAs for microinjection T7 promoter was added by Hi Fidelity PCR (KAPA, HiFi Hotstart PCR Kit) amplification using Px330 as template. The following primers were designed for each gene:

Forward: **T7 promoter**, sgRNA sequence, crRNA sequence:

5′- **TGTAATACGACTCACTATAGG**NNNNNNNNNNNNNNNNNNNgtttta gagctagaaatagc-3′

Reverse: 5′-AGCACCGACTCGGTGCCACT-3′

The PCR reaction contained 1.5 µl dNTP Mix, 10 µl 5X PCR Buffer, 1.5µl of each primer (10 µM), 1 µl of Px330 plasmid template, 0,5 µl KAPA Hi-Fi DNA polymerase and 34 µl sterile water. At least 8 reactions were prepared in order to obtain enough material for the following step. T7-sgRNA product was gel purified and used as template for *in vitro* transcription to RNA by using MEGAshortscript T7 Transcription Kit (Ambion). RNA was purified by MEGAclear Kit (Ambion) and quality was verified by Bioanalyzer. This process was performed for each target gene, as well as for Cas9.

Microinjections were performed in collaboration with the Transgenic Mice Unit in CNIO. Zygotes were derived from the therapeutic strain. 30 ng/µl sgRNA and 50 ng/µl Cas9 mRNA was microinjected into the cytoplasm of the one-cell state embryos. Next, the mouse embryos were transferred into foster mothers and chimeras were born.

3.1.5.3 Genotyping strategy

3.1.5.3.1 T7 endonuclease assay

This assay detects heteroduplex DNA that results from annealing DNA stands that have been modified after a sgRNA/Cas9 mediated cut to DNA strands without modifications. PCR products amplified from each sample were purified by QIAquick Gel Extraction Kit. Briefly, 600 ml of QG buffer was added to the PCR product, mixed well and loaded on the Qiagen spin column. Samples were washed two times with 500 ml ethanol containing PE buffer. T7 endonuclease (NEB) was used to detect mismatched DNA. To do this, 200 ng of PCR product was mixed with 2 ml of NEB2 buffer and reaction volume was filled up to 20 ml with sterile water. Hybridization was perfomed in thermocycler as following: 5min, 95ºC; ramp down to 85ºC, at -2C/s; ramp down to 25ºC, at -0.1C/s; hold at 4ºC. 1 µl of T7 endonuclease was added to each sample and incubated at 37ºC for 15 minutes. Reaction was directly loaded on 10% polyacrylamide gel (4 ml

30% Acryamide, 6,8 ml water, 2,4 ml Tris-Borate-EDTA (TBE), 200 µl 10% APS, 10 µl TEMED) to separate DNA fragments. 9 µl DNA ladder was used as standard. Electrophoresis was performed in TAE buffer on 100-150 mV. Detection of DNA fragments was done in ethidium-bromide containing water.

3.1.5.3.2 Subcloning and sequencing

In order to identify mutations, we used pGEM-T Easy Vector System for subcloning PCR products. This vector contains a T7 and an SP6 sequence, as well as a β-galactosidase coding sequence and a standard ampicillin selection cassette to screen for recombinant clones. Purified PCR products were ligated to linearized pGEM-T vector containing a 3'-terminal thymidine at both ends by T4 DNA ligase enzyme overnight at 4ºC. DNA insert was used at 1:3 ratio of vector to insert, respectively. Transformation was done in DH10B *E. Coli* bacteria strain by adding the ligation mix and performing heat shock at 42ºC for 90 seconds. This was followed by a 2-minute incubation on ice. Then, 300 µl of LB medium was added to the tube and bacteria was incubated for 1.5-2 hours at 37 ºC, shaking at 120 rpm. Then, 100 µl of transformation culture was plated on agar plates with Ampicillin resistance and IPTG/X-Gal. Recombinant colonies (white) were picked and plasmids were purified by Qiagen Mini Kit. Products were sequenced by T7 or SP6 primers at the CNIO Genomics Unit. Sequences were aligned and analyzed utilizing MultAlin program.

3.1.6 Subcutaneous and orthotopic allograft models

Immunodeficient NU-*Foxn1*^{nu} mice (females, 5-weeks-old) were purchased from Harlan Laboratories. Tumor ($0.5x10^6$) cells only or in combination with ($0.5x10^6$) CAFs or NPFs were injected in PBS:Matrigel (1:1) into dorsal flanks of the mice. Growth was measured every 3 days until humane end point. Orthotopic injection was performed by surgery under anesthesia (4% Isofluorane) utilizing the same number of cells for injection as in the subcutaneous model. Tumor growth was monitored by micro-ultrasound (Vevo 770, Visualsonics, Toronto, Canada). Mice were sacrificed 3-weeks-post-injection. Tumor volume was limited to 1,500 mm^3. Tumors were measured by caliper and calculated as Length x $Width^2/2$.

3.2 Isolation of cells – tissue culture

3.2.1 Generation of fibroblasts and tumor cells by outgrowth

Primary fibroblasts were isolated from fresh tissue samples collected from tumor-bearing KPeCY or WT mice. The tissue was minced by a sterile surgical blade and cells were incubated in collagenase P solution (1,5 μg/ml in Hank's Balanced Salt Solution, HBSS) solution for 30-60 minutes at 37°C. Cells were washed with 5% FBS-HBSS, centrifuged and plated in 6 cm Petri dish with DMEM+10% FBS and 1% Penicillin/Streptomycin. The following day, tissue pieces were removed and placed in a new Petri dish to avoid epithelial cell contamination of fibroblast cultures and tumor cells were allowed to growth out from tissue pieces. In the case of CAFs, differential trypsinization was used in order to eliminate remnant tumor cells. This method takes advantage of the faster attachment/detachment of fibroblasts compared to other cell types. Cells were washed with PBS, which was followed by trypsinizing the cells for 30 seconds at 37°C and seeding them to a separate culture plate. The second washing and trypsinization step (5 mins, 37°C) contained the tumor cells in higher proportion. Culture media was changed every 3 days.

3.2.2 Isolation by cell sorting

CAFs and tumor cells were obtained by mechanical dissociation of freshly dissected tumor tissue and digested in Collagenase solution (0,5 mg/ml Collagenase P – HBSS with 0,2 %BSA) for 30 min, at 37ºC shaking in a 250-ml flask. Then cells were washed and centrifuged in ice cold 5% FBS-HBSS washing buffer containing 0,01% DNase. After two steps of filtration (100 μm and 40 μm cell strainer), erythrocytes were lysed by 30s incubation with ACK lysis buffer (Lonza), and cells were resuspended in PBS containing 0.5% BSA and 2 mM EDTA. Before analysis, single cell suspensions were preincubated with purified anti-mouse CD16/32 antibodies (1:200; BD Pharmingen) for 15 min on ice to block nonspecific Fc receptor-mediated binding. Aliquots of $0{,}5\times10^6$ cells were stained for 30-45 min at room temperature with the following antibodies: APC anti-mouse CD31 (1:200, clone MEC 13.3, BD Biosciences), APC anti-mouse CD45 (1:200, clone 30-F11, BD Biosciences), FITC anti-mouse CD326 (EpCAM, 1:200, clone: G8.8, Biolegend), PE anti-mouse CD140a (PDGFRα, 1:100, clone: APA5, eBioscience). Samples were processed to Influx cell sorter (BD Pharmingen) and separated directly into Trizol (RNA isolation) or PBS (cell culture). Cells were plated in 6 cm Petri dishes and

cultured in DMEM+10%FBS. Primary cultures were expanded and frozen at passage 2 (P2). Çell lines were generated by serial passaging.

3.2.3 Tumor organoid – fibroblast co-cultures

Organoids were established from tumor tissues obtained from KPeCY mice at humane end point based on previously described protocol (216). Fibroblasts were plated ($1x10^5$) in 24 well glass bottom plates (Greiner Bio-One). Organoids were passed at 1:6 dilution from confluent 24 well plates. Organoids were co-cultured with fibroblast in basic media without factors (Advanced DMEM + Hepes + Glutamax) for 5 days. Images were acquired in a Leica DMI6000B wide field microscope (Leica Microsystems) equipped with a 5X NA, 0.15 dry objective and an incubator chamber at 37ºC and 5% of CO_2. Leica AF and Leica HCS-A software were used for the acquisition.

3.2.4 Wound healing and migration assay

To perform wound healing and migration assays $0,5x10^6$ cells were plated into 6-well cell culture plate. Cells were allowed to grow in 10% FBS containing DMEM medium to confluence into 6-well plates. Three vertical 1- mm wide scratches were made across the cell layer using a sterile pipette tip. After washing with PBS, serum free DMEM medium was added (217). Wound healing assays were acquired in a Leica DMI6000B wide field microscope (Leica Microsystems). Images were acquired with bright-field method every 10 minutes during 20 hours and were processed by Fiji software.

3.2.5 Lentiviral infection of cells

Lentiviral supernatants were prepared through transfection of HEK293T cells at 70%-80% confluence. Packaging plasmids pLP1 (1.95µg), pLP2 (1.3µg), pLP/VSVG (1.64µg) (Invitrogen) and the lentiviral shRNA sequence (5µg) were mixed and added to 40µl of Polyethylenimine (1mg/ml) and 500µl serum free DMEM. The mixture was vortexed for 5 seconds and incubated at RT for 15 minutes. HEK293T cells were transfected dropwise. Transfected cells were incubated at 37°C overnight. The following day, cells were placed at 32°C for 24-48 hours. Lentiviral supernatant was collected and filtered (0.45µm) into DMEM containing Polybrene (8µg/ml). Cells were infected at 50 % confluency. After infection cells were grown for 24 hours at 32°C followed by a growth period for additional 24 hours at 37°C. Subsequently, cells were selected with 2µg/ml puromycin for 1 week. For *Saa3* (TRCN0000100095, TRCN0000100248), *Lum*

(TRCN0000094640), *Has1* (TRCN0000028846) and *Mpp6* (TRCN0000361747) knockdown assays, cells were infected using lentiviral particles generated with Mission-shRNA plasmids (Sigma). Non-Target shRNA control vector (sh-Ctrl) was used as a negative control.

3.3 Gene expression profiling

3.3.1 RNA extraction from sorted cells

Total RNA was extracted from 5000-20000 cells directly sorted into 1 ml Trizol and the tubes were directly frozen on dry ice to avoid degradation of RNA. After thawing, samples were vortexed for 15 seconds and 200 µl of chloroform was added. To separate phases, samples were mixed thoroughly and let for 2 mins at RT followed by 10 mins of centrifugation at 4ºC, 12000 rpm. Next, aqueous phase was transferred carefully into a new tube and 1 volume of 70% ethanol was added. This tube already contained 1 µl of Glycogen and 3 µl of Linear Polyacrylamide (LPA) in order to enhance precipitation of the small amount of RNA. Samples were mixed and centrifuged at 13200 rpm at RT. Supernatant was aspirated using vacuum and samples were air-dried for 30-60 mins at RT. RNA clean-up was performed when necessary by Qiagen (see 3.10.1). RNA quality was measured by Bioanalyzer.

3.3.2 RNA sequencing, gene expression profiling and GSEA analysis

Poly-A pull-down was utilized to enrich mRNAs from total RNA samples (200 ng-1 µg per sample, RIN>8 required) and proceeded to library preparation by using Illumina TruSeq RNA prep kit. Libraries were then sequenced using Illumina HiSeq2000 at Columbia Genome Center. Samples were multiplexed in each lane, which yields targeted number of single-end/paired-end 100bp reads for each sample, as a fraction of 180 million reads for the whole lane. RTA (Illumina) was used for base calling and bcl2fastq (version 1.8.4) for converting BCL to fastq format, coupled with adaptor trimming. Reads were analyzed with the Next*presso* pipeline (218). Sequencing quality was checked with FastQC v0.11.0. Reads were aligned to the human genome (GRCh37/hg19) with TopHat-2.0.10 using Bowtie 1.0.0 (219) and Samtools 0.1.1.9 (220), allowing two mismatches and 20 multihits. Gene Set Enrichment Analysis was performed with GSEAPreranked (221), setting 1000 gene set permutations. Only those gene sets, with significant enrichment levels (FDR q-value < 0.25) were considered.

3.4 Imaging

3.4.1 Tumor monitoring by micro-ultrasound

Mice were anesthetized with 4% isoflurane (Braun Vetcare) in 100% oxygen at a rate of 1.5 liter/min. Hypothermia associated with anesthesia was avoided using a bed-heater. Abdominal hair was removed by depilation cream to prepare the examination area. Mice were screened for PDAC and tumors were measured with a micro-ultrasound system Vevo 770 (Visualsonics, Toronto, Canada) with an ultrasound transducer of 40 MHz (RMV704, Visualsonics, Toronto, Canada). PDAC size was calculated as Length x $Width^2/2$.

3.4.2 Imaging by contrast agent

Tumor perfusion and vascularization study was performed by administration of MicroMarker Contrast agent (VisualSonics). Gas filled bubbles surrounded by phospholipid monolayer were injected intraveniously directly before ultrasound measurements. Efficiency of contrast agent perfusion was measured within the tumor.

3.5 Treatments

Mice were treated twice a week with Gemcitabine (Gemzar) (100 mg/kg) or Saline IP, 100µl volume. Combination treatment of Gemcitabine and anti-VEGF monoclonal antibody B20 4.1.1 (5 mg/kg, Genentech) or macrophage depleting agent Clodronate (50 mg/kg, Clodronate Liposomes) were administered at the same time IP. Tumor growth was followed weekly by microultrasound. Mice were treated until humane end point to study survival.

3.6 Processing of mouse tissues

3.6.1 Necropsies

Necropsies were performed in the CNIO Pathology laboratory. Mice were euthanized in a CO_2 chamber, tissue samples were collected either in 10% buffered formalin, embedded in OCT and/or frozen to be sectioned at a later time on a microtome-cryostat or directly frozen in dry ice for extraction of protein, DNA or RNA. The Comparative Pathology Unit of CNIO processed all the formalin-fixed tissues samples.

3.6.2 Histology – Immunohistochemistry

For histological analyses, tissues were fixed in 10% buffered formalin and embedded in paraffin. Hematoxylin & Eosin (H&E) staining and IHC analyses were performed on 3 μm paraffin sections. For IHC, the following antibodies were used: anti-mouse CD31 (1:50, Abcam), anti-mouse F4/80 (1:20, ABD Serotec, CI: A3-1), anti-mouse CK19 (TROMA III, CNIO Monoclonal Antibody Unit), anti-mouse Ki67 (SP6, Master Diagnostica), GFP Mouse Monoclonal (1:500, Roche), anti-mouse Cleaved Caspase 3 (Asp 175) (1:750 Cell signaling, 9661), anti-mouse Phospho-Histone H3 (Ser10) (1:500, Millipore), anti-mouse CD3 (1:250, Santa Cruz Biotechnology, M20), anti-mouse MPO (1:1250, Dako, A0398), anti-mouse Pax5 (1:500, Santa Cruz Biotechnology, C-20). Digital images of immunostained slides were obtained at 40X magnification (0.12 μm/pixel) using a whole slide scanner (Mirax scan, Zeiss) fitted with a 40X/0.95 Plan Apochromat objective lens (Zeiss). Images were analyzed by ZEN2 software. At least 4 tumors were sectioned and one section was analyzed for quantification of each staining.

3.6.3 Immunofluorescence

CAFs and NPFs ($5x10^5$ cells/well) were plated in 24-well plates using BioCoat Poly-D-Lysin (Cellware) coverslips and allowed to grow for 24h. Tissue samples were sectioned (10μm) by Cryostat from OCT blocks. Samples were fixed in 4% paraformaldehyde (Electron Microscopy Sciences). Permeabilization was performed by 0.2% Triton X-100 solution. Primary antibodies including those elicited against αSMA (1:100, Biocare Medical), anti-mouse PDGFRα (CD140a, 1:100, clone: APA5, eBioscience) were incubated overnight at 4^0C followed by the addition of secondary antibody, Alexa Fluor 594 at 1:200 for 1h at room temperature, then Hoescht (Invitrogen) staining was applied. Sections were mounted with Mowiol. Captures were performed with a TCS SP5 confocal microscope (Leica Microsystems) equipped with a 20X NA, 0.7 dry, a 20X 0.7 multi-immersion and a 40X NA, 1.25 oil objectives. Leica AF software was used for acquiring and processing the images.

3.7 FACS analysis

Single cell preparation was performed as described above, otherwise cell were trypsinized and resuspended in PBS. Before analysis, cells were preincubated with purified anti-mouse CD16/32 antibodies (1:200; BD Pharmingen) for 15 min on ice to

block nonspecific Fc receptor-mediated binding. Cells were immunostained with APC-Cy7 anti-mouse αSMA (1:75, Abcore), PE anti-mouse CD140a (PDGFRα, 1:100, clone: APA5, eBioscience). For cancer stem cell (CSC), population PE anti-mouse CXCR4 (1:100, clone: 2B11, BD Biosciences), APC anti-mouse CD133 (1:100, clone:13A4, eBioscience) PE-Cy7 anti-mouse CD44 (1:100, clone: IM7), FITC anti-mouse CD326 (EpCAM, 1:200, clone: G8.8 Biolegend) were used. Monocyte/macrophage profiling: anti-mouse F4/80 (1:100, clone: BM8, eBioscience), anti-mouse PE-Cy7 CD11b (1:100, clone: M1-70, BD Biosciences), PerCP-Cy5.5 anti-mouse CD11c (1:100, clone: N418, eBioscience), anti-mouse CD206 PE (1:50, Serotec). Samples were processed on a FACS CANTO II flow cytometer (BD Pharmingen) and analyzed using FlowJo (Tree Star).

3.8 Western blot

3.8.1 Protein extraction

Cells were washed and collected in NP40 lysis buffer: 50mM Tris-HCl pH 7.4, 150mM NaCl, 0.5% NP40, and a freshly added cocktail of protease and phosphatase inhibitors (cOmplete Mini, Roche; Phosphatase Inhibitor Cocktail 2 and 3, Sigma-Aldrich). Samples were incubated on ice for 30 minutes and were centrifuged for 20 minutes at 13,000 rpm and 4ºC. Supernatant was transferred to a new tube and protein concentration was measured by Bradford reagent (Bio-Rad). Standard curve was prepared from 1mg/ml Bovine Serum Albumin (BSA). 2µl of the protein extract was added to 1ml of 1:4 Bradford reagent and the absorbance was read at 595nm by spectrophotometer. Standard curve was prepared from 1mg/ml Bovine Serum Albumin (BSA).

3.8.2 Blotting

Cell lysates (50µg) were mixed with 4X loading buffer and 10X reducing agent (Thermo Fisher Scientific). To denature protein, samples were boiled for 4 minutes at 95ºC. After spin down, they were loaded on 4-12% Nupage Bis-Tris gels (Thermo Fisher Scientific) and separated in MES 1X buffer (Thermo Fisher Scientific). 8µl of Spectra Multicolor Broad Range Protein Ladder (Thermo Fisher Scientific) was used for molecular weight reference. Nitrocellulose transfer membrane (GE Healthcare) and Whatman 3MM (Sigma- Aldrich) paper were sized to gel and prewet in transfer buffer (Tris-Glycine 1X, Lonza; Methanol 20%). A “transfer sandwich” was assembled in the following order: cathode, sponge, 3x Whatman paper, gel, nitrocellulose membrane 3x Whatman paper, sponge, anode. The gel was transferred for 60 minutes at a constant

current of 400 mA and maximum power on ice or at 4ºC. Afterwards, staining with Ponceau S solution (Sigma) was performed to check the efficiency of protein transfer. Membranes were blocked by incubation with 5% non-fat milk in TBST (1X Tris-Buffered Saline (TBS) solution; 0.1% of Tween-20) for 45 minutes at RT, shaking. Incubation with primary antibodies diluted in milk was performed overnight, 4ºC. The next day, the membranes were washed three times with 1X TBST buffer for 15 minutes on a shaking platform at RT. Next, blots were incubated for 1h with HRP (1:2000, Dako) labelled secondary antibodies. Protein visualization was done with chemiluminiscent system (ECL; Amersham, GE Healthcare). Membranes were blotted with antibodies against Lumican (1:2000, rabbit monoclonal, EPR8898, Abcam), and Gapdh (1:10000; Mouse monoclonal; Sigma-Aldrich G8795) for loading control.

3.9 Genotyping

Most of the genetic modifications were genotyped by Transnetyx (Cordoba, TN, USA). For *Saa3* alleles, PCR reaction was done as following. Genomic DNA was isolated from mouse tails, genotyping was performed by PCR. Each reaction contained: 1µl $MgCl_2$ (25mM), 2µl Taq-Polymerase Buffer 1X, 0.25µl dNTPs 10mM, 0.2µl BSA 10 mg/ml, 0.2µl Taq-Polymerase (5U/µl EcoTaq, Ecogen), 0.5µl of each of the primers (10µM, Sigma), 1µl of DNA filled up to 20µl of sterile water. The following primers were used for genotyping the Saa3 alleles:

Forward WT: 5-AAGCTCTCTCTGAAATGGTCCAG-3

Reverse WT: 5-TTTCTCCCATTGCTTTGTGCTAGGC-3

Reverse KO: 5-GTGGGAAGTGATTTTGCCATCAGCC-3

3.9.1 DNA extraction

At weaning, mouse tail was cut to extract genomic DNA. Cells were cultured, harvested and collected in pellets. Tissues and cells were incubated with a lysis buffer (20mM Tris-HCl pH 8.0, 100mM NaCl, 0.5% SDS, 10mM EDTA pH 8.0 and MilliQ H_2O) and 400µg/ml of proteinase K overnight at 55ºC. The next day, 300µl of saturated NaCl were added to the digested sample. After mixing vigorously by inversion, the mix was incubated on ice for 10 minutes. The samples were then centrifuged at 13,200 rpm for 10 minutes at 4ºC. The supernatant was transferred into a clean tube, and DNA was precipitated by adding 800µl of isopropanol. After mixing and incubating the solution for

at least 5 minutes at RT, the samples were centrifuged at 13,200 rpm for 30 minutes at 4ºC. The supernatant was discarded and the pellets were washed with 500µl of 70% ethanol. The samples were centrifuged again at 13,200 rpm for 5 minutes at 4ºC. Finally, the pellets were left to air dry. Dry pellets were resuspended in 100µl of sterile water.

3.9.2 General PCR reaction

Genomic DNA from mouse tails was used for genotyping by Polymerase Chain Reaction (PCR). Each reaction contained: 1µl $MgCl_2$ 25mM, 2µl Taq-Polymerase Buffer 1X, 0.25µl dNTPs 10mM, 0.2µl BSA 10 mg/ml, 0.1µl Taq-Polymerase (5U/µl EcoTaq, Ecogen), 0.75µl of each of the primers (10µM, Sigma), 1µl of DNA and up to 20µl of MilliQ H_2O. General PCR program used: denaturation at 94°C for 1 minute, followed by 35 cycles of denaturation at 94°C for 30 seconds, annealing at 60°C for 30 seconds and extension at 72°C for 30s, and a long extension at 72°C for 10 minutes as final step.

3.10 Quantitative Real Time – PCR (qRT-PCR)

3.10.1 RNA isolation

Total RNA was extracted from cultured cells or from frozen tissue by Qiagen RNeasy Mini Kit. Briefly, cells were washed with PBS and were collected with cell scraper in 600 ml of RLT buffer. Tissues were mechanically disrupted using zirconium beads in capped tubes and were centrifuged at 2000 rpm. This lysate was loaded on QiaShredder columns to eliminate cell aggregate remnants. Next, 1 volume of 70% ethanol in RNase free water was added, the lysate was mixed and loaded to RNeasy spin columns. Columns were centrifuged at 10,000 rpm for 30 seconds. The RNA bound to the membrane of the column was washed by 700 µl RW1 buffer and on-column DNA digestion was performed by RNase free DNase Set (Qiagen) for 15 mins.

3.10.2 cDNA synthesis and q – RT – PCR reaction

cDNA synthesis was performed by reverse-transcription of 1 µg RNA using Super Script II Reverse Transcriptase (Invitrogen) and random primers (Invitrogen) following the manufacturer's instructions. 20 µl cDNA reaction was diluted 1:5 in RNase free water and was ready to use. qRT-PCR assays were performed with a FAST7500 Real-Time PCR System using Power SYBR Green PCR Master Mix (Applied Biosystems) with the primers indicated below. Reaction was set up for 10 µl containing: 5 µl of SYBR Green

master mix; 0.25 µl of forward and reverse primers (10 µM); 2.7 µl RNase free water; and 1.8 µl cDNA. Triplicates were loaded for each reaction on 96 well plate. Data analysis was performed using ΔΔCT method (ΔΔCt = ΔCt sample – ΔCt reference). GAPDH was used for normalization.

Primers for *Saa1* amplification:

5-AGGAGACACCAGGATGAAGC-3 (forward)

5-GGAAAGCCTCGTGAACAAAT-3 (reverse)

Primers for *Saa2* amplification:

5-CCACAAGCCTCTCTCTGTGA-3 (forward)

5-AGTTCCCTGTTTCCATCGAC-3 (reverse)

Primers for *Saa3* amplification:

5-TGCCATCATTCTTTGCATCT-3 (forward)

5-AGTAGGCTCGCCACATGTCT-3 (reverse)

Primers for *CD68* amplification:

5-AGCCATTCAAGACAAAGCCT-3 (forward)

5-CAAGGTGAACAGCTGGAGAA-3 (reverse)

Primers for *CK19* amplification:

5-TGTCGACCTAGCCAAGATCC-3 (forward)

5-AAGGTAGGTGGCTTCAGCAT-3 (reverse)

Primers for *Vimentin* amplification:

5-CGGCTGCGAGAGAAATTGC-3 (forward)

5-CCACTTTCCGTTCAAGGTCAAG-3 (reverse)

Primers for *FAP* amplification:

5-TTTCCAGGCGATGTGGTACT-3 (forward)

5-ATGGTCCAAGTCGTCCATGT-3 (reverse)

Primers for *PDGFR*α amplification:

5-AGCCAGAAGTAGCGAGAAGC-3 (forward)

5-GGCAGTATTCCGTGATGATG-3 (reverse)

Primers for *Mpp6* amplification:

5-GATCTGGTAATCGCCCGAATC-3 (forward)

5-GGTGCCTCTCCATATTGACGTA-3 (reverse)

Primers for *GAPDH* amplification:

5-CGACTCAGATGTCCCTGGAT-3 (forward)

5-GCCTGTCCAAGCAATGAAAT-3 (reverse)

3.11 Human samples

Primary tumors were obtained from the Tumor Bank of the Hospital 'Virgen de la Arrixaca' Murcia, Spain (BIOBANC-MUR, B.0000859). Specific informed consent for tumor implantation in mice was obtained from all patients, and the study received the approval of the CNIO Ethics Committee.

DKFZ human PDAC dataset: a different set of primary tumors were used to isolate cell populations by cell sorting were obtained from PDAC patients at the University Hospital Heidelberg, Germany in collaboration with the German Cancer Research Center (DKFZ). The study was approved by the ethical committee of the University of Heidelberg and conducted in accordance with the Helsinki Declaration; written informed consent was obtained from all patients. Human PDAC-CAFs and normal fibroblasts were obtained from fresh primary PDAC specimens and adjacent normal pancreas by cell sorting: immunostained with FITC anti-human CD326 (EpCAM, 1:11, Clone: AC128, Miltenyi Biotec); VioBlue anti-human CD45 (1:11, Clone: 5B1, Miltenyi Biotec); APC anti-human CD31 (1:11, Clone: HEA-125, Miltenyi Biotec). Fibroblasts were defined as EpCAM-/CD45-/CD31- population.

3.12 Statistical Analysis

Data are mean ± SD except for FACS analysis where representative images were used. Significance between two groups was assessed by the Student's two-tailed *t*-test. Data sets consisting of more than 2 groups were analyzed by analysis of variance (ANOVA). The product limit method of Kaplan-Meier was used for generating the survival curves, which were compared by using the log-rank (Mantel-Cox) test. Difference of metastasis appearance between two groups was analyzed by Chi-square test. P values < 0.05 were considered to be statistically significant (*P < 0.05, **P<0.001 ***P < 0.001). All statistical analysis was performed using GraphPad Prism software.

4 Results

4.1 Targeting CAFs in PDAC

Pancreatic Ductal Adenocarcinoma is characterized by an abundant desmoplastic microenvironment that constitutes up to 90% of the total tumor volume. Around 80% of this stroma is composed (around 80%) of cancer-associated fibroblasts (CAFs), which produce massive amount of ECM components and are responsible for establishing physical and chemical barrier to chemotherapeutic drugs (222). Therefore, CAFs may represent attractive target in pancreatic cancer in combination with standard of care treatments. To better understand tumor stroma interactions generating the defense mechanism of pancreatic tumors we decided to study transcriptome profiles of CAFs and their role in PDAC development by using mouse models.

4.1.1 Characterization of stromal cell populations in PDAC mouse model

To explore the populations of CAFs present in PDAC, we used a GEM tumor model previously generated in our laboratory, the K-*Ras*$^{+/LSLG12Vgeo}$;*Trp53*$^{lox/lox}$;*Elas*-tTA/*tetO*-Cre compound strain, in which we can selectively induce the expression of a resident K-Ras^{G12V} oncogene and disable the Trp53 tumor suppressor in acinar cells during late embryonic development (92). We added a *Rosa26*^{LSLEYFP} allele in order to have a color marker (EYFP) to identify those cells carrying the tumor initiating mutations: expression of the K-*Ras*^{G12V} oncogene and loss of *p53*. These mice, designated as KPeCY, develop PDAC tumors with complete penetrance and a latency of 3-4 months. More importantly, they recapitulate the human disease including the formation of a massive stromal desmoplasia made up of heterogeneous CAF populations.

Interestingly, analysis of stromal tissue with antibodies elicited against αSMA and PDGFRα, a marker associated with inflammation (140), revealed that whereas most fibroblastic stromal cells of KPeCY tumors expressed αSMA, only a fraction contained PDGFRα (Fig 8*A*). FACS analysis of fresh tumors showed at least four distinct populations of fibroblast cells (Fig 8*B*). Whereas one population only expressed αSMA (39% of the total), other population, representing 36% of the cells, contained both markers, (αSMA and PDGFRα). We also identified two additional populations represented by those cells that only expressed PDGFRα (9%) and those that did not express either marker or expressed them at very low levels (16%) (Fig 8*B*).

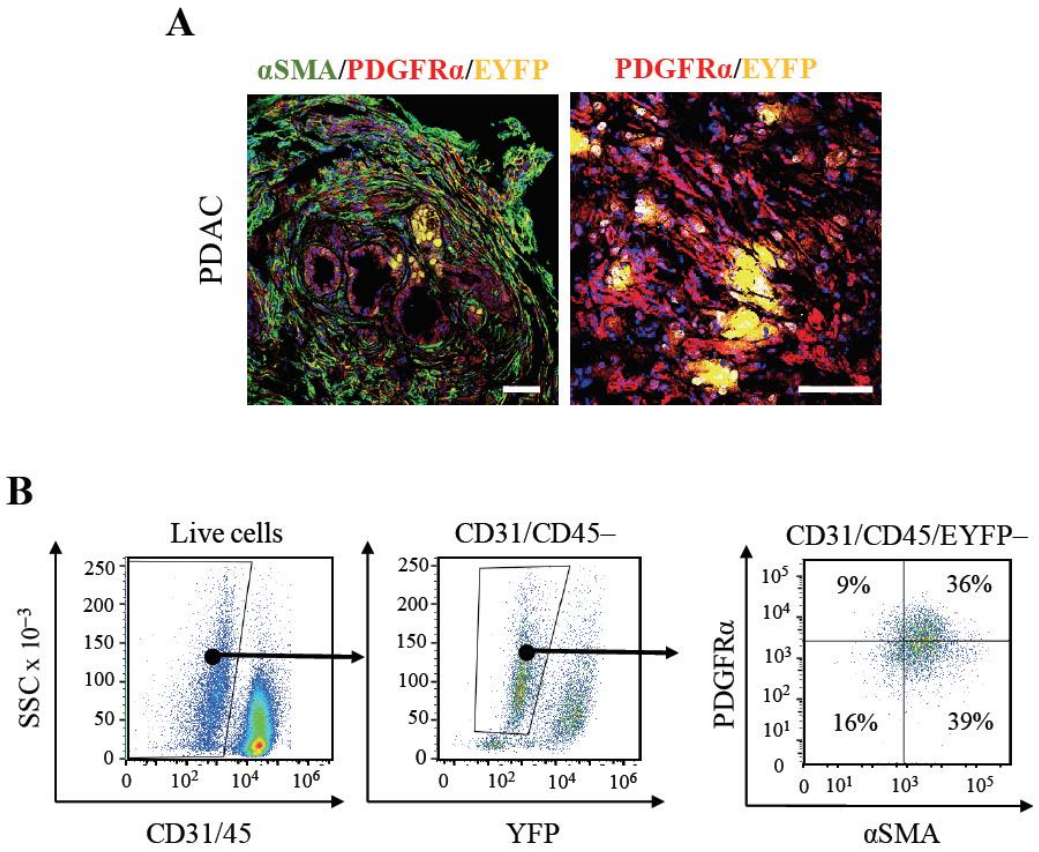

Figure 8. Immunofluorescence and FACS analysis of CAFs. *(A) (Left)* Immunofluorescence staining with anti-αSMA (green) and anti-PDGFRα (red) antibodies and with EYFP (yellow) of a KPeCY PDAC tumor. *(Right)* Higher magnification of PDGFRα (red) and EYFP (yellow) positive cells. Scale bars, 100 μm. *(B) (Left)* FACS analysis of fresh tumor samples with CD31/CD45 and EYFP markers. *(Right)* FACS analysis of CD31/CD45/EYFP negative cells with anti-αSMA and anti-PDGFRα antibodies. The percentages of αSMA and PDGFRα single positive cells as well as αSMA/PDGFRα double negative and double positive cells are indicated.

4.1.2 Isolation of CAFs from PDAC and NPFs from normal pancreas

Several methods were used previously to isolate fibroblasts from different tumor types and from normal tissues (155, 157, 223). In order to establish an efficient way to separate fibroblasts and to compare distinct populations we isolated stromal cells by two methods.

4.1.2.1 Fibroblast isolation by "outgrowth"

First, we isolated CAFs and normal pancreatic fibroblasts (NPFs) by "outgrowth method" [(155), section 1.3.1], where all types of cells are allowed to grow out from

tissue pieces and attach to the culture plate. However, separation of a mixed cell population needs to be addressed afterwards. We used differential trypsinization to obtain pure fibroblast population. This method takes advantage of the faster detachment of fibroblasts compared to epithelial cells upon trypsinization. Purity was verified by the expression of fibroblast-specific genes (Vimentin, PDGFRα and αSMA) qPCR and immunofluorescence and the lack of tumor and immune cell markers Cytokeratin 19 (CK19), CD45, CD68, F4/80 respectively analyzed by qPCR.

This method is simple and fast but has important disadvantages: the culture is a mixture of populations and CAFs adapt to the plate, resulting in expression pattern alterations and can influence target identification. To bypass this issue, we selected a more physiological isolation method.

4.1.2.2 Fibroblast isolation by cell sorting using PDGFRα

We isolated CAFs by FACS. For this method, it is essential to use cell surface specific markers. We selected a subset of fibroblasts by the cell surface marker PDGFRα+. We sorted PDGFRα+/EYFP-/CD45-/CD31- stromal cells from PDAC tumors of KPeCY mice as well as from normal pancreata of control *Elas*-tTA/*tetO*-Cre;*Rosa26*$^{+/LSLEYFP}$ animals (Fig 9*A* and *B*). These cells represented 21% and 15% respectively, of the EYFP-/CD45-/CD31- population and were subjected to direct RNA isolation with the aim of performing RNAseq analysis. We also established primary cells in culture and cell lines for *in vitro* studies. These cultured cells retained αSMA and PDGFRα expression and displayed the spindle shape characteristic of fibroblasts, at least until 30 passages (Fig 9*C, D*). The fibroblastic nature of these cells was further verified by the expression of fibroblast-specific genes including FAP, Vimentin, PDGFRβ, as well as by the lack of immune (CD45, CD68) and tumor (CK19, EpCAM) cell markers (Fig 9*B* and *E*). These results show that this cell population does not contain tumor or immune cells. In addition, we considered these fibroblasts sorted from tumors as CAFs and cells sorted from normal pancreas as NPFs. Altogether, these results indicate that the PDGFRα+ stromal cells isolated from KPeCY tumors represent CAFs whereas those obtained from normal pancreata represent NPFs. The latter had slightly higher levels of αSMA than CAFs, a property that has been proposed to represent a marker of myo-fibroblast activation (Fig 9*D*) (127).

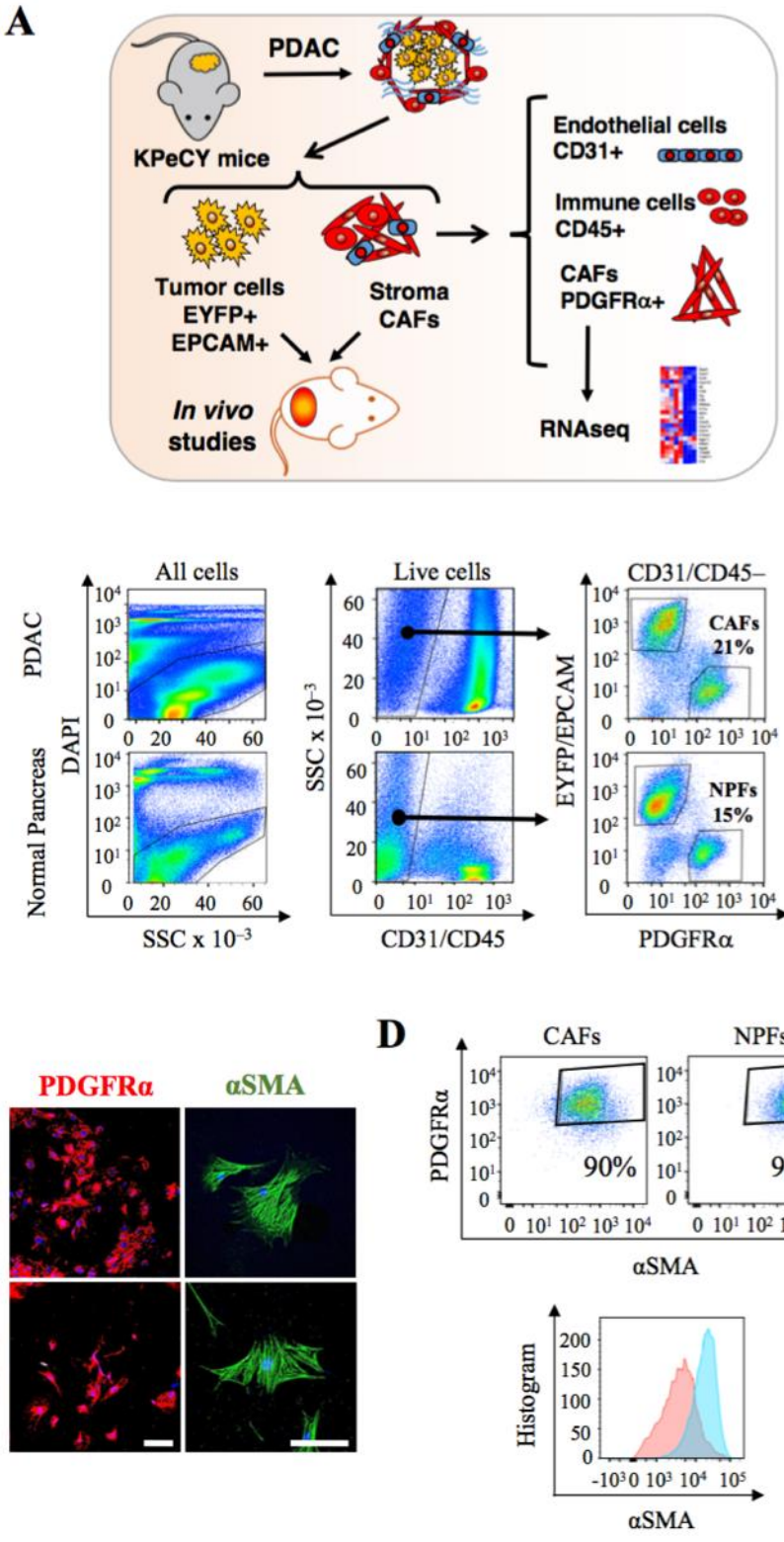
A
PDAC
KPeCY mice
Tumor cells
EYFP+
EPCAM+
Stroma
CAFs
In vivo
studies
Endothelial cells
CD31+
Immune cells
CD45+
CAFs
PDGFRα+
RNAseq
B
All cells
Live cells
CD31/CD45–
PDAC
Normal Pancreas
DAPI
SSC x 10⁻³
CD31/CD45
EYFP/EPCAM
PDGFRα
CAFs
21%
NPFs
15%
C
PDGFRα
αSMA
CAFs
NPFs
D
CAFs
NPFs
PDGFRα
90%
98%
αSMA
Histogram
αSMA

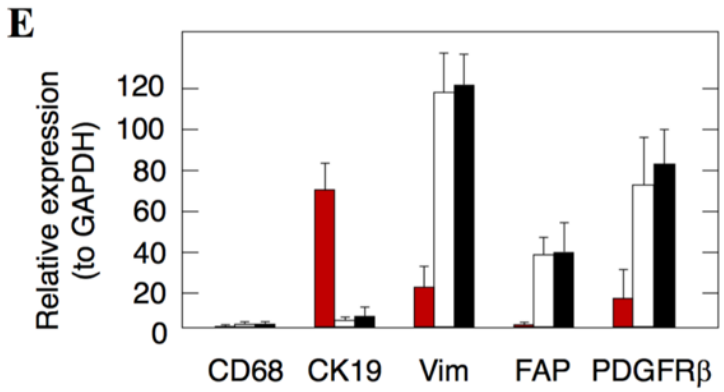

Figure 9. FACS isolation and verification of PDGFRα+ CAFs and NPFs. *(A)* Schematic diagram of the strategy followed in this study to sort the different cell populations from GEM PDAC tumors. Immune cells were separated by CD45 expression, endothelial cells by CD31 staining, tumor cells by the EYFP marker and EPCAM-FITC staining and CAFs by PDGFRα expression. Cells were used for cell culture, RNAseq and in vivo tumor growth studies. *(B)* Cell sorting of KPeCY PDAC tumors and normal pancreata from control mice selected with DAPI, anti-CD31 and CD45, anti-EPCAM, and anti–PDGFRα and EYFP. The percentages of NPFs and CAFs are indicated. *(C)* Immunofluorescence staining of sorted CAFs and NPFs after expansion in culture with anti-αSMA (green) and anti-PDGFRα (red) antibodies. Scale bars, 50 μm. *(D) (Upper)* A representative FACS analysis of αSMA/PDGFRα co-expression in CAF and NPF cells. *(Lower)* FACS histogram representing the αSMA expression intensity in CAFs (red) and NPFs (blue). *(E)* Expression levels of CD68 (immune cell marker), CK19 (tumor cell marker); and Vimentin (Vim), FAP and PDGFRα (fibroblast markers) analyzed by qPCR (relative to GAPDH expression) in tumor cells (red bars), NPFs (open bars) and CAFs (solid bars).

4.1.2.3 Tumor promoting PDGFRα+ CAFs and tumor suppressing PDGFRα+ NPFs

It was described by several groups that CAFs display pro- and anti-tumorigenic properties (130, 173). To determine whether PDGFRα+ CAFs can promote tumorigenesis, we compared their tumor supporting capabilities with those of NPFs using *in vivo* assays. EYFP+ sorted PDAC tumor cells ($0.5x10^6$) isolated from tumor-bearing KPeCY mice were subcutaneously inoculated alone or in combination with CAFs ($0.5x10^6$) or NPFs ($0.5x10^6$) into the flanks of immunocompromised mice. Whereas CAFs stimulated tumor growth by as much as 75%, NPFs inhibited the proliferation of

the pancreatic tumor cells by as much as 65% (Fig 10). These results illustrate the pro-tumorigenic activity of the PDGFRα+ subpopulation of CAFs used in this study.

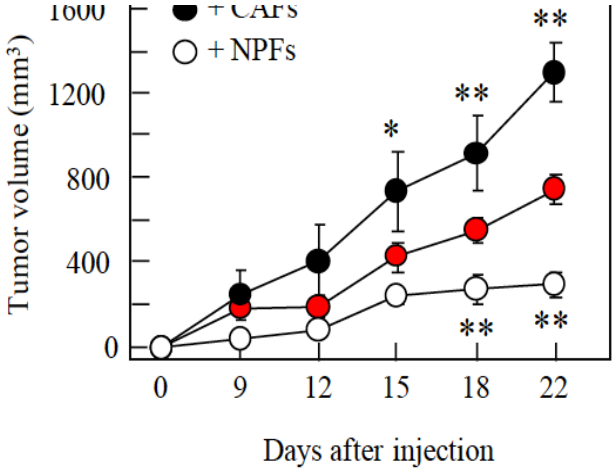

Figure 10. Pro- and anti-tumorigenic fibroblasts in a subcutaneous mouse model. Growth of PDAC tumor cells (0.5 x 10^6) injected subcutaneously in immunocompromised mice either alone (red circles) or co-injected with the same amount of CAFs (solid circles) or NPFs (open circles) (*P < 0.05, **P<0.001).

4.1.2.4 Comparative transcriptional profiling of CAFs versus NPFs

Understanding the biology and the molecular pattern changes of heterogeneous CAF populations is increasingly important in order to develop efficient therapies targeting the stroma in PDAC. In this thesis work, we compared transcriptome profiles of distinct CAF populations isolated by two different methods.

4.1.2.4.1 Gene expression profiling of fibroblasts from "outgrowth"

To better characterize the cells isolated by outgrowth from normal (WT) pancreas and PDACs we performed RNA sequencing (RNAseq) of NPFs (n = 3) and CAFs (n = 3). It is important to take into consideration that these cells were cultured *in vitro* at least for 2 weeks, time that could presumably alter their gene expression profiles compared to freshly isolated cells.

To broaden our understanding of general CAF characteristics, first, we performed a pathway analysis comparing CAF to NPF expression patterns. Gene Set Enrichment Analysis (GSEA) revealed significantly increased activity in the Complement Cascade, Toll-like receptor and NFκB signaling, as well as upregulation of Cytokine-Receptor Interaction (Fig 11*A*) suggesting highly elevated innate immune response. On the other

hand, we observed downregulation of genes from Cell cycle and Vascular smooth muscle contraction gene sets in CAFs compared to NPFs (Fig 11*A*).

Differential expression study demonstrated a high number of differentially regulated genes (n = 730). Among the top upregulated genes (Fig 11*B*), there were Serum Amyloid A3 (Saa3, log2 fold change = 7,42), Haptoglobin (Hp, log2 fold change = 6,51) and Apolipoprotein B (Apob, log2 fold change = 6,50). These three genes are associated with 'Acute phase response', suggesting a key role of this complex pathway in CAF reprogramming.

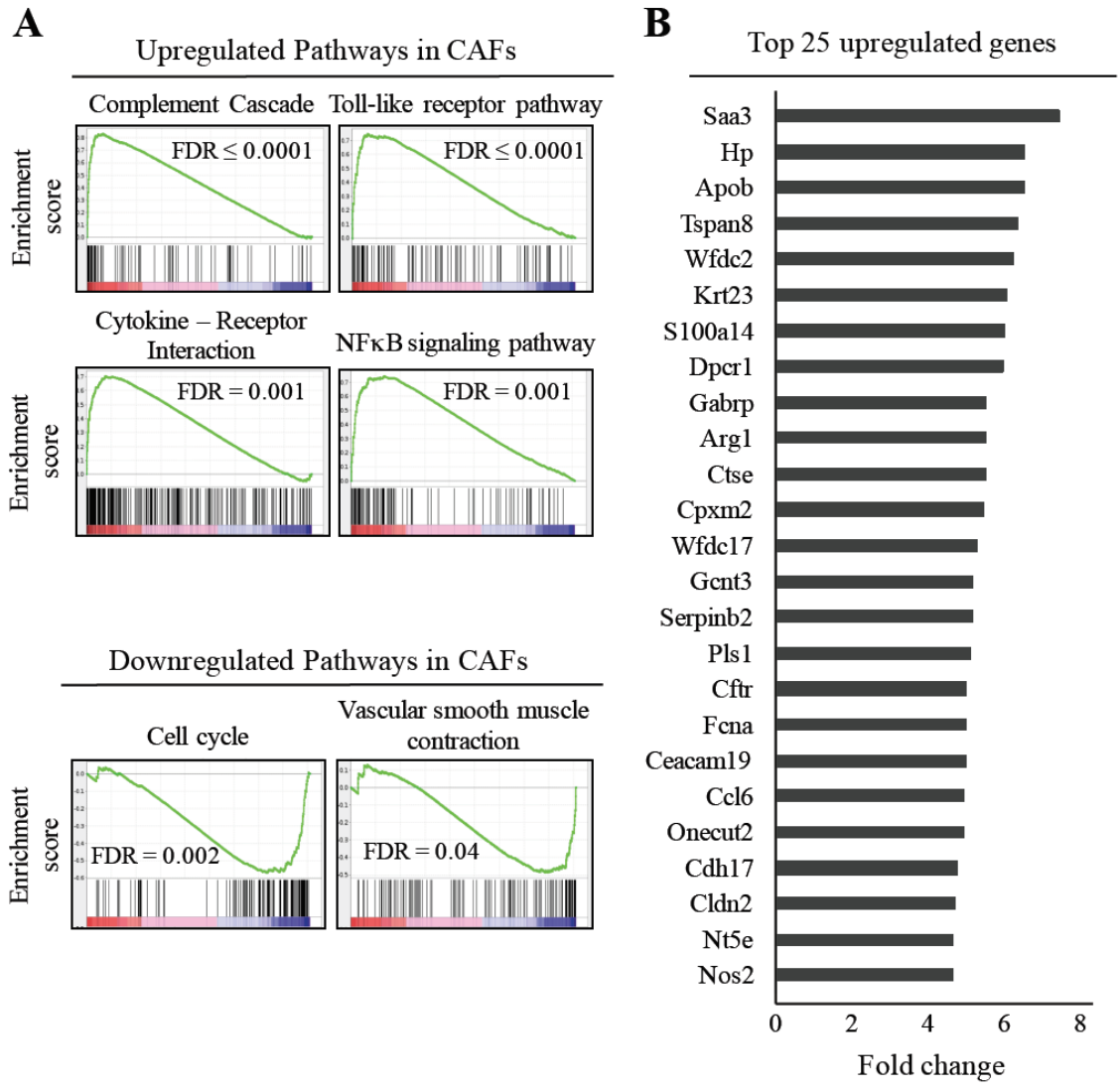

Figure 11. Transcriptional profiling of CAFs by "outgrowth". *(A)* GSEA pathway analysis of CAFs compared to NPFs isolated by outgrowth. *(B)* Top 25 upregulated genes identified in CAFs compared to NPFs.

4.1.2.4.2 Gene expression profiling of PDGFRα+ CAFs and NPFs isolated by cell sorting

To understand the molecular bases responsible for the tumor-promoting activity of PDGFRα+ CAFs compared to the PDGFRα+ NPFs, we performed a comparative study of the transcriptome profiles of freshly isolated CAFs (n = 5) with those of NPFs (n = 3) by RNA sequencing analysis. As illustrated in Figure 12*A*, CAFs displayed a strong inflammatory profile, in which many of the top upregulated genes included those encoding cytokines, such as *Il1ß* and *Il6*, chemokines like *Cxcl1* and *Ccl22*, as well as other interleukins and TNF family members related to the innate immune response. Furthermore, Gene Set Enrichment Analysis (GSEA) confirmed the upregulation of the immune cell recruiting Complement Cascade, IL-1R signaling, and JAK-STAT pathways in CAFs. This analysis also identified the Cytokine/Receptor signaling as one of the most significantly upregulated pathways in CAFs compared to NPFs (Fig 12*B* and *C*). In addition, we observed a high enrichment in cell-to-cell junction pathways suggesting the presence of active contact-mediated signaling in CAFs (Fig 12*B* and *C*), a property that may have an important role in tumor promotion (224). CAFs also displayed upregulation of TGF-ß and Hedgehog signaling pathways as well as ECM/Receptor interactions (Fig 12*C*), a set of transcriptional changes thought to result from their crosstalk with the tumor cells (151, 170).

Downregulated hallmarks included Oxidative Phosphorylation suggesting that CAFs have undergone a metabolic reprogramming and oxidative stress (Fig 12*C*). The latter was further supported by significant downregulation of genes involved in Peptide Elongation, Translation and Protein Metabolism, hallmarks of stress responses indicating mitochondrial dysfunction. We also observed a significant reduction of P53 signaling-related genes, suggesting cell death evasion (148, 225). These results, taken together, support the concept that the CAFs used in this study possess a unique secretory-inflammatory gene signature with emphasis in the activation of the innate immune response (Fig 12) as well as impaired oxidative phosphorylation (Fig 12*C*).

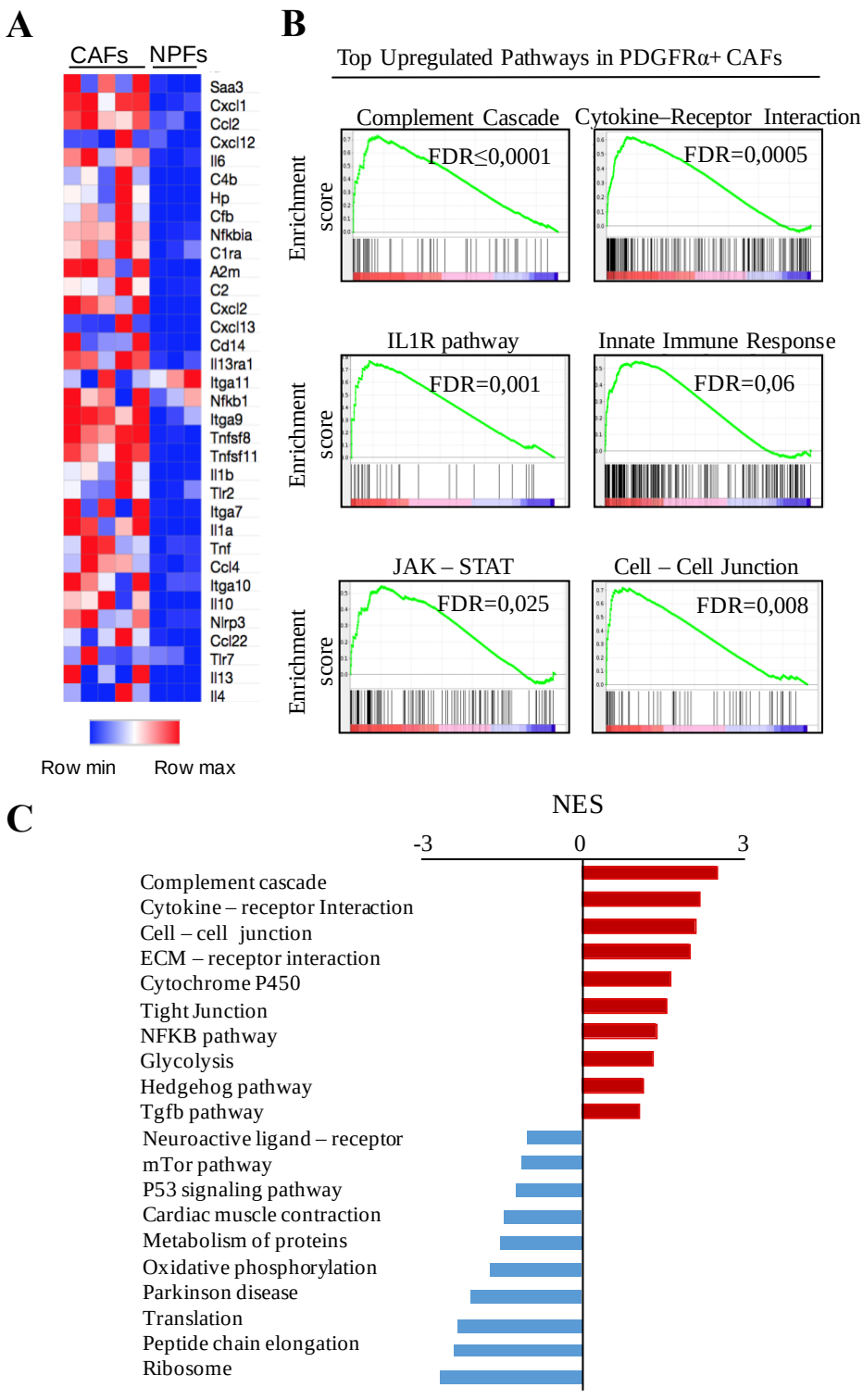

Figure 12. Transcriptional profiling of PDGFRα+ CAFs. *(A)* Heat map representing color-coded expression levels of differentially expressed inflammatory genes in CAFs (n = 5) versus NPFs (n = 3). *(B)* GSEA gene set enrichment analysis of CAFs: significantly upregulated inflammatory and cell adhesion pathways (FDR: False Discovery Rate). *(C)*

GSEA pathway analysis illustrating 10 significantly up- and downregulated pathways in CAFs. The Normalized Enrichment Score (NES) ranking was generated by the GSEA.

4.1.2.4.3 Target selection and validation

Comparison of gene expression profiling data of fibroblasts isolated by either outgrowth or by cell sorting led us to a list of differentially regulated genes. The difference in expression patterns is mainly due to the CAF isolation method and to the nature of the isolated populations (pool of CAFs vs. PDGFRα+ population). We found 488 genes significantly upregulated in CAFs compared to NPFs isolated by the outgrowth method and 297 genes upregulated in PDGFRα+ CAFs isolated by FACS. Only 117 genes were found in both groups, including Saa3 as the top overexpressed gene (Fig 13*A*). On the other hand, downregulated genes were present in a lower number, however in PDGFRα+ population up- and downregulated genes were distributed more evenly compared to the one isolated by outgrowth (Fig 13*B*). PDGFRα+ CAFs displayed 165 genes downregulated, whilst the other group had only 80, where 27 was shared (Fig 13*B*).

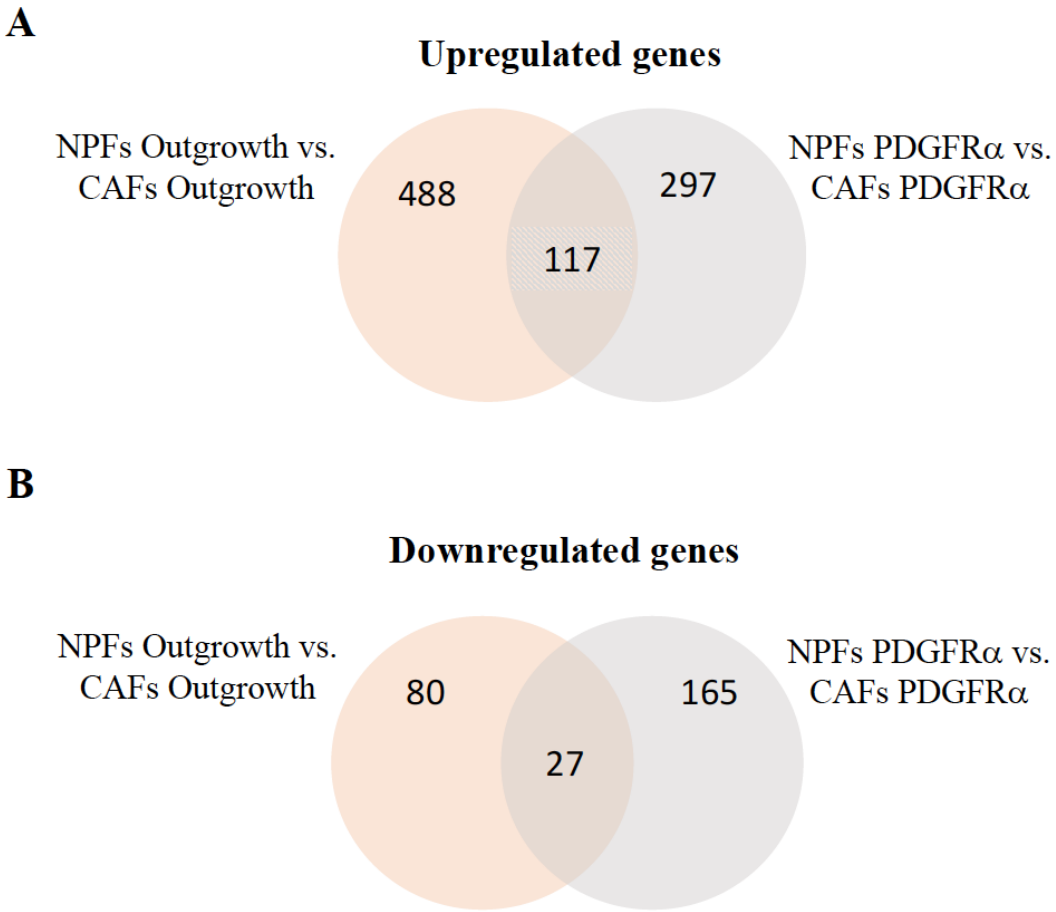

Figure 13. Differentially regulated gene comparison in distinct CAF populations. *(A)* Venn diagram of upregulated genes shared by CAFs compared to NPFs isolated by distinct methods: outgrowth or sorted by PDGFRα. *(B)* Venn diagram of downregulated genes in common between the two CAF populations.

Pharmacologically, targeting overexpressed proteins by inhibiting their function is more feasible than to increase the activity of downregulated genes. Therefore, to select potentially "druggable" targets we considered the upregulated genes. We identified 117 commonly overexpressed genes in both CAF populations and submitted for Gene Ontology analysis (GO). Interestingly, the majority of the encoded proteins are secreted proteins (n = 48) and membrane-associated proteins (n = 27) (Fig 14*A*). To further characterize these genes, we annotated them to GO terms by molecular function, where more than 50% presented cytokine, chemokine or growth factor activity followed by groups enriched in receptor or protein binding (Fig 14*B*).

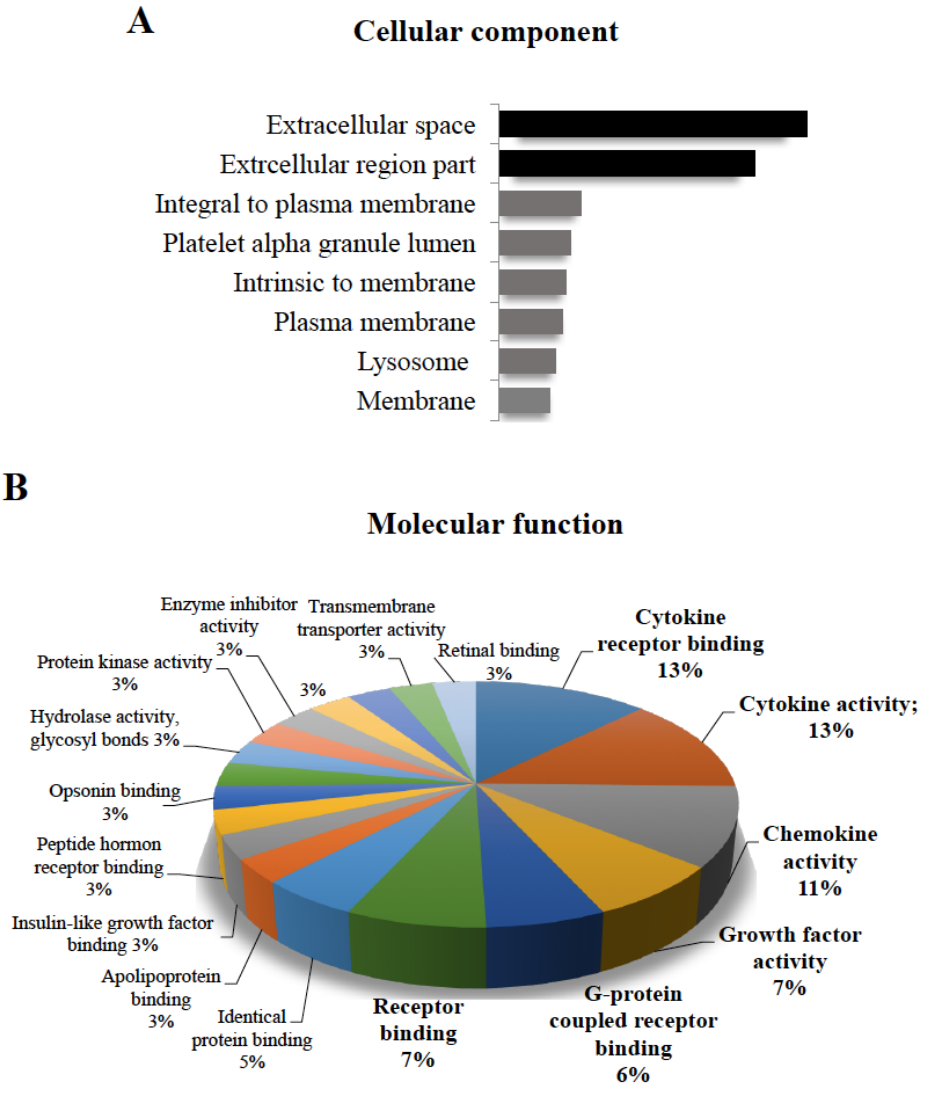

Figure 14. Molecular function of target candidates. *(A)* Gene Ontology study of the 117 commonly overexpressed genes in CAFs grouped by cellular component. *(B)* Gene annotations at molecular level by functions.

4.1.2.4.4 Validation of RNAseq results by quantitative RT-PCR

Next, we selected potential targets from the list of 117 commonly overexpressed genes for validation at RNA level by quantitative RT-PCR. Gene expression was validated in PDGFRα+ NPFs, PDGFRα+ CAFs and tumor cell samples isolated by cell sorting. Only secreted, extracellular or membrane proteins were considered with a putative role in CAF – tumor cell cross talk.

A

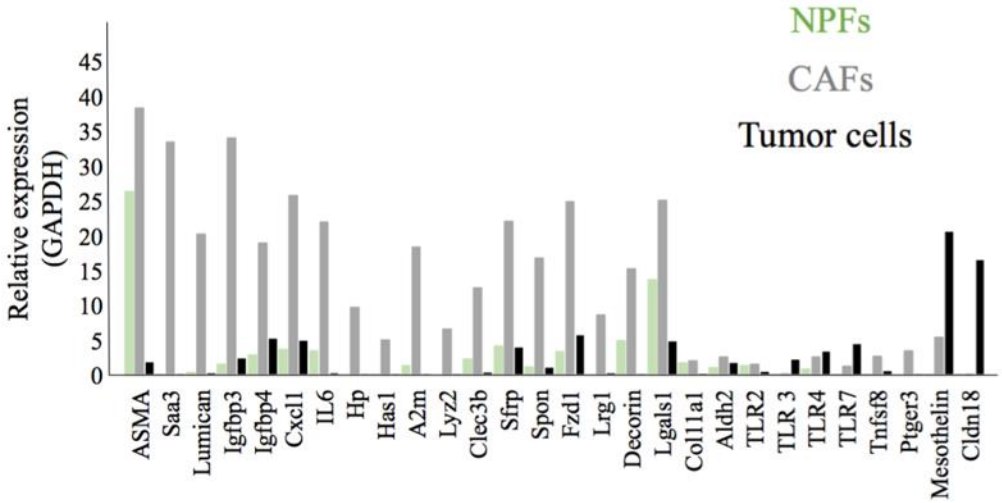

B

NPFs \ CAFs		Expression: High	Expression: Low
Expression	No	Saa3, Lum	Msln, Tnfsf8, Ptger3
	Low	Igfbp 3/4, Cxcl1, IL6, Hp, Has1, A2m, Lyz2, Clec3b, Sfrp, Spon, Fzd1	Igf2, Lrg1, Chi3l, Aldh2
	high	Dcn, Cfh, Thbd, Lgals1	Arg1, Itga11, Hpse, Col11a1

Figure 15. Target validation and selection. *(A)* qRT-PCR validation of RNA seq gene expression results in PDGFRα+ NPFs (green) and CAFs (grey), as well as tumor cells. *(B)* Table of selected candidate genes. Expression values are divided in No/Low/High in the case of NPFs and into High/Low in CAFs.

Taken all together after verifying the expression by qRT-PCR we defined the following criteria for target selection and further validation:

- Secreted or membrane protein – 'druggability'.
- Significant overexpression in CAFs compared to NPFs.
- No or low expression in NPFs on order to avoid toxicity upon therapeutic inhibition.
- Functional relevance in tumor development.
- Strategic tools for functional studies (available antibodies).
- Information of viability of germline knock-out mouse models.
- Relevance to human disease: expression in human PDAC.

Among the overexpressed targets, Saa3 presented the highest expression in CAFs with almost no expression in NPFs suggesting no harmful effect on normal homeostasis upon inhibition. In addition, based on the above criteria and on literature evidence of functional relevance *Lumican* (*Lum*), *Haptoglobin* (*Hp*) and *Hyaluronic acid synthase 1* (*Has1*), as well as *Mesothelin* (*Msln*) were selected for further functional validation and *in vivo* characterization. Saa3 and Haptoglobin are acute phase proteins and are associated with chronic inflammation (175, 226). Lumican and Has1 have an important role in ECM remodeling. Lumican overexpression in tumor cells was associated with better prognosis, however stromal expression was correlated with significantly worse survival, invasiveness and metastasis (227). Has1 is responsible for hyaluronic acid production, the matrix component that defines structure and physical properties of the stroma, as well as for regulation of inflammatory processes (163, 228). Mesothelin is a tumor differentiation antigen and is proposed as a reliable marker of pancreatic cancer (22), yet its function has not been addressed properly.

From this point onwards, all experiments were performed only in fibroblasts isolated by cell sorting, selected by PDGFRα and will be referred as CAFs and NPFs.

4.1.3 *In vivo* functional validation – mouse models

4.1.3.1 Subcutaneous allograft models

To functionally validate the selected targets, we decided to use an *in vivo* system by injecting tumor cells alongside with CAFs subcutaneously into the flanks of nude mice and monitor tumor growth as previously shown (Fig 10). In order to address the effect of the target genes in CAFs on tumor growth we used RNA interference to knock-down the

selected gene's activity. CAFs were infected with 'shTarget' or 'shControl' containing virus, knock-down efficiency was measured by qRT-PCR (Fig 16*A* and *B*). However, since we couldn't obtain a 100% downregulation, the most efficient sequence was used to perform co-injection experiments.

As depicted on Figure 16, tumor cells ($0.5x10^6$) inoculated with CAFs treated with non-target shRNA control ($0,5x10^6$) favored tumor growth and increased tumor size by 75% compared to tumor cells alone. While knock-down of *Has1* in CAFs resulted in reduced tumor growth compared to CAFs treated with control shRNA, however these differences were not significant (Fig 16*C*). Similarly, downregulation of *Lum* decreased tumor size in a non-significant manner. Finally, *Saa3* knock-down caused the highest reduction of tumor cell growth (Fig 16*C*). These results indicate that each of these three genes (*Lum*, *Has1* and *Saa3*) have a functional role in PDAC promotion and suggest that a significant reduction in tumor size could be obtained by achieving a complete elimination of any of these targets.

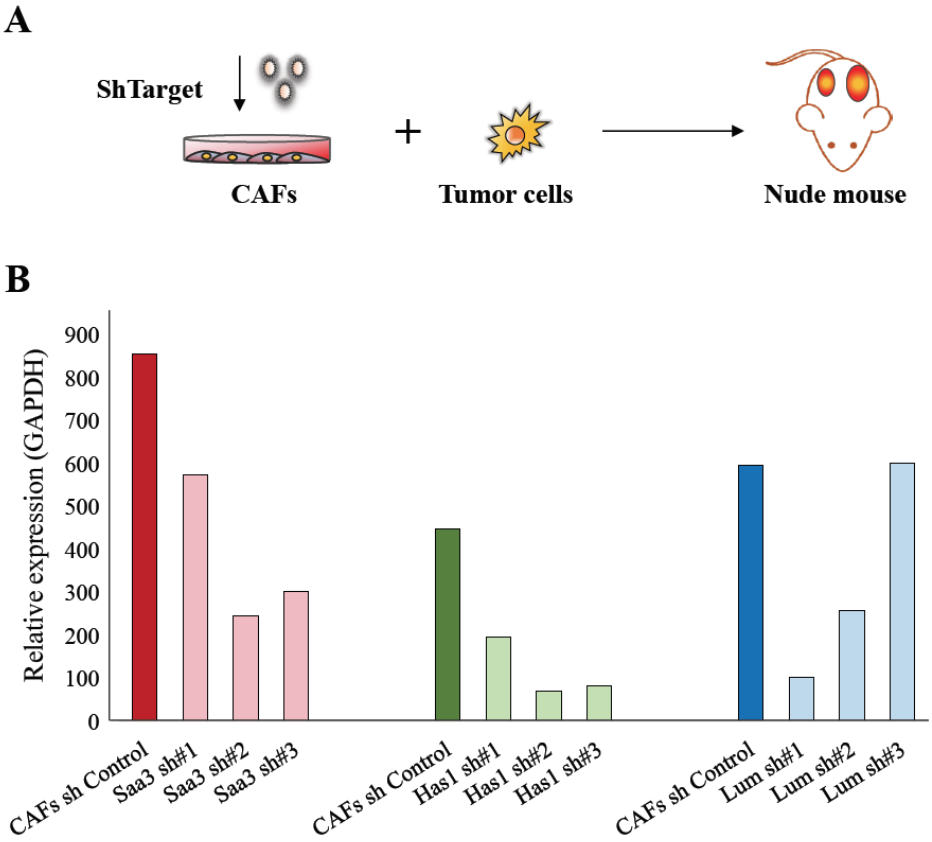

C

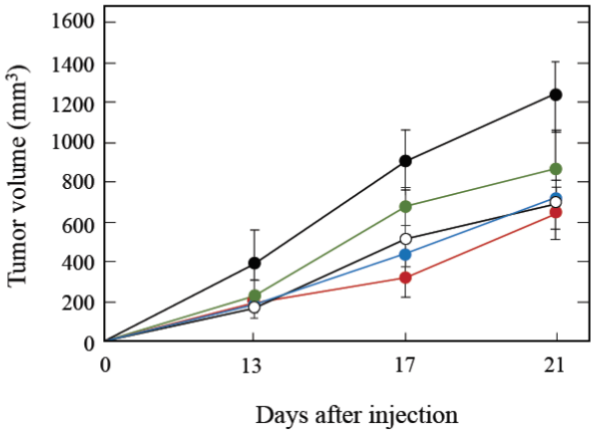

Figure 16. *In vivo* target validation by shRNA mediated gene silencing. *(A)* Scheme of experimental design of in vivo functional target validation. CAFs were treated with shRNA against the specified 'Target' and co-injected with tumor cells into the flanks of nude mice. *(B)* shRNA knock down efficiency for each target measured by qRT-PCR. *(C)* Tumor growth curve of tumor cells co-injected with CAFs subcutaneously into the flanks of nude mice. Tumor size was monitored during the experimental period (3 weeks). CAFs were treated with shRNA sequences against the different targets or a control shRNA. Combinations with tumor cells are indicated on the graph by colors: shControl CAFs (black) (n = 5), sh Has1 CAFs (blue) (n = 3), sh Lum CAFs (green) (n = 4), shSaa3 CAFs (red) (n = 4), only tumor cells (grey).

4.1.3.2 Generation of mouse models to study the role of the targets in PDAC

Given the results obtained with the knock-down experiments in nude mice we decided to further validate these target genes in vivo in our PDAC mouse model. Therefore, we selected *Saa3*, *Lumican*, *Has1* and additionally two other genes from our target list encoding secreted proteins: Mesothelin and Haptoglobin, both elevated in human PDAC development and described as potential biomarkers (229).

Viable knockout mouse models were generated previously for all these genes (209, 230–232) with a few phenotypic changes. *Lum null* mice displayed fragile skin, corneal opacification and disorganized dermal connective tissue with abnormal collagen fibril assembly (232). *Has1* and *Msln* knockout mice are viable with no particular phenotypic changes (231, 233). *Hp null* mice had a small reduction in postnatal viability and impaired tissue regeneration properties (230). Saa3 knockout mice were generated and cryopreserved sperm was available in the KOMP repository (see section 3.3.2.). For the

other four genes, we decided to use a novel and fast approach to obtain germline KO and developed mouse models by CRISPR gene editing technology. (see section 3.3.4.).

4.1.3.3 Generation of mouse models by CRISPR targeting the stroma

4.1.3.3.1 Single guided RNA design and validation in CAF cell lines

First, we designed guide RNA sequences targeting the first coding exons (Fig 17*A*) of each candidate gene in order to generate an early stop codon in the protein coding sequence upon activation of the Cas9 protein, taking advantage of the cells own DNA repair mechanisms, such as Non-Homologous End Joining (NHEJ). We validated the guide RNAs *in vitro* by transferring them to CAFs utilizing a dual lentiviral vector system. Mutations induced by the target sgRNA and the Cas9 protein were confirmed at DNA level by T7 endonuclease assay and Sanger sequencing. First, we performed T7 endonuclease assay on PCR products generated in the region of the target sgRNA. This method uses enzymes that cleave heteroduplex DNA at mismatches and extrahelical loops formed by single or multiple nucleotides. Figure 17*B* displays the detection and verification of one mutation induced by Lumican sgRNA. Mutated samples were further analyzed by subcloning and Sanger-sequencing the DNA fragments (Fig 17*B*). Several mutational events were observed: insertions, deletions (*indels*) with each sgRNA. Indels, that induced frame shift mutation and thereby prevented the gene from translation into functional protein (Fig 17*C*), were selected for validation at protein level (Fig 17*D*) and for further experimental procedures. We repeated the same process with other genes: *Has1*, *Hp* and *Msln*.

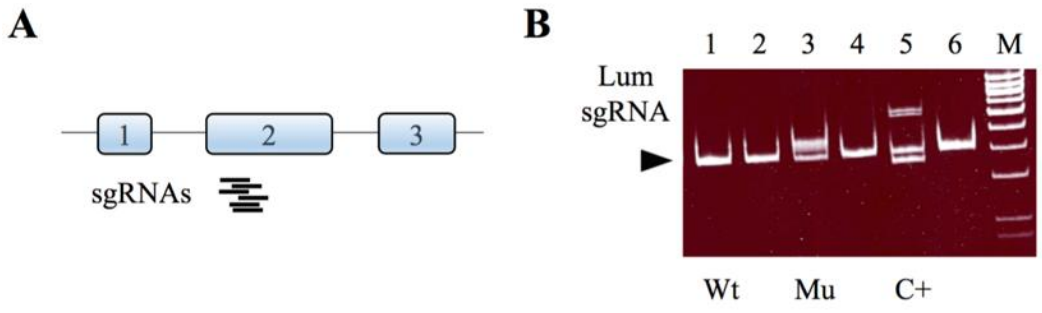

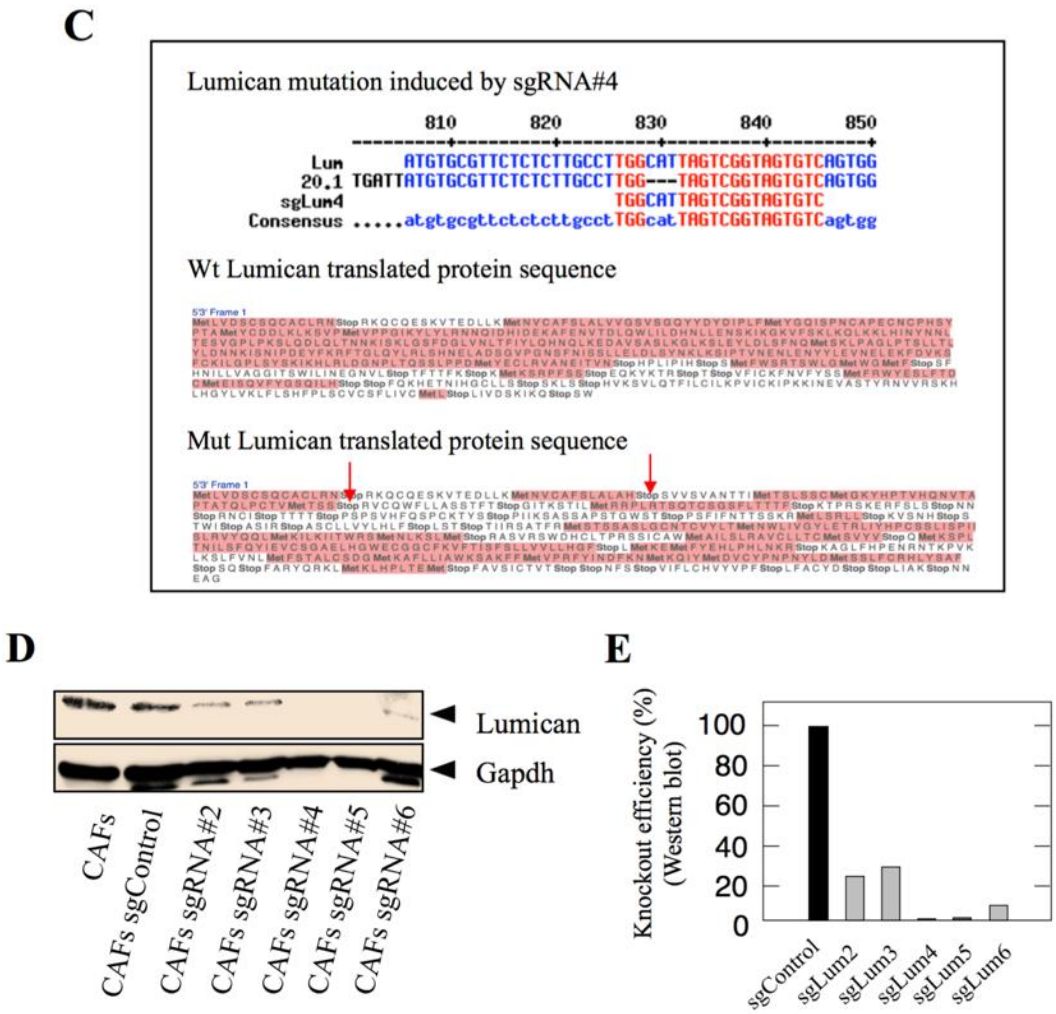

Figure 17. sgRNA design and validation of Lumican. *(A)* Scheme of sgRNA design of Lumican displaying the localization of the sequences on the second exon. *(B)* Example of T7 endonuclease assay of CAFs treated with sgRNA containing lentivirus. Mutant cells generated heteroduplex DNA displaying double band (Mu), whereas WT cells show only 1 band (WT). Positive control sample is depicted on the image (C+). *(C) (Upper)* Alignment of the WT Lumican sequence, the result of the sgRNA treated cells and the sgRNA sequence. *(Lower)* WT amino acid sequence of Lumican. Below the amino acid sequence predicted after the modification induced in sgRNA treated cells. The red arrows depict the STOP codons generated by the frameshift mutation occurred. *(D)*Western blot analysis of sgRNA efficiency validated in CAF cell line. sgRNA 4 and 5 reulted in complete elimination of Lumican protein. *(E)* Efficiency comparison of 5 sgRNA sequences targeting Lumican analyzed by western blot displayed in (*D)*.

4.1.3.3.2 Direct microinjection of sgRNA into zytgotes to generate single mutant mice

To confirm these results *in vivo* and to investigate complete ablation of the targets in mice, we targeted zygotes derived from our *"therapeutic model"*, the K-*Ras*$^{+/FSFG12V}$;*Trp53*$^{frt/frt}$;Elas-tTA/tetO-FLp(o);*Egfr*$^{lox/lox}$;*c-Raf*$^{lox/lox}$;Ub-CreERT2 strain. This model takes advantage of a dual recombinase system (Cre/LoxP and Flp/Frt) which allows temporal and spatial separation of tumor development and target elimination. These animals will express the Flp(o) recombinase in Elastase positive cells during late embryonic development leading to the expression of the resident K-Ras^{G12V} oncogene and to the ablation of the Trp53 tumor suppressor gene. When the tumor is developed, tamoxifen induced elimination of *Egfr* or *c-Raf* targets occur ubiquitously in cells expressing the Cre-recombinase driven by the human Ubiquitin C promoter (Blasco et al. unpublished). Therefore, this approach provides the possibility to mimic better the therapeutic response of well-established tumors.

We microinjected *Has1* targeting sgRNA along with Cas9 encoding mRNA into the cytoplasm of one-cell state embryos. Blastocysts derived from the injected embryos were transplanted into foster mothers and newborn pups were obtained (9). Efficiency of F0 generation mice carrying mutations was determined at weaning by the same 'PCR – T7 assay' strategy as described above. As illustrated in Figure 18, mice positive for DNA mismatch heteroduplexes (2, 3, 5, 7) were set up for sequencing analysis. The multiple mutational events occurred during embryo development were determined by Sanger sequencing in order to select frame shift alterations. Mice were then crossed again with the *'therapeutic strain'* to generate heterozygous F1 pups. These pups were analyzed by PCR strategy for germ line transmission of the selected CRISPR alterations.

In conclusion, development of single mutated Has1 KO mouse model resulted in 44% efficiency in the F0 generation revealed by T7 assay. Future studies will address the role of this gene on PDAC development.

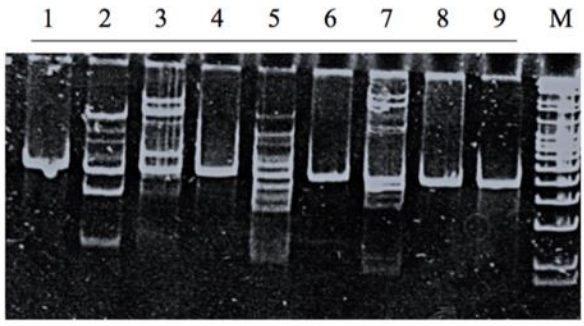

Figure 18. Has1 single mutated mouse strain validation. T7 endonuclease assay depicting 4 mice (2, 3, 5, 7) with DNA heteroduplex (multiple bands) products and 5 WT mice (1, 4, 6, 8, 9) with only one band. DNA ladder is marked on the right side (M).

4.1.3.3.3 One-step generation of triple mutant mice by zygote injection

To achieve greater therapeutic benefit and to generate faster knockout mouse models, we tested the efficiency of multiple stromal target deletion at once by direct microinjection of three different target sgRNAs. Lum, Hp and Msln guide RNAs were introduced along with Cas9 mRNA into the cytoplasm of zygotes derived from our *"therapeutic strain"*. To test the incorporation of the mutated alleles and to obtain homozygous triple KO mice, a complex strategy was designed as illustrated on Fig 19. Briefly, F0 mice were subjected to triple PCR analysis, as well as T7 endonuclease assay followed by sub-cloning and sequencing of the DNA fragments for each target. Mice positive for T7 assay with a frame shift mutation were selected for breeding. Germline transmission of indels was determined from the F1 generation by the same process as in the case of the F0. F1 generation was crossed possibly with mice that already incorporated mutated alleles of at least one of the target genes. However, extraordinary number of crosses were necessary to reach the final desired genotype to study the role of the absence of these three genes in PDAC development. After two years, this strain is still under generation.

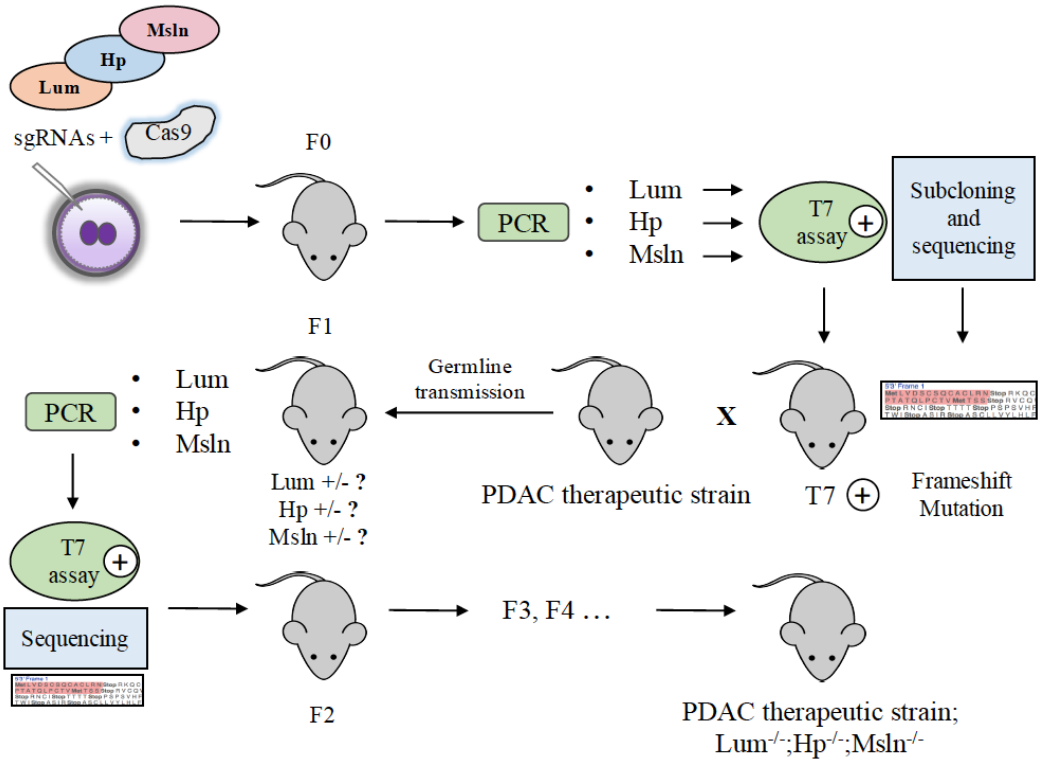

Figure 19. Triple knockout mice by CRISPR. The scheme depicts the generation and the genotyping strategy of triple mutant mice. SgRNA of Lum, Hp, Msln was injected along with Cas9 mRNA into the cytoplasm of zygotes derived from the therapeutic strain resulting in F0 knockout mouse generation. PCR strategy was designed to amplify the target region. The PCR product was used for T7 endonuclease assay and DNA sequencing of subclones to identify *indels*. Mice with frameshift mutations were selected to generate knockout mouse strain by intercrosses. F1 generation was subjected to verify mutations with the same strategy. Intercrosses were repeated until the appropriate genotype was obtained.

Table 1 shows the efficiency of each step in the process of triple KO PDAC strain establishment. In three microinjection sessions, a total number of 25 pups were born. T7 assay and sequencing analysis demonstrated various single – and bi-allelic mutational events in the F0 generation. In few occasions, even 4 different *indels* were found per target per mouse, such as in the case of Lumican (Table 1). This data suggests possible remaining activity of the Cas9 protein during first cell divisions.

Only 11 mice carried mutations in at least one gene (44%), the rest of the mice (56%) were WT. From the 11 mutant mice, 3 contained *indels* only in 1 target, 6 mice carried mutations in 2 genes and 2 triple knockout mice were obtained. However, several

mutated alleles were not transmitted to the F1 generation and the final numbers were reduced to 4 *single*, 5 *double* and 1 *triple* mutant mice.

Table 1. Summary of mutations and efficiency of Triple KO mice. The table shows the number of mutated alleles found for each gene in the F0 generation found in each gene as well as the number of *single*, *double* and *triple* mutant mice distributed among the target genes. The efficiency of each target gene generating mutated mice upon injection of the combined sgRNAs is shown in the last column. The efficiency of simultaneously mutant mice is depicted in the lower line.

Gene	Max. mutant alleles/mouse (F0)	Single	Double	Triple	Total	Efficiency of target
Lum	4	0	2		6	24%
Hp	2	0	2		6	24%
Msln	2	3	5	1	10	40%
Efficiency of mutants		**12%**	**24%**	**12%**	**44%**	

In conclusion, simultaneous deletion of three target genes and generation of a triple KO strain by the CRISPR/Cas9 genome editing technology resulted in lower efficiency than single mutated KO mice intents. In addition, NHEJ – mediated gene mutations produced mutations in a highly unpredictable and rather inefficient manner.

4.1.3.4 Generation of Saa3 null mice by conventional targeted deletion

The role of Saa3 in tumor development has not been investigated yet. A germline knockout mouse model has been described in the context of obesity-induced inflammation (209) with no major effect on normal homeostasis.

Preliminary results demonstrated pro-tumorigenic effect of this protein when silenced by shRNA. Thus, we decided to eliminate Saa3 in our PDAC mouse model. The Saa3 null allele was generated by homologous recombination using a BAC vector, where a LacZ gene cassette and a Neomycin resistance cassette at the ATG transcription start site replaces the entire protein coding sequence (Fig 20 *A*). The Saa3 null mouse sperm was used for *in vitro* fertilization of KPeCY females. By intercrosses we obtained homozygous Saa3 null mice (Fig 20*B*) at the expected Mendelian ratio and mice were healthy as reported before (209).

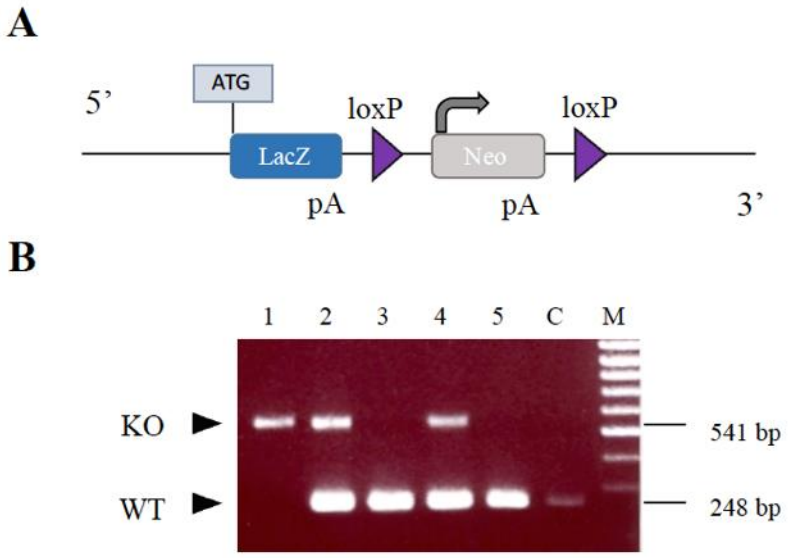

Figure 20. Generation of Saa3 null mice. *(A)* Scheme of the Saa3 null allele. LacZ reporter cassette is at the ATG transcription start site, followed by Neomycin resistance cassette (Neo) flanked by loxP sites (triangles). *(B)* PCR analysis of the Saa3 null allele in mouse tail DNA. Lane 1: $Saa3^{-/-}$; lane 2 and 4 $Saa3^{+/-}$; lane 3 and 5: $Saa3^{+/+}$. KO: null allele; WT: wild type allele. Expected fragment size of each allele is depicted.

4.1.4 Saa3 in mouse PDAC development

To study the effect of ablating *Saa3* expression in PDAC development, we incorporated *Saa3 null* alleles to our PDAC mouse model, the K-*Ras*$^{+/LSLG12Vgeo}$;*Trp53*$^{lox/lox}$;*Rosa26*$^{+/LSLEYFP}$;*Elas*-tTA/*tetO*-Cre, KPeCY strain.

4.1.4.1 PanIN formation and survival

Saa3 null K-*Ras*$^{+/LSLG12Vgeo}$;*Elas*-tTA/*tetO*-Cre mice displayed the same number of PanIN lesions and PDAC tumors as Saa3 competent animals (Fig 21*A*). Likewise, KPeCY mice carrying either wild type *Saa3* alleles (n = 18) or *Saa3 null* alleles (n = 20) developed PDAC with 100% penetrance succumbing to pancreatic tumors before 23 weeks of age with median survivals of 15 and 16 weeks, respectively. These observations, taken together, indicate that the absence of Saa3 expression from their germline has no significant effect on tumor development (Fig 21*B*).

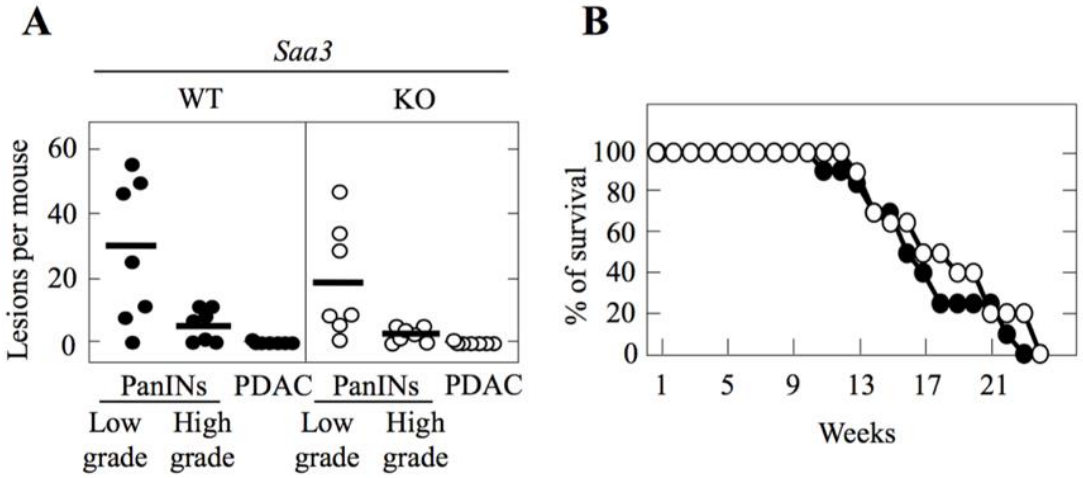

Figure 21. PanIN formation and survival. *(A)* Quantification of low and high grade PanIN lesions as well as PDACs in KPeCY mice expressing or lacking Saa3. *(B)* Kaplan-Meier survival curve of KPeCY mice expressing (open circle) or lacking Saa3 (closed circle). Saa3 WT, open circle; Saa3 null, closed circles.

4.1.4.2 Stroma reorganization in Saa3 tumors

Histological analysis revealed that *Saa3 null* tumor cells were more packed than in control tumors and exhibit a significant reorganization of their extracellular matrix as revealed by their reduced levels of collagen content (Fig 22*A*). *Saa3 null* tumors had a higher proportion of EYFP+ tumor cells and displayed less dense fibrotic stroma, albeit these differences were not statistically relevant in FACS analysis (Fig 22*B*). Interestingly,

we did not observe a significant reduction in the PDGFRα+ population, indicating that the reduced stromal content is not due to the loss of this CAF subpopulation (Fig 22*C*).

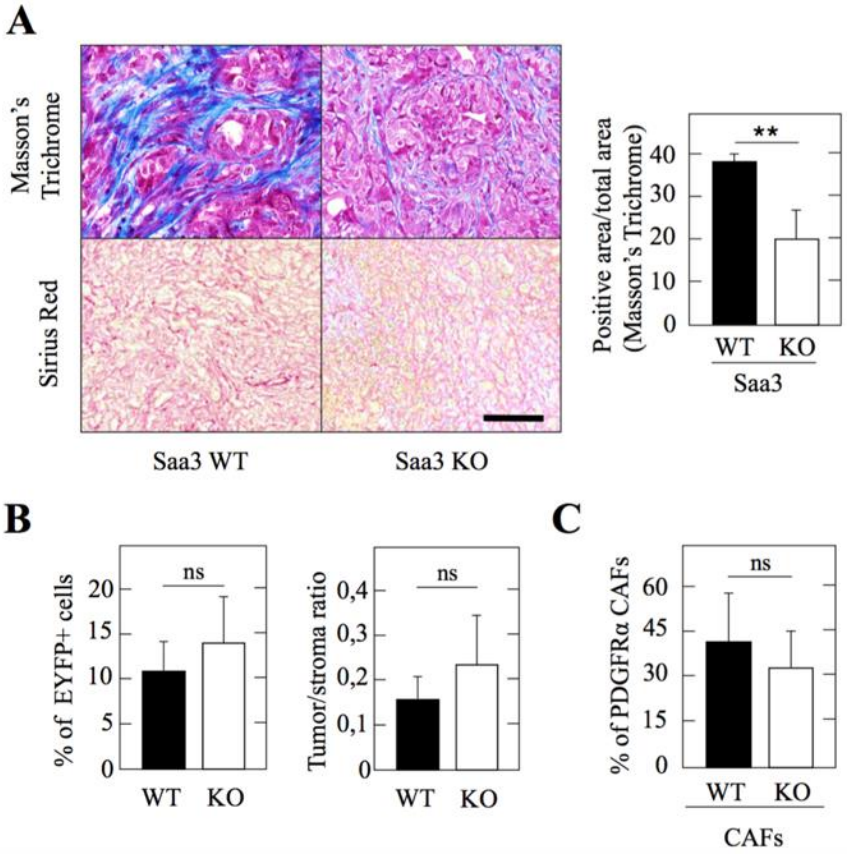

Figure 22. Characterization of the stromal component of *Saa3 null* tumors. *(A)* (*Left)* Masson's Trichrome and Sirius Red staining of collagen in *Saa3* competent (WT) and *Saa3 null* (KO) tumors. Scale bar, 50 μm. *(Right)* Quantitative analysis of Masson's Trichrome stained sections of *Saa3* competent (WT) and *Saa3 null* (KO) tumors (n = 4). *(B)* (*Left*) Quantitative FACS analysis of EYFP+ tumor cells and (*Right*) Tumor/stroma ratio in PDAC tumors of *Saa3* competent (solid bars) and *Saa3 null* (open bars) KPeCY mice (n = 6). Tumor/stroma ratio was calculated as the percentage of tumor cells vs. the percentage of immune (CD45), endothelial (CD31) and fibroblast (PDGFRα+) compartments all together (n = 6). *(C)* Quantitative FACS analysis of PDGFRα+ cells in PDAC tumors of *Saa3* competent (solid bars) and *Saa3 null* (open bars) of KPeCY mice.

Moreover, we observed a significant increase in the levels of macrophage infiltration in the *Saa3 null* tumors (12,5% vs. 3,8% of total area, Fig 23*A*). The increase in tumor-infiltrating macrophages was observed in both the anti-tumorigenic M1 as well as the pro-tumorigenic M2 populations (Fig 23*B*). However, this increase appeared to be more pronounced in the M2 populations, which has been associated with worse clinical

outcome in PDAC patients (234). In contrast, there were no obvious differences in the amount or localization of neutrophils or T and B lymphocytes (data not shown). *Saa3 null* tumors also displayed a significantly elevated number of endothelial CD31+ cells, indicating increased vessel density (Fig 23*A*). These vessels were functional as assessed by the greater perfusion observed upon injection of a contrast agent (Fig 23*C*). Whether increased angiogenesis was promoted by the infiltrating macrophages, as previously suggested (235), remains to be determined.

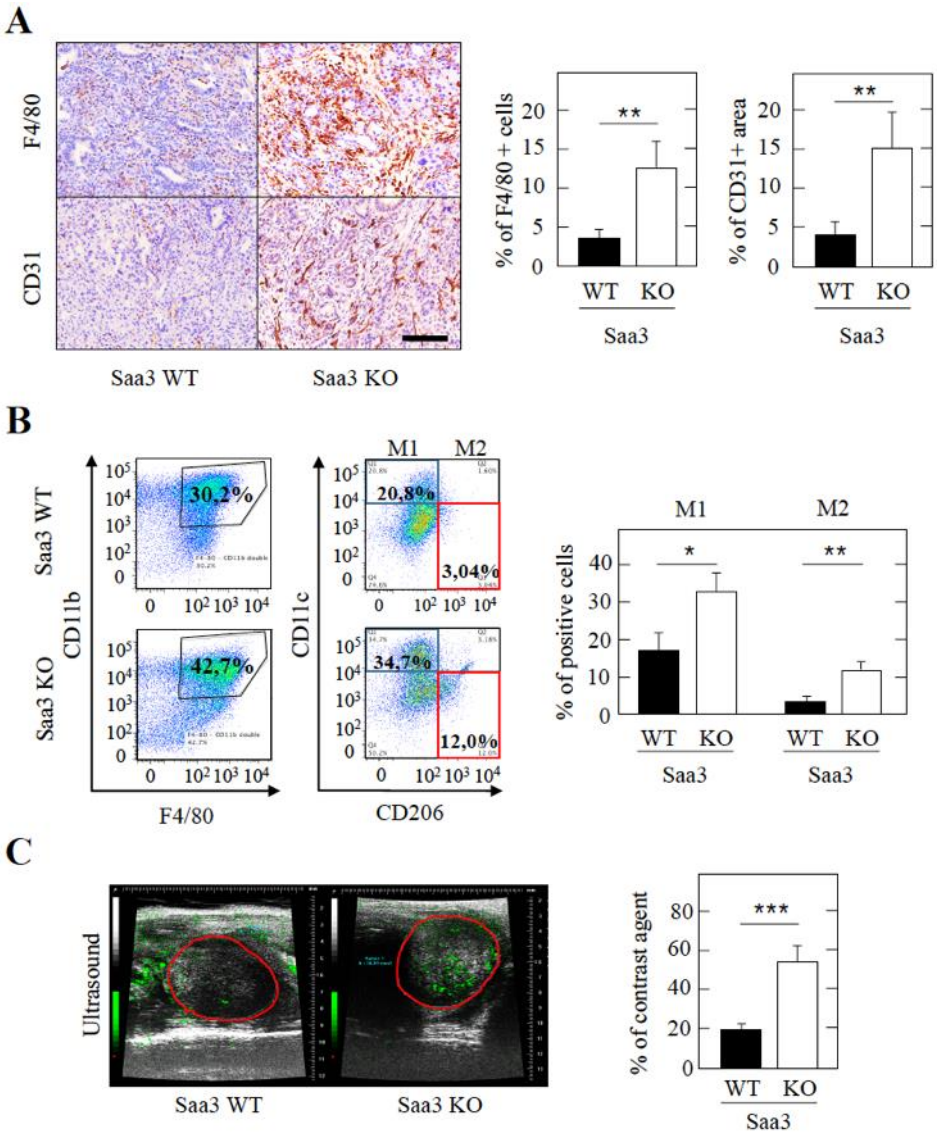

Figure 23. Stroma reorganization in Saa3 null tumors. *(A) (Left)* Representative images of F4/80 and CD31 immunostaining in *Saa3* competent (WT) and *Saa3 null* (KO) tumors. Scale bar, 50 µm. *(Right)* Quantitative analysis of F4/80 and CD31 stained sections of *Saa3* competent (WT) and *Saa3 null* (KO) tumors (n = 5). *(B) (Left)* FACS

analysis of fresh *Saa3* competent (WT) and *Saa3 null* (KO) tumor samples with anti-F4/80 and anti-CD11b antibodies. *(Center)* FACS analysis of F4/80+/CD11b+ double positive macrophages with anti-CD11c and anti-CD206 antibodies. The percentage of M1 ($CD11c^{high}/CD206^{low}$) (blue square) and M2 ($CD11c^{low}/CD206^{high}$) (red square) macrophage populations is indicated for each tumor type. *(Right)* Quantitative analysis of M1 and M2 macrophages in *Saa3* competent (WT) and *Saa3 null* (KO) tumors (n = 2). (C) (Left) Micro-ultrasound images of *Saa3* competent (WT) and *Saa3 null* (KO) tumors after injection of contrast agent. *(Right)* Quantitative analysis of vessel density in *Saa3* competent (WT) and *Saa3 null* (KO) tumors (n = 5). (*P < 0.05, **P<0.001 ***P < 0.001).

4.1.4.2.1 Stroma remodeling has low impact on treatment efficiency

Next, we interrogated whether the effect of *Saa3* ablation on stroma remodeling improved the therapeutic benefit of drug treatments. We reasoned that a reduction in fibrosis and increase in functional angiogenesis could increase the efficacy of the standard of care therapy, gemcitabine (GEM). We treated control *Saa3* expressing and *Saa3 null* KPeCY mice with GEM and vehicle starting when tumors were detected by ultrasound and finishing at humane end point. Surprisingly, tumors progressed slightly faster in *Saa3* wild type (n = 7) mice than in *Saa3* knockout (n = 5) mice (Fig 24). Interestingly, there was a better response to GEM treatment in *Saa3* wild type (n = 6) mice than in *Saa3* knockout (n = 5) mice as illustrated by tumor growth (Fig 24*A*). However, the slight increase in survival of *Saa3* knockout mice treated with GEM could explain that their tumors were bigger at humane end point (Fig 24*B*).

Furthermore, we studied the therapeutic strategy of depleting macrophages by Clodronate in combination with GEM, since targeting tumor-infiltrating macrophages was previously shown to be beneficial in PDAC (50) The effect in tumor growth in *Saa3* knockout (n = 5) mice was highly improved compared to GEM alone. Moreover, in these mice a small benefit in relative tumor volume was observed compared with *Saa3* wild type (n = 4) mice. However, this combination treatment did not enhance significantly the survival, maybe due to toxicity (Fig 24*B*).

Since PDAC is inherently poorly vascularized antiangiogenic therapies might not be beneficial. However, in preclinical trials VEGF inhibition reduced tumorigenicity (236). On the other hand, Phase III clinical trials with Gemcitabine alone or in combination with Bevacizumab resulted in questionable improvement of overall survival

probably due to lack of patient classification (237). Therefore, we tested if there was increased therapeutic benefit in *Saa3* knockout mice, where angiogenesis is highly induced. Indeed, treatment with the antiangiogenic agent (anti-VEGF antibody, B20.4.1.1, Genentech) in combination with GEM, displayed better therapeutic outcome in *Saa3* knockout mice (n = 5) compared to *Saa3* wild type mice (n = 6) (Fig 24*A*). Additionally, in both cohorts, mice survived significantly longer compared to vehicle treated littermates (Fig 24*B*).

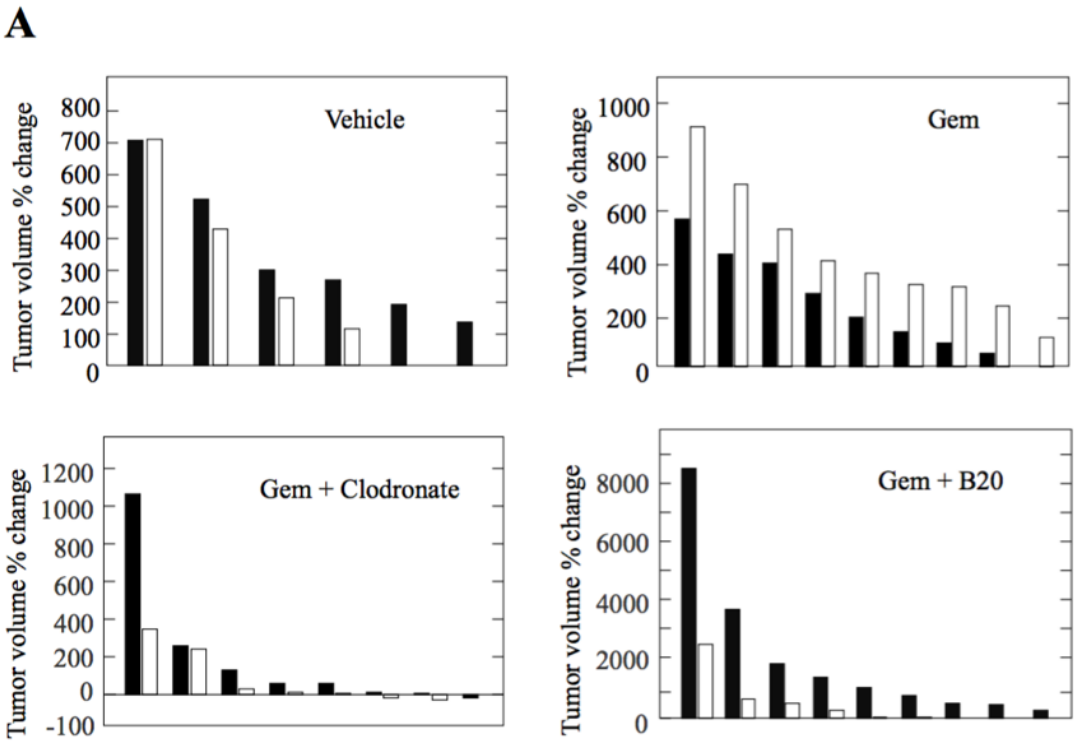

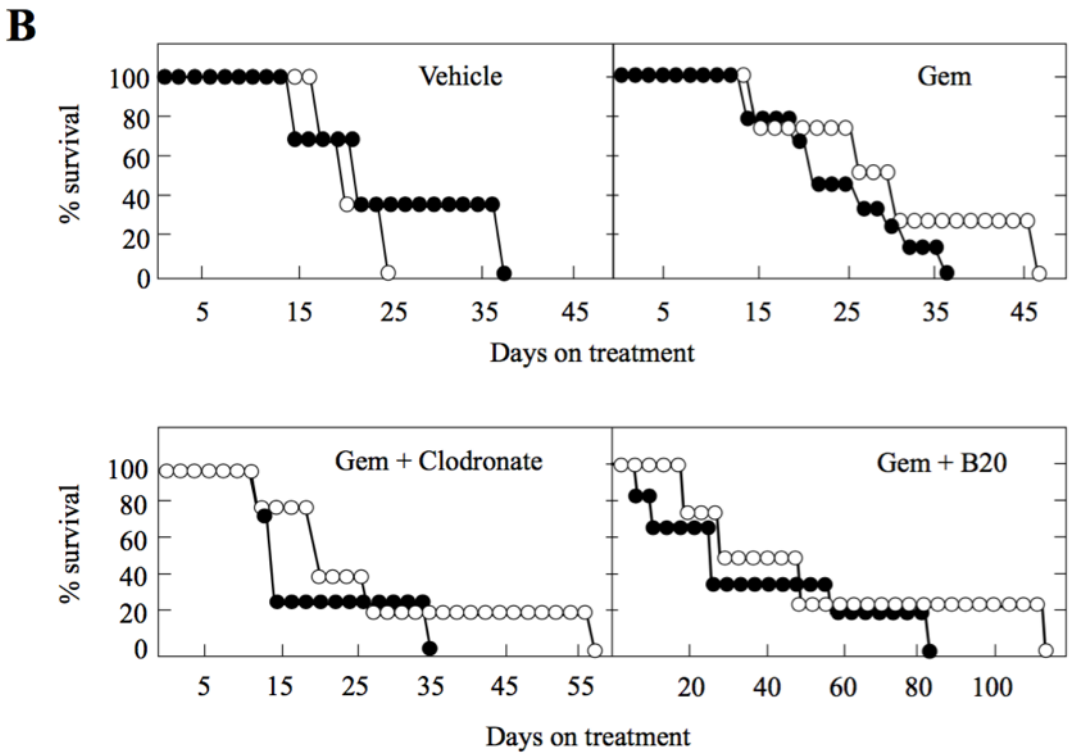

Figure 24. Treatments of tumor-bearing mice. *(A)* Tumor volume change in *Saa3* competent (solid bars) and *Saa3 null* (open bars) KPeCY mice after exposure to the indicated treatments: Vehicle (n = 5), Gemcitabine (Gem) (n = 5), Gemcitabine + Clodronate (n = 5) and Gemcitabine + B20 antibody (n = 4). ns, not significant. *(B)* Kaplan-Meier survival analysis of the same *Saa3* competent (solid circles) and *Saa3 null* (open circles) KPeCY mice upon treatment.

4.1.4.3 Undifferentiated tumor phenotype

4.1.4.3.1 Stem cell-like tumor cells

Tumors lacking *Saa3* appeared less differentiated upon Hematoxylin & Eosin (H&E) and CK19 staining (Fig 25*A*). Undifferentiated tumor phenotype has been associated with a cancer stem-like state in pancreatic cancer (238). Therefore, we assessed the cancer stem cell compartment (CSC) in *Saa3* competent and *Saa3 null* tumors. As illustrated in Figure 25*B*, we found a marked increase in CSC (CD133+) and metastatic CSC (CD133+/CXCR4+) populations in *Saa3* competent PDAC tumors versus those lacking *Saa3* expression (0.56% vs 4.02% CD133+ cells and 0.15% vs 0.43% in CD133+/CXCR4+ cells, respectively). These results suggest that the absence of *Saa3* confers a more invasive phenotype (239). Indeed, *Saa3 null* tumors showed a higher Ki67 proliferation index (Fig 25*C*).

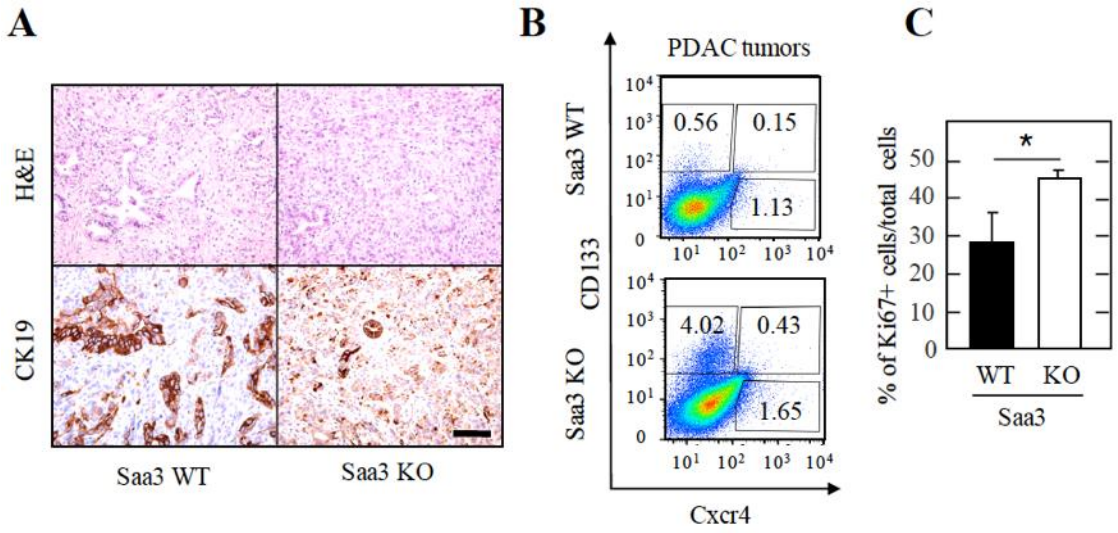

Figure 25. Undifferentiated Saa3 null tumors. *(A) (Top)* H&E staining and *(Bottom)* CK19 immunostaining of *Saa3* competent (WT) and *Saa3 null* (KO) tumors. Scale bar, 50 μm. *(B)* FACS analysis of fresh tumor samples *Saa3* competent (WT) and *Saa3 null* (KO) tumors from KPeCY mice with anti-CD133 and anti-CXCR4. *(C)* Quantitative analysis of Ki67 positive cells in *Saa3* competent (WT) and *Saa3 null* (KO) tumor sections.

Moreover, EYFP+ tumor cells present in the pancreas of 8-week old *Saa3 null* mice displayed a considerably higher percentage of PDGFRα+ cells than those expressing Saa3 (2.43% vs. 0.21%, respectively) (Fig 26*A*). Since PDGFRα expression is a marker for epithelial to mesenchymal transition (EMT), these results suggest that the absence of *Saa3* expression might promote the appearance of a migratory phenotype (143, 240, 241).

4.1.4.3.2 Migratory properties – metastasis

Since PDAC tumor cells most frequently metastasize to the liver we examined the presence of *Saa3* competent and *Saa3 null* EYFP+ pancreatic tumor cells in this tissue. As illustrated in Figure 26*B*, we detected an unusually high number of disseminated tumor cells in the liver of KPeCY *Saa3 null* animals, representing as many as 15.3% of all liver cells. In contrast, the number of tumor cells in *Saa3* competent animals only represented 0.07% of the liver cell population (Fig 26*B* and *C*).

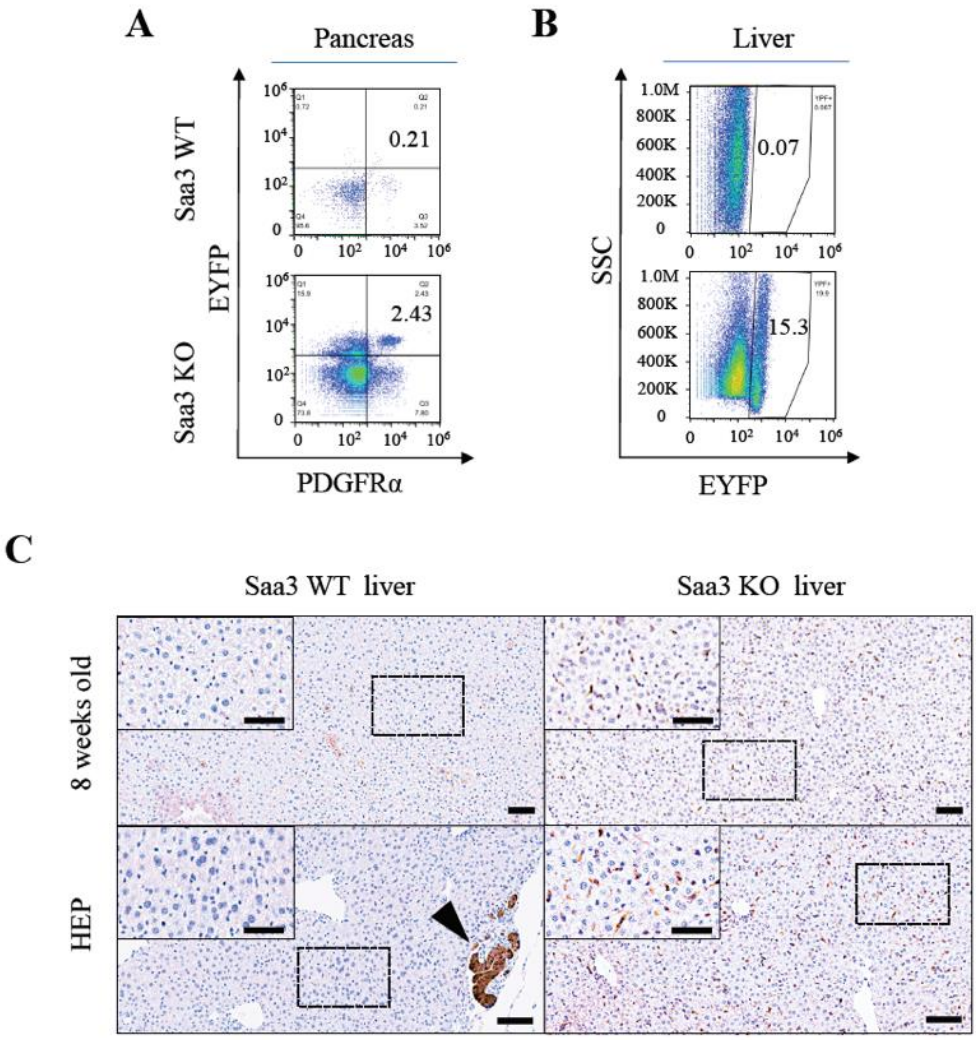

Figure 26. Disseminated EYFP+ tumor cells. *(A)* FACS analysis of EYPF expressing PDGFRα+ pancreatic tumor cells in pancreas isolated from 8-week-old *Saa3* competent (WT) and *Saa3 null* (KO) KPeCY mice. *(B)* FACS analysis of EYPF expressing cells in livers isolated from the same mice. *(C)* Images of GFP staining in livers of *Saa3* competent (WT) and *Saa3 null* (KO) KPeCY mice sacrificed at 8 weeks old age or humane end point (HEP). Scale bar, 100 µm. Insets display high magnification images. Scale bar, 30 µm.

However, these disseminated *Saa3 null* tumor cells did not proliferate and failed to propagate after colonization (Fig 27*A*). Indeed, whereas 12 out of 63 (19%) Saa3 competent mice displayed metastatic outgrowths, only 2 out of 40 (5%) Saa3 *null* animals presented metastatic lesion in their livers (P = 0.043) (Fig 27 *B*). These reduced levels of metastatic outgrowth were not due to a reduction in the inflammatory cell population, CD11b+ and F4/80+ monocyte derived-immune cells, which are known to establish the

metastatic niche (36, 37) (Fig 27*C*). Thus, this suggest that the reduced metastatic potential of *Saa3 null* tumors is an intrinsic property of the tumor cells. Indeed, these infiltrated *Saa3 null* tumor cells were negative for Ki67 immunostaining, indicating that they have limited proliferative properties (Fig 27*A*). However, it is also possible that absence of Saa3 expression in the liver may contribute to the limited proliferative and metastatic properties of these tumor cells.

It has been reported that Saa1 is a potent inducer of liver metastasis (191). In addition, SAA1 is among the top 50 upregulated genes in metastatic liver expression profile in a human PDAC dataset analyzed by Moffitt et al., suggesting that SAA1 may be relevant in liver metastasis formation (72). Thus, we examined the levels of expression of other Saa family members in livers of *Saa3* competent and *Saa3 null* tumor bearing mice sacrificed at humane end point. As illustrated in Fig 27*D*, the levels of expression of *Saa1* and *Saa2* are high in the livers of *Saa3* competent, but not in *Saa3 null* tumor bearing mice. These results may also contribute to explain why the abundant pancreatic tumor cells present in the livers of *Saa3 null* mice have limited metastatic potential.

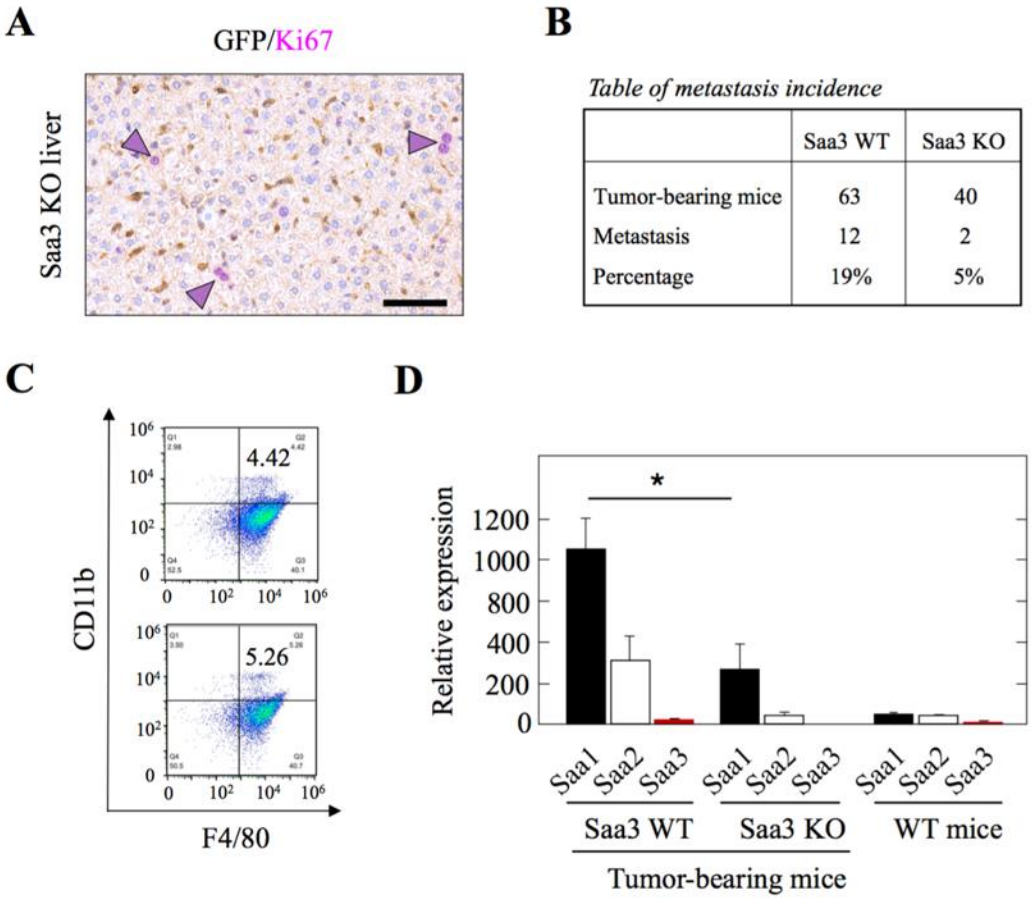

Figure 27. Metastatic properties of *Saa3 null* mice. *(A)* Co-staining of GFP (brown) and Ki67 (magenta) to mark EYFP+ tumor cells that proliferate (Ki67+) on liver sections

of 8 weeks old *Saa3 null* KPeCY mice. Scale bar 50 µm. *(B)* Incidence of metastasis in tumor-bearing mice sacrificed at humane end point. *(C)* FACS analysis of the macrophage population in livers of 8-week-old *Saa3* competent (WT) and *Saa3 null* (KO) KPeCY mice with F4/80 and CD11b antibodies (n = 4). *(D)* Expression analysis by qPCR of *Saa* family members in livers of *Saa3* competent (Saa3 WT) (n = 3) and *Saa3 null* (Saa3 KO) (n = 3) tumor bearing KPeCY mice sacrificed at HEP and in WT control livers (n = 2). Saa1 (solid bars), Saa2 (open bars) and Saa3 (red bars) are indicated.

To better characterize the effect of *Saa3* ablation on the migratory properties of PDAC tumor cells, we generated cell lines from pancreatic tumors lacking this protein. FACS analysis confirmed that the number of CD133+/CD44+ CSCs was higher in *Saa3 null* EYFP+ tumor cell lines (46.6% vs. 18.8%) (Fig 28*A*) demonstrating a clear enrichment in this population (239). Migration assays revealed that tumor cells lacking Saa3 displayed increased migratory properties (Fig 28*B*). While Saa3 expressing tumor cells advanced towards the scratch as a solid layer, cells lacking Saa3 moved freely throughout the scratch as individual cells (Fig 28*B*). CAFs lacking Saa3 expression also had increased motility and closed the gap more efficiently than those expressing the protein (61,5% in *Saa3 null* vs. 40.8% in wild type CAFs in a 16 hr period) (Fig 28*C*).

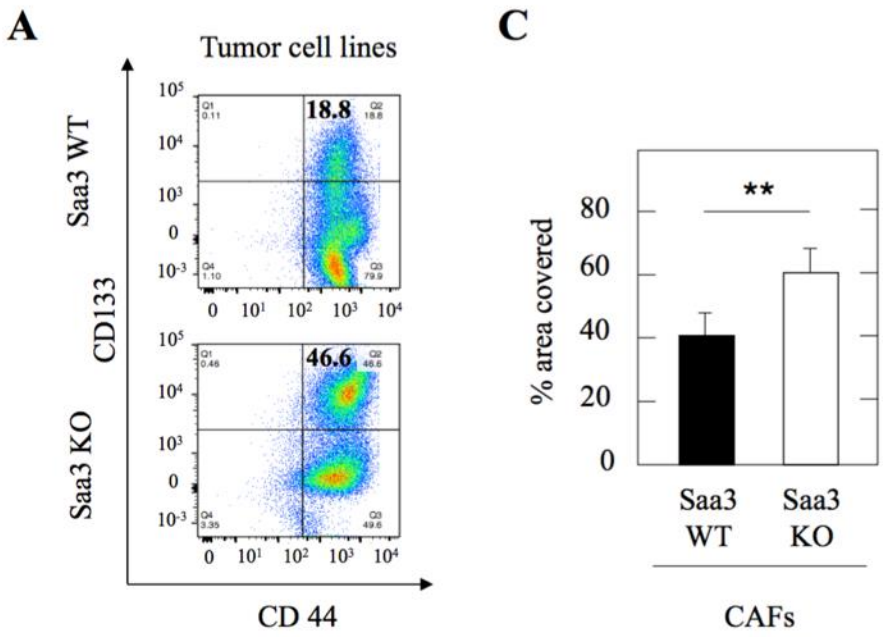

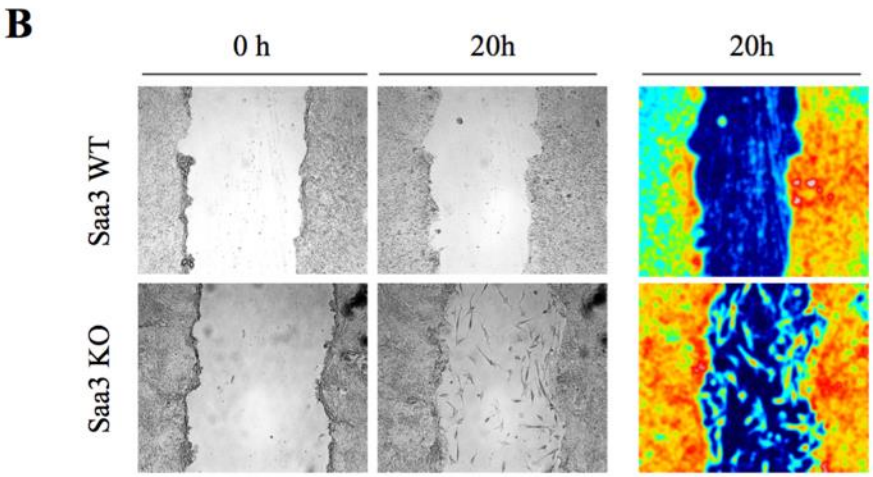

Figure 28. In vitro migratory cells. *(A)* FACS analysis of pancreatic tumor cell lines with anti-CD133 and anti-CD44. *(B)* Migratory properties of *Saa3* competent (WT) and *Saa3 null* (KO) tumor cells in an *in vitro* scratch assay. The right panel depicts a color enhanced picture for better visualization. *(C)* Quantitative analysis of migration assays in *Saa3* competent (WT, solid bar) and *Saa3 null* (KO, open bar) CAFs. The percentages represent the area covered by CAFs in 16 hours after the generation of the scratch.

4.1.4.4 Anti-tumorigenic properties of Saa3 null CAFs

Germline elimination of Saa3 did not induce significant survival benefit in PDAC mouse model. However, CAF specific knock-down of Saa3 previously showed reduction in tumor size upon co-injection with tumor cells subcutaneously into the flanks of nude mice (Fig 10). To study further the anti-tumorigenic properties of CAFs lacking Saa3 we isolated CAFs from tumor bearing *Saa3 null* KPCY mice by cell sorting using PDGFRα and established primary *Saa3 null* CAF cell lines.

4.1.4.4.1 Organoid co-culture of Saa3 competent and null CAFs and tumor cells

To characterize the effect of Saa3 on the interaction between pancreatic tumor cells and CAFs *in vitro*, we examined the growth properties of organoids generated from PDAC tumors of KPCY mice co-cultured with CAFs expressing or lacking Saa3. As illustrated in Figure 29*A*, Saa3 expressing CAFs significantly increased the number and size of individual organoids (Fig 29*B*). In contrast, *Saa3 null* CAFs failed to promote tumor growth resulting in organoid cultures similar to those grown in the absence of CAFs. As expected, NPFs effectively reduced the growth of organoids (Fig 29*A* and *B*). These results clearly indicate that Saa3 plays a key role on the ability of CAFs to support tumor cell growth.

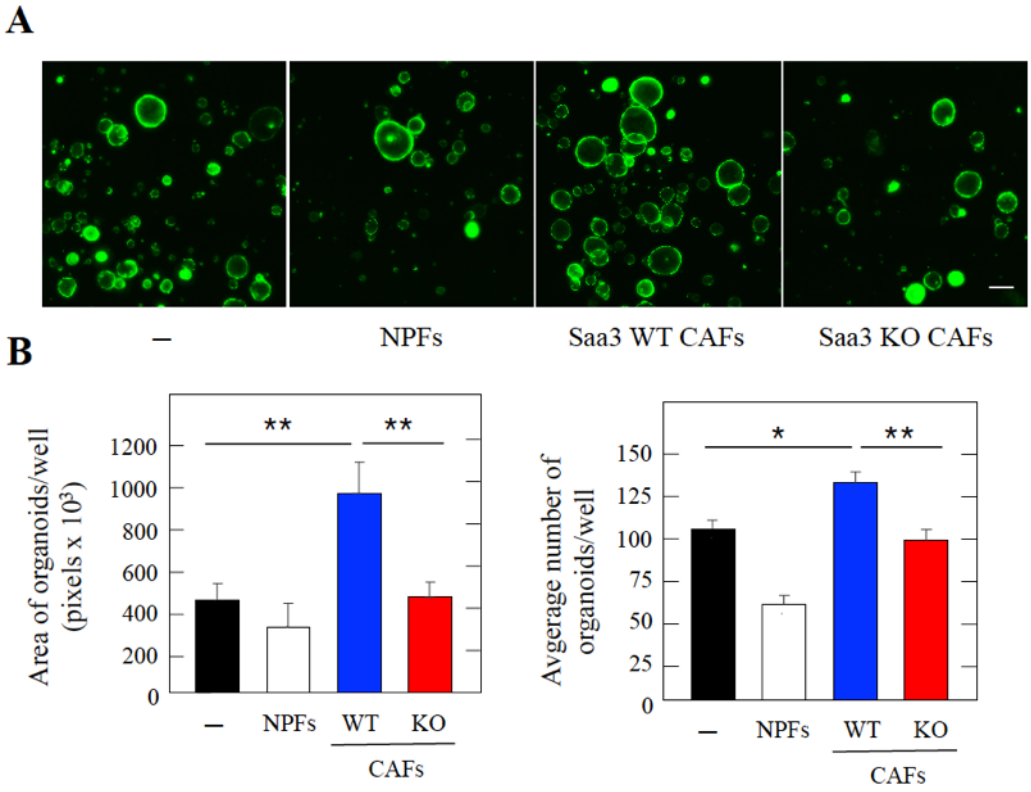

Figure 29. Anti-tumorigenic properties of Saa3 null CAFs *in vitro*. *(A)* Cultures of EYFP+ tumor organoids grown in the presence of NPFs, *Saa3* competent (WT) and *Saa3 null* (KO) CAFs. Scale bar, 100 µm. *(B)* Quantification of *(Left)* area and *(Right)* number of organoids under the indicated cultured conditions.

4.1.4.4.2 Orthotopic allografts of Saa3 competent and null CAFs and tumor cells

To explore the effect of Saa3 in the cross-talk between tumor cells and CAFs *in vivo*, we inoculated orthotopically in immunocompromised mice CAFs as well as tumor cells ($0.5x10^6$ each) either expressing or lacking *Saa3* (Fig 30*A*). As illustrated in Figure 24*B*, ablation of *Saa3* in tumor cells (n = 6) had no effect on their ability to induce tumors. As expected, based on the results described above using *in vitro* assays, co-injection of *Saa3* expressing tumor cells with NPFs (n = 6) reduced tumor growth whereas co-injection with *Saa3* expressing CAFs (n = 8) led to a significant increase in tumor volume. Interestingly, when these tumor cells were co-injected with CAFs lacking *Saa3* (n = 8), tumor growth was significantly reduced to levels even lower than those observed with NPF, indicating that Saa3 is essential for the ability of CAFs to stimulate tumor growth *in vivo*. However, this effect was not observed when we co-injected *Saa3 null* tumor cells along with *Saa3 null* (n = 6) CAFs (Fig 30*B*). No significant differences were observed in the proliferation (Ki67) or apoptosis (cleaved Caspase 3) levels that could explain the

differences in tumor volume induced by *Saa3* competent versus *Saa3 null* CAFs (Fig 30*C*). These observations indicate that whereas Saa3 provides pro-tumorigenic properties to CAFs, the anti-tumorigenic effect of *Saa3 null* CAFs requires that the corresponding tumor cells express the Saa3 protein. Likewise, we also observed a pro-tumorigenic effect when we co-injected *Saa3 null* tumor cells with *Saa3* null CAFs, suggesting that when both cell types are deficient in *Saa3* expression there is an alternative cross-talk that promotes tumor progression. These results provide an explanation as of why tumor development in *Saa3 null* mice is not affected, since the potential tumor inhibitory effect of *Saa3* ablation in CAFs does not take place when their neighboring tumor cells also lack *Saa3*.

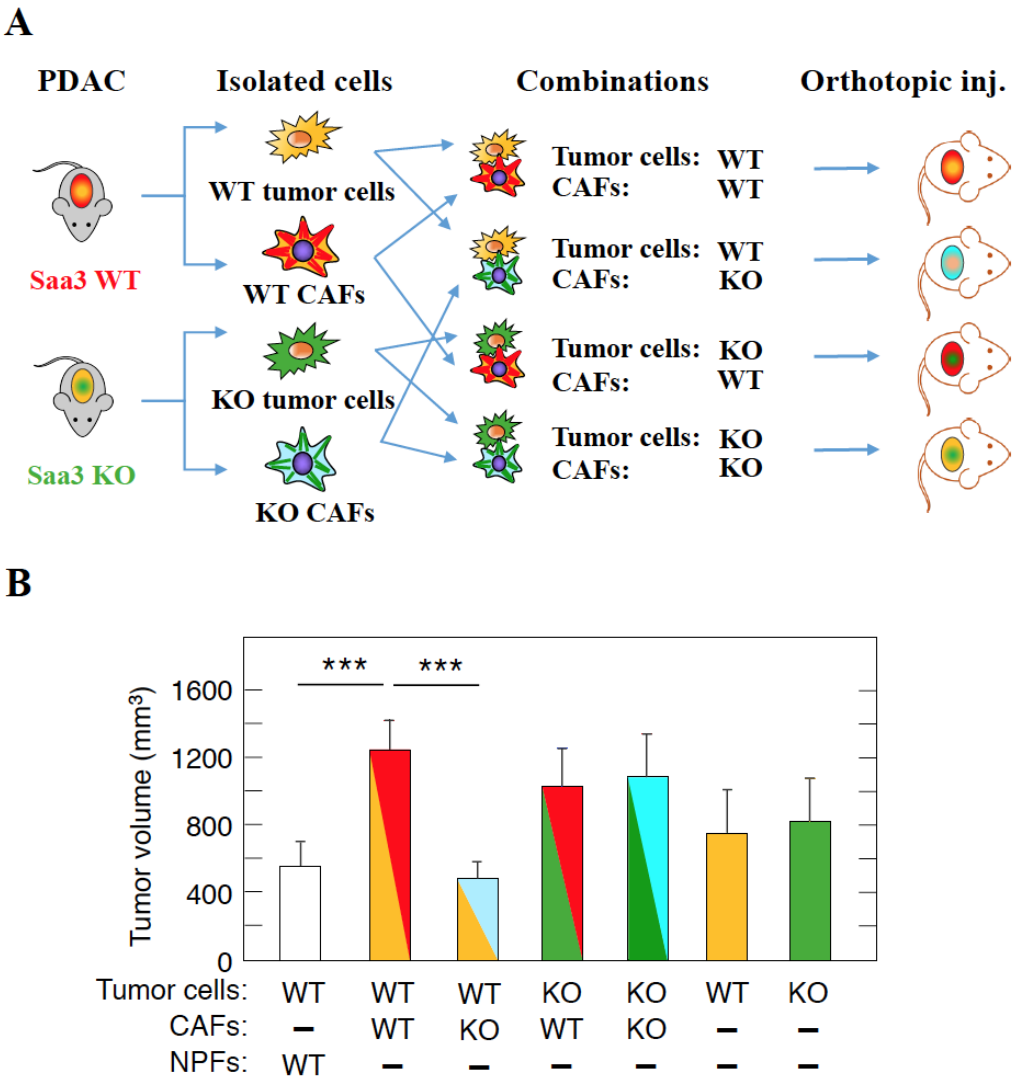

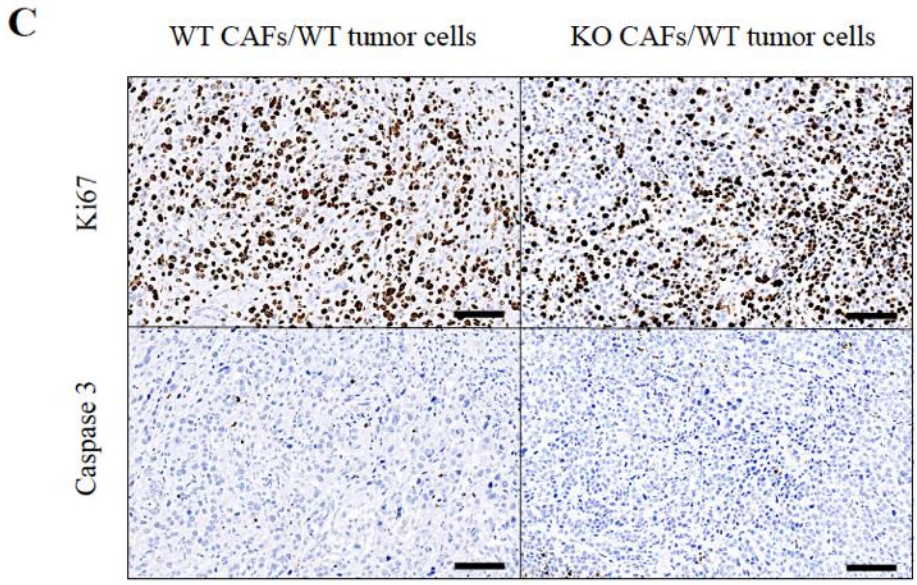

Figure 30. Anti-tumorigenic properties of Saa3 null CAFs *in vivo.* *(A)* Diagram depicting the *in vivo* orthotopic tumor assays in immunodeficient mice carried out to determine the pro-tumorigenic properties of *Saa3* competent (WT) (red) and *Saa3 null* (KO) (light blue) CAFs on pancreatic tumor cells isolated from *Saa3* competent (WT) (yellow) and *Saa3 null* (KO) (green) tumors. *(B)* Quantitative analysis of orthotopic tumor growth in immunodeficient mice inoculated with the indicated combinations of *Saa3* competent (WT) and *Saa3 null* (KO) CAFs and pancreatic tumor cells. Colors used to represent the corresponding bars are those indicated in (B). NPFs (open bar) were used as a negative control. *(C)* Immunohistochemical representation of apoptosis (Cleaved Caspase 3 and proliferation (Ki-67) of orthtotopic tumors. (***P < 0.001).

Taken altogether, in the following table we summarize the most important findings obtained with the *Saa3 null* PDAC mice.

Table 2. Most relevant features of Saa3 competent and Saa3 null KPeCY mice. Grading of the phenotypes is illustrated from not observed (–) to low (+), normal (++), high (+++), or very high (++++).

Features of KPCY mice	*Saa3 WT*	*Saa3 KO*
Stroma reorganization		
• ECM	+++	+
• Vascularization	+	++++
• Macrophage number and infiltration	+	++++
• Other immune cell infiltration	+	+
CAFs		
• Tumor growth support (nude mice assays)	+++	–
• Wound healing property (*in vitro*)	++	+++
Tumor cells		
• Differentiation	++	+
• Cancer stem cells (CSCs)	+	+++
• Migratory properties (*in vitro*)	+	++++
Liver metastasis		
• Macro-metastasis	++	–
• Micro-metastasis	++	+
• Migratory tumor cells	+	++++

4.1.4.5 Transcriptional profiling of Saa3 null cells

4.1.4.5.1 Comparative expression profile of Saa3 null and competent CAFs

To dissect the mechanism by which *Saa3* confers tumor stimulatory properties to CAFs, we used RNAseq to compare the transcriptome of *Saa3 null* and *Saa3* proficient CAFs. GSEA pathway analysis of *Saa3 null* CAFs revealed a significant enrichment in Proliferation and Angiogenesis hallmarks, as well as upregulation of Sonic Hedgehog, TNF-α NF-κB and IL-6 pathways. Moreover, we observed enrichment in genes implicated in EMT, suggesting increased plasticity of *Saa3 null* CAFs as well as their potential effect in inducing an undifferentiated phenotype in their neighboring tumor cells (242). In addition, the *Saa3 null* CAFs displayed upregulation of the Apical Junction pathway, a property that predicts increased physical contact between stromal and tumor cells (224). Finally, *Saa3 null* tumor cells displayed upregulation of the Tight Junction pathway suggesting increased cell-to-cell contact properties (Fig 31).

The most downregulated gene sets included the Oxidative Phosphorylation and Drug Metabolism pathways (Fig 31). Moreover, loss of Saa3 expression also downregulated other metabolic pathways such as Glycolysis. This pathway is activated

in Saa3 competent CAFs possibly playing a role to provide metabolites to their neighboring tumor cells (148). These observations suggest that loss of Saa3 might induce metabolic reprogramming of CAFs along with a reduction in the production of nutritional metabolites available to the adjacent tumor cells.

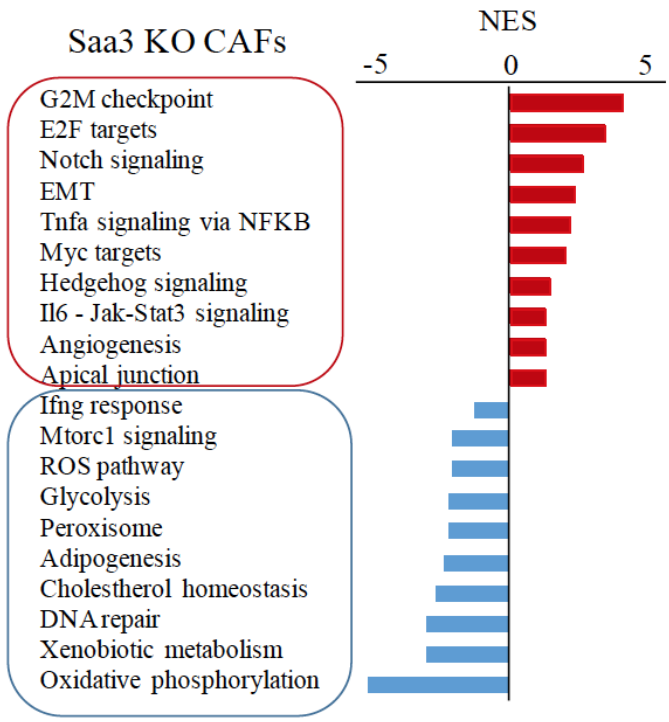

Figure 31. Transcriptional profiling of Saa3 KO CAFs. GSEA pathway analysis of Saa3 null vs. Saa3 proficient CAFs. The Normalized Enrichment Score (NES) ranking was generated by the GSEA.

4.1.4.5.2 Comparative expression profile of Saa3 null and competent tumor cells

We also interrogated of the transcriptomes of *Saa3* competent and *Saa3 null* tumor cells (Fig 26). This analysis revealed that loss of *Saa3* expression in pancreatic tumor cells results in a significant enrichment of cell cycle and metabolism related gene sets. Thus, confirming the increased proliferative capacity of the *Saa3 null* tumor cells. In addition, these mutant tumor cells displayed upregulation of the Tight Junction pathway suggesting increased cell-to-cell contact properties. On the other hand, we observed significant downregulation in ECM reorganization related pathways, suggesting a decrease in the levels of extracellular collagen, a feature that might explain the higher migratory properties of *Saa3 null* tumor cells (Fig 26).

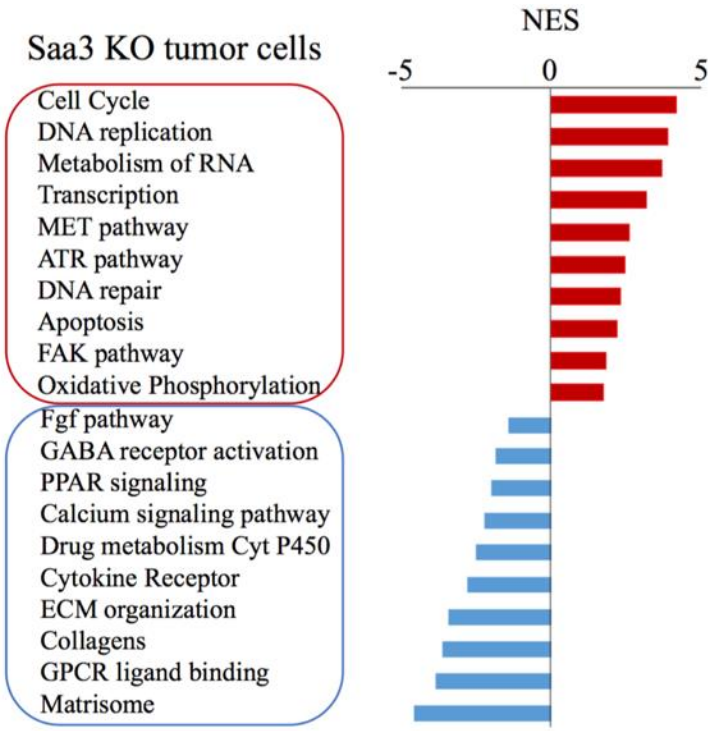

Figure 32. Transcriptional profiling of Saa3 KO tumor cells. GSEA pathway analysis of Saa3 null vs. Saa3 proficient CAFs. The Normalized Enrichment Score (NES) ranking was generated by the GSEA.

4.1.4.5.3 Cytokine profiles

Saa3 is involved in the regulation of several inflammatory cytokines (191, 243). Thus, we examined the profile of cytokine enrichment changes by GSEA analysis utilizing a specific signature of 144 cytokines. As illustrated in Figure 33, elimination of Saa3 downregulated global cytokine profile not only in CAFs but also in the tumor cell compartment (Fig 33). These results suggest that elimination of this inflammatory protein has an important role in the regulation of inflammatory cytokines and probably in systemic inflammation.

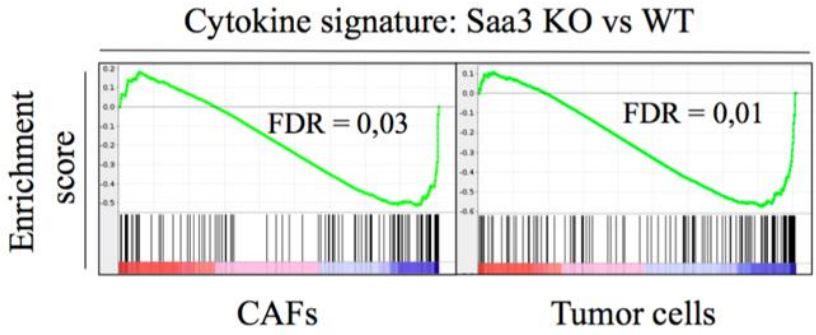

Figure 33. Cytokine profiles of *Saa3* competent and *null* cells. Specific cytokine signature was found significantly downregulated in both *Saa3 null* CAFs (FDR = 0.03) and in *Saa3 null* tumor cells (FDR = 0.01) by GSEA analysis. Enrichment score was generated by the GSEA software.

Taken together, transcriptome profiling result of *Saa3 null* cells indicate that elimination of Saa3 induces proliferation, metabolic reprogramming and cell-to-cell contact in both CAFs and tumor cell population. On the other hand, lack of Saa3 reduces overall cytokine secretion with the exception of the TNF-α and IL-6 pathways in CAFs.

4.1.4.5.4 Mpp6 – Saa3 axis

Differential expression analysis of the above data set revealed the presence of three significantly upregulated genes in *Saa3 null* CAFs. In particular, the gene encoding the Membrane Palmitoylated Protein 6 (*Mpp6*) (fold change = 15.8), a member of the palmitoylated membrane protein subfamily of peripheral membrane-associated guanylate kinases (MAGUK) (Fig 34*A* and *B*). The other upregulated genes included those encoding the g-aminobutiric acid receptor 3 (*Gabra3*, fold change = 3.2) and *Cbl*, an E3 ubiquitin-protein ligase involved in cell signaling and protein ubiquitination (fold change = 2.3) (Fig 34*A*). These observations were validated for *Mpp6* using qRT-PCR analysis of *Saa3 null* and competent CAFs (Fig 34*C*).

To determine whether *Mpp6* upregulation was functionally involved in the anti-tumorigenic effect of *Saa3 null* CAFs, we knocked down *Mpp6* expression using specific shRNAs that resulted in a significant decrease of its expression levels. *Mpp6*-downregulated *Saa3 null* CAFs were co-injected orthotopically with Saa3 competent PDAC tumor cells. These tumor cells grew significantly faster than those co-injected with *Saa3 null* CAFs reaching proliferation levels similar to those observed with Saa3 competent CAFs (Fig 34*D*). Downregulation of *Mpp6* also reverted the undifferentiated phenotype of tumor cells in the presence of *Saa3 null* CAFs (Fig 34*D*). These observations, taken together, indicate that the growth inhibitory activity of *Saa3 null* CAFs on their adjacent tumor cells is mediated by the upregulation of the tight junction protein Mpp6. Interestingly, Saa3 ablation did not alter the levels of expression of *Mpp6* in pancreatic tumor cells (Fig 34*B*) indicating that Saa3 selectively controls the expression of *Mpp6* in CAFs.

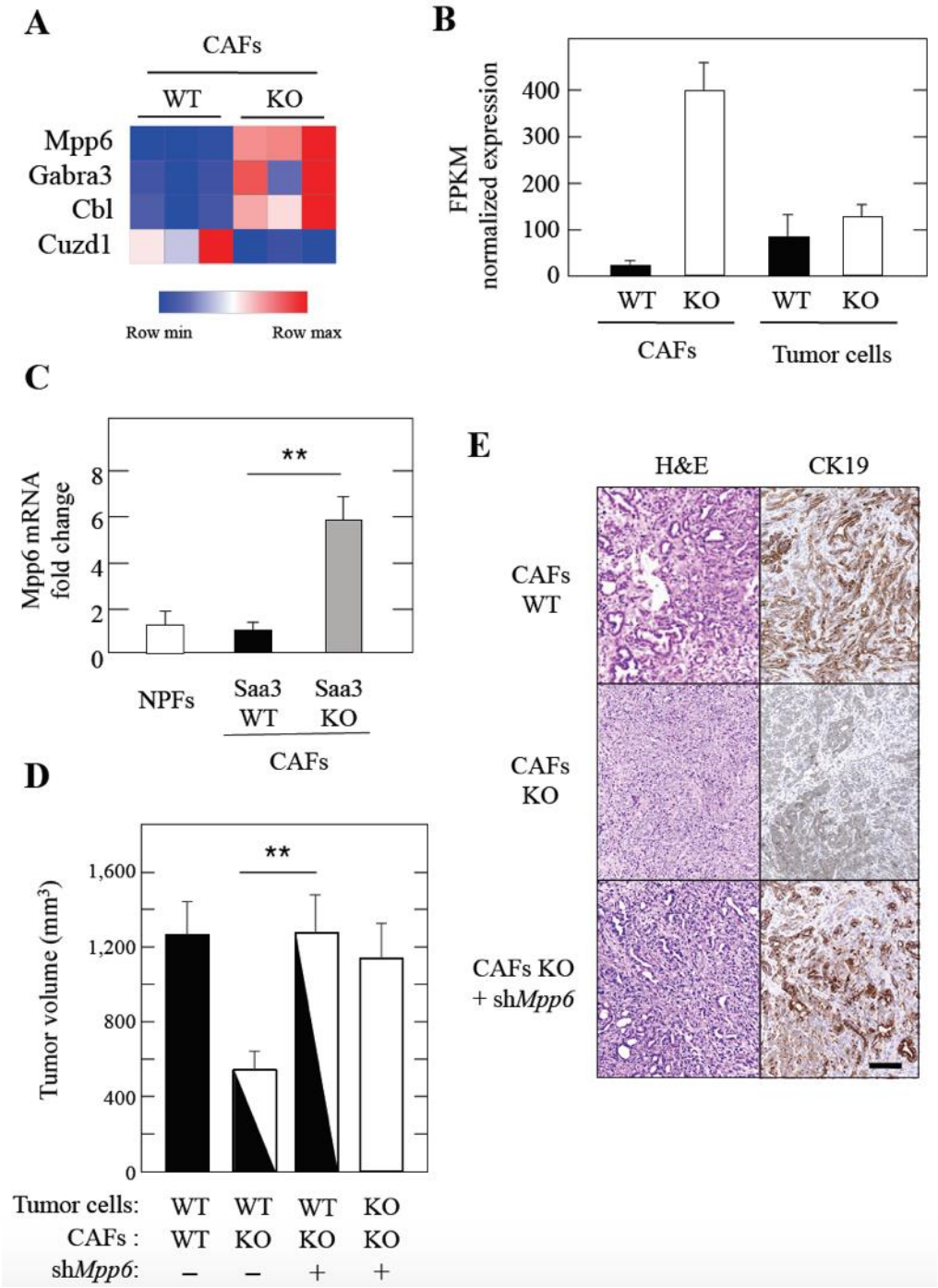

Figure 34. Identification and downregulation of Mpp6 in *Saa3 null* CAFs. *(A)* Heat map of the differentially expressed genes in *Saa3 null* (KO) CAFs compared to Saa3 competent (WT) CAFs. *(B)* RNAseq analysis of Mpp6 expression in *Saa3* competent (WT, solid bars) and *Saa3 null* (KO, open bars) CAFs and tumor cells. *(C)* qPCR validation of Mpp6 expression levels in NPFs (open bar), *Saa3* competent (WT) and *Saa3 null* (KO) CAFs (grey bar). *(D)* Tumor growth of orthotopic allografts of immunocompromised mice of *Saa3* competent (WT) and *Saa3 null* (KO) pancreatic tumor cells in the presence of *Saa3* competent (WT) and *Saa3 null* (KO) CAFs treated

(+) or non-treated (–) with a shRNA against *Mpp6*. Tumor volume is indicated by solid (WT cells), open (KO cells) and mixed solid/open (WT and KO cells) bars. *(E)* H&E and CK19 staining images of orthotopic tumors obtained from *(E)*. Scale bar, 100 μm. (**P<0.001).

4.1.5 SAA1 in human PDAC

The human genome contains three genes encoding highly related SAA family members (40% amino acid identity), SAA1, SAA2 and SAA4 (244). It also contains a non-functional *SAA3* pseudogene (SAA3P) (183). Among the three *SAA* functional genes, *SAA1* is the most similar in structure and function to murine *Saa3*. The SAA1 protein is expressed in several stromal cell types including activated synovial fibroblasts (194). Moreover, SAA1 has been shown to control neutrophil plasticity and has anti- and pro-tumorigenic inflammatory properties in melanoma (245). *SAA1* is highly expressed in a variety of tumors including PDAC (TCGA database).

4.1.5.1 Gene expression profiling of human CAFs

To validate our findings in human disease, we isolated hCAFs and hNPFs from PDAC patient samples and adjacent normal tissues by outgrowth method (155). We compared their expression profile by RNAseq and verified significant enrichment between human and mouse CAF expression profiles shown by GSEA analysis (Fig 35*A*). Indeed, the most upregulated gene sets were Cytokine-Receptor Interaction and Complement Cascade pathways in hCAFs compared to hNPFs, similar to our observation in mouse CAFs.

Next, we examined the expression levels of all SAA family members in our RNA seq dataset, which revealed SAA1 with the highest expression in hCAFs (Fig 35*B*). We validated these results by qPCR in primary CAF samples and observed distinct expression values of SAA1 suggesting variability among CAF samples (Fig 35*B*).

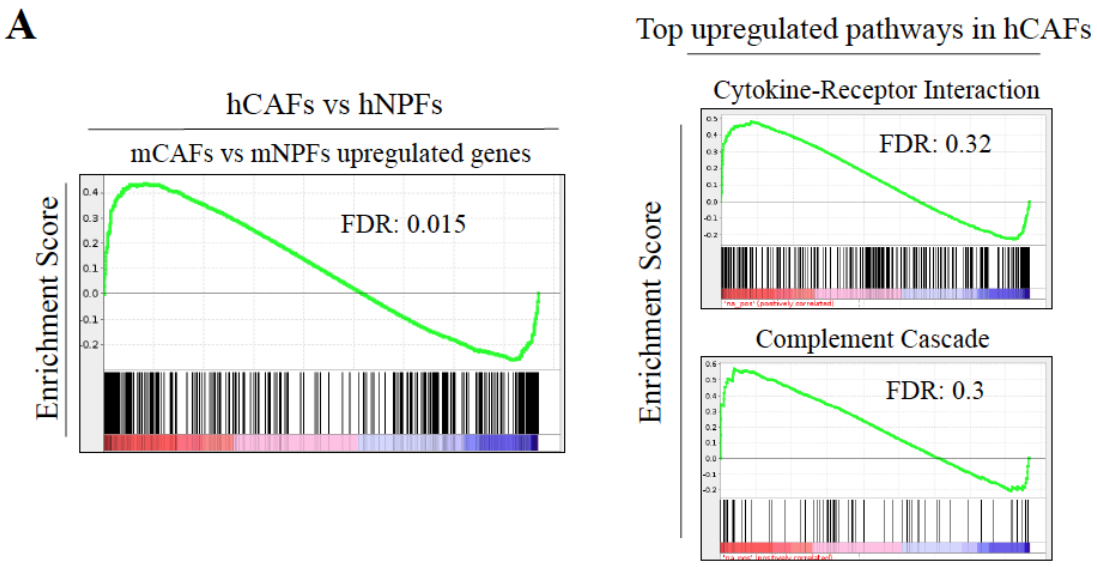

B

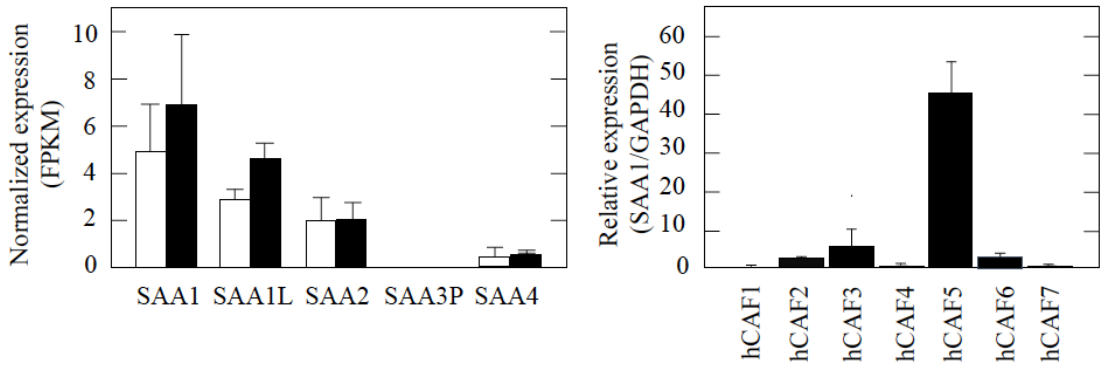

Figure 35. RNAseq analysis of human CAFs. *(A)(Left)* Comparison of mouse and human fibroblast signatures by GSEA analysis. Genes that were upregulated in mouse CAFs were downregulated in hNPFs. *(Right)* Upregulated pathways in hCAFs shown by GSEA pathway analysis. *(B)(Left)* Expression levels of *SAA* family members: SAA1, SAA-like 1 (SAA1L) SAA2, SAA3 pseudogene (SAA3P) and SAA4. Values are displayed in normalized FPKM derived from RNAseq results. *(Right)* Validation of SAA1 expression levels by qPCR in different primary hCAFs.

4.1.5.2 Analysis of SAA1 in the DKFZ human PDACdata set

Since gene expression signatures can be altered during cell culture we decided to analyze cellular populations isolated by cell sorting, similarly to the method we utilized for mouse samples. Hence, we established a collaboration with the group of Andreas Trumpp (DKFZ). This group has an unpublished dataset obtained from freshly isolated CAFs from tumor samples of PDAC patients (n = 7) and from adjacent normal pancreas (n = 5). The analysis of his data set revealed that *SAA1* is upregulated in the CAF samples compared to those obtained from normal pancreata (log2 fold change = 3.74; P<0.005). In contrast, the levels of *MPP6* expression were lower in CAFs than in normal pancreatic fibroblasts (Fig 36*A*). That is, the levels of both genes, *SAA1* and *MPP6*, inversely correlated in both types of fibroblasts (Fig 36*B*).

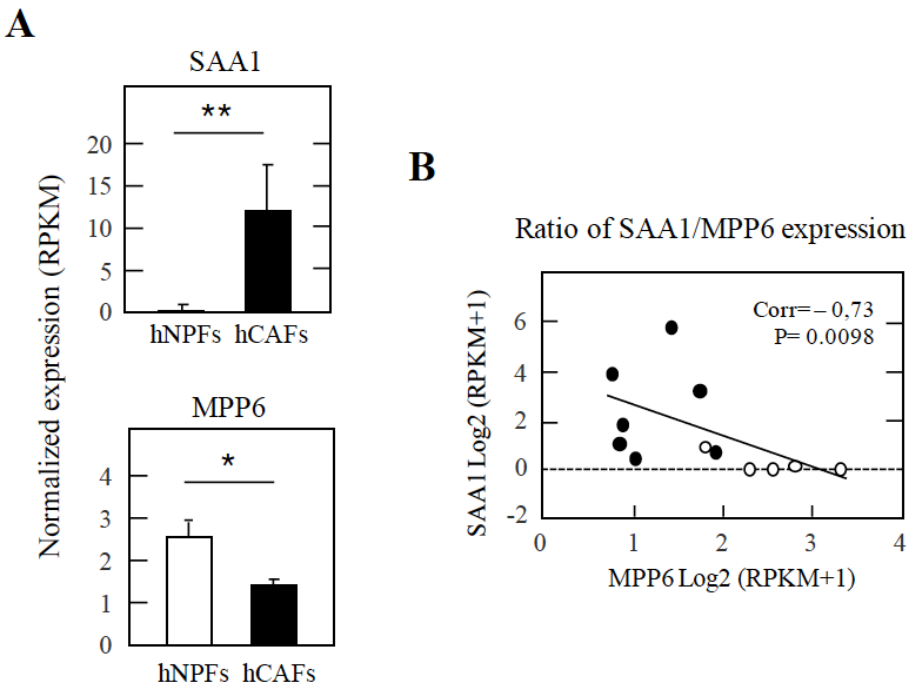

Figure 36. SAA1 in human sorted fibroblasts in DKFZ dataset. *(A) (Top) SAA1* and (Bottom) MPP6 expression in freshly sorted human NPFs (n = 5) (open bars) and CAFs (n = 7) (solid bars). *(B)* Correlation of *SAA1* and *MPP6* expression in freshly sorted human CAFs (n = 7, solid circles) and human NPFs (n = 5, open circles). Spearman Correlation (Corr) and P value are indicated. (*P < 0.05, **P<0.001).

4.1.5.3 Analysis of the Moffitt human PDAC data set

To further confirm these observations, we examined the *SAA1* expression levels in the PDAC RNAseq and microarray data set recently published by Moffitt and coworkers (72). RNAseq data revealed high but variable expression of *SAA1* both in tumors and in CAFs isolated from PDAC samples (Fig 37*A*). Moffitt´s report described two types of PDAC-associated stroma, "normal" or "activated", based on stromal signatures considering high αSMA expression or an inflammatory signature, respectively (72). Although, *SAA1* was primarily found expressed in tumor samples with "activated" stroma signature, high levels of *SAA1* expression correlated with significantly worse survival in both tumor samples containing "normal" or "activated" stroma (Fig 37*B*). In those tumor samples that contained low amounts of stroma, high *SAA1* expression correlated with a slight increase in survival, suggesting that the pro-tumoral effect of *SAA1* overexpression is primarily mediated by the stromal cells. In addition, *SAA1* was identified among the top 50 genes of liver specific metastatic PDAC signature in Moffitt´s analysis. These

results support the concept that SAA1 may play a role in human PDAC similar to that described for Saa3 in mouse tumors. Similarly, as shown in the previous dataset, SAA1 expression negatively correlated with MPP6 levels in PDAC stroma (Fig 37*C*).

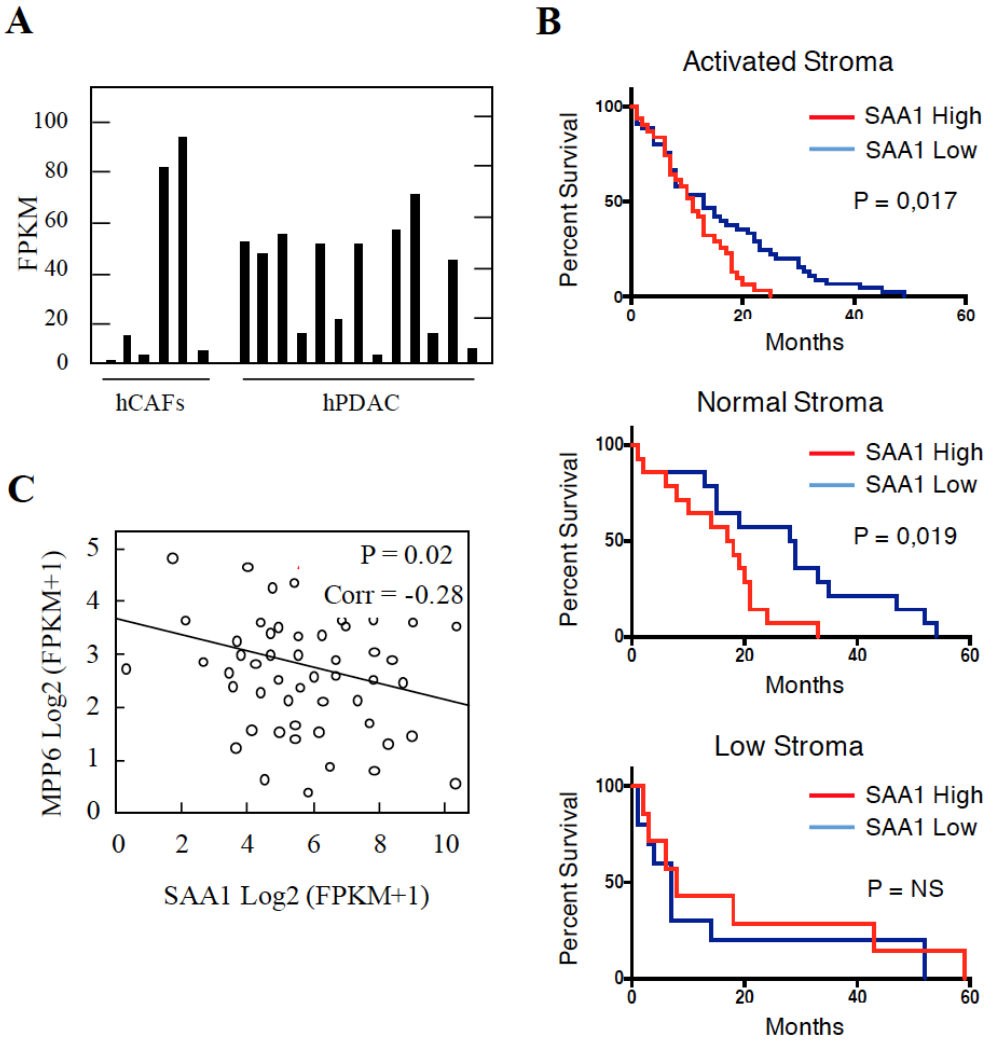

Figure 37. Analysis of the Moffitt dataset. *(A)* Fragments Per Kilobase Million (FPKM) values of SAA1 expression by RNAseq in human CAFs and PDAC samples obtained from Moffitt´s dataset (72). *(B)* Kaplan-Meier survival analysis of PDAC patients with high (red) or low (blue) *SAA1* expression levels classified by the presence of (Top) activated or (Middle) normal stroma signatures as well as in (Bottom) PDAC tumors with low stroma content based on microarray data from Moffitt´s dataset (72). *(C)* Correlation of SAA1 and MPP6 expression and human PDAC stroma signatures. Spearman Correlation = -0.28 with P value = 0.02.

5 Discussion

5.1 Targeting the stroma in PDAC by reprogramming CAFs

Pancreatic ductal adenocarcinoma (PDAC) is a lethal cancer, due to the inefficient current therapeutic strategies. PDAC is characterized by a rich desmoplastic stroma mainly composed by a heterogeneous population of cancer-associated fibroblasts (CAFs). CAFs contribute to promote cancer progression, immune-suppression and to treatment resistance (222). Targeting the stroma has gained interest with the aim to enhance drug delivery or inhibit its role in cancer cell chemoresistance or immune-suppression.

In contrast to the previous concept that pancreatic tumor stroma is solely tumor promoting (246), certain components, such as myofibroblasts can function in tumor suppression (152). However, this property may be highly dependent on tumor stage, tissue context and composition of the microenvironment. Indeed, elimination of proliferating αSMA myofibroblasts resulted in more aggressive tumors (170). Similarly, reduction of fibrotic stroma by genetic inhibition of stroma related Hedgehog pathway promoted tumor progression (51). On the contrary, blockade of stroma derived soluble factors (87), as well as Vitamin D mediated reprogramming of CAFs resulted in decreased tumor volume and increased chemotherapy efficacy. Interestingly, other studies have shown that normal fibroblasts have oncogenic suppressive potential (247, 248). Inhibitory property of normal tissue fibroblasts on tumor growth was reported earlier in various organs via governing epithelial homeostasis and proliferative quiescence (149, 150). This suggests that, normal fibroblasts could act as tumor suppressors, a function that is lost upon reprogramming to become CAFs.

Thus, we hypothesized that reprogramming of CAFs to become phenotypically closer to normal pancreatic fibroblast (NPF) characteristics, will retain cancer promotion and will not have the negative effects of stroma elimination.

5.1.1 Isolation and gene expression profiling of CAFs

To confirm our hypothesis, we isolated CAFs and NPFs by two different methods, by outgrowth and by cell sorting, and compared their expression profile in order to better understand their role in tumor development. Differential expression study identified 117 commonly upregulated genes in the two CAF populations. Nevertheless, among the most upregulated genes we found several of them belonged to the acute-phase response proteins, where *Serum amyloid A3* presented the highest expression levels. Moreover,

GSEA analysis displayed numerous pathways shared by these two CAF populations including Complement Cascade as the most significantly upregulated one, as well as Cytokine-Receptor Interaction and Innate Immune Response related pathways, such as NFκB. However, it has to be taken into consideration that CAFs isolated by outgrowth method do not represent a pure fibroblast population and may undergo gene expression alterations affected by culture conditions. This can explain the discrepancies between the differential expression analysis of CAFs isolated by outgrowth vs cell sorting.

Hence, we decided to further characterize PDGFRα+ subpopulation of CAFs to avoid contamination by other cell types and to study a more physiological scenario of freshly isolated CAFs.

5.1.2 PDGFRα+ CAFs are protumorigenic

A CAF subpopulation expressing PDGFRα is thought to mediate an inflammatory response (140). However, their putative pro-tumorigenic activity has not been properly documented. In this study, we show that PDGFRα+ CAFs possess pro-tumorigenic properties *in vivo* based on their ability to promote growth of co-injected pancreatic tumor cells in immunocompromised mice. This property is specific for PDGFRα+ fibroblasts isolated from PDAC tumors since the corresponding PDGFRα+ fibroblasts isolated from normal pancreata inhibited tumor growth (Fig 38).

Recent studies have described distinct populations of CAFs (127, 130, 162). A subpopulation, designated as myCAFs, is characterized by elevated expression of αSMA and appear to localize immediately adjacent to the neoplastic cells. A distinct subpopulation, iCAFs, located more distantly from the neoplastic cells and express low levels of αSMA. Instead, these cells display higher levels of secreted IL-6 as well as of other inflammatory mediators (162).

The CAFs isolated in our study, based on the expression of PDGFRα, also have high levels of IL-6, suggesting that they may represent iCAFs. Other similarities between these iCAFs and the PDGFRα+ CAFs isolated here include significant upregulation of cytokine/chemokine-receptor signaling pathways, as well as JAK-STAT signaling. However, the PDGFRα+ CAFs characterized in this study display significant overexpression of innate immune response-related signaling and high enrichment in cell-to-cell junction pathways, two properties not reported for iCAFs. Thus, it is plausible that the PDGFRα+ CAFs described here might represent, as yet another subpopulation of inflammatory CAFs.

5.1.3 Target selection validation in CAFs

We selected and validated candidate genes that fulfilled our criteria in PDGFRα+ CAFs and NPFs. Among those, druggability, significant overexpression in CAFs but no or low expression in NPFs; functional relevance in PDAC development, as well as in human disease were the more important for selection. Validation of overexpression of candidate genes in CAFs by qPCR narrowed down our list, which finally resulted in the selection of the following genes: *Saa3*, *Has1*, *Lumican*, *Haptoglobin* and *Mesothelin*. For all of these genes, overexpression has been reported in cancer (175, 227, 229). Some of them were found expressed in tumor cells as well (227, 249). Saa3 and Hp are acute-phase response inflammatory proteins associated to chronic inflammation (198, 226). These two genes appeared among the top 25 upregulated genes in inflammatory CAFs of mouse PDAC in a recent study by Ohlund et al (162). Lum and Has1 have important role in fibrosis and ECM remodeling (232), the latter is responsible for producing hyaluronic acid, the matrix component that defines structure and physical properties of the stroma (124). Whereas, Mesothelin is a tumor antigen and is proposed as a reliable marker of pancreatic cancer, its function has not been addressed properly. We hypothesized, that functional studies of these genes would help to better understand to role of CAFs in PDAC development either in immunosuppression or in physically induced therapy resistance.

5.1.3.1 Functional validation of targets by RNAi silencing

shRNA mediated knock down of these targets revealed functional role of the selected target genes in tumor stroma crosstalk. We co-injected tumor cells with CAFs, in which expression of either Saa3, Has1 or Lumican was downregulated, as well as CAFs infected with control shRNA, subcutaneously in the flanks of immunodeficient mice. Tumor growth monitoring exhibited reduction in tumor size for all the three genes silenced in CAFs compared to CAFs treated with control shRNA. However, the differences were not significant. One explanation could be the low efficiency of the knock down by shRNA. On the other hand, we did not find a candidate for which silencing would enhance pro-tumorigenic activity of CAFs. Further experiment for overexpression of these proteins should be performed in order to ensure the significance of these result.

5.1.3.2 Generation of knockout mouse models by CRISPR in PDAC stroma

To further investigate to role of the selected genes in PDAC development we took advantage of the novel and fast gene editing technology, CRISPR/Cas9, and generated

knockout mouse models. By this method, it is also possible to induce mutations simultaneously and efficiently ablate genes at the same time.

We injected guide RNA of *Has1* into one cell state embryos derived from our *"therapeutic strain"*, which resulted in 4 knockout chimeras with the ability to transmit the modification germ line. However, several crosses were utilized in order to finalize a mouse strain for characterization. In addition, multiple mutational events and their identification has to be taken into consideration when using CRISPR/Cas9 system. Nevertheless, these events occurring through DNA repair mechanism, are not entirely sure to result in knockout mutations. Taken altogether, development of single mutated *Has1* knockout mouse model resulted in 44% efficiency.

Next, we challenged the capacity of the system, to generate triple mutant mice to eliminate *Lumican, Haptoglobin* and *Mesothelin* at the same time. Indeed, the three sessions of microinjection resulted in 25 chimeras born, from which 3 were single-, 5 double- and 2 triple-mutant mice that were able to transmit the modification to the next generation. However, numerous crosses were necessary to reach the final genotype for characterization. This is due to the problem that NHEJ – mediated gene modifications produced mutations in a highly unpredictable and rather inefficient manner. Therefore, this mouse strain is still under generation, however preliminary data shows normal viability when eliminating these genes. Future studies will address the functional role of these genes in PDAC development.

5.2 Saa3 is protumorigenic in CAFs but not in tumor cells

Transcriptome analysis of the PDGFRα+ CAFs studied here revealed a series of selectively upregulated genes when compared with those fibroblasts present in normal pancreata. The top-scoring gene was *Saa3*, a member of the gene family encoding Saa proteins (Fig 38). In humans, SAA1 and SAA2 are secreted during acute phase of inflammation and have been implicated in several chronic inflammatory diseases, such as rheumatoid arthritis, atherosclerosis and amyloidosis. Another member of this gene family, *SAA3*, is not expressed in human cells but has been shown to be a major acute phase reactant in other species such as rabbits and rodents (250). Murine Saa3 has been shown to be expressed in macrophages (251) and adipose tissue (252). During inflammatory processes, Saa3 expression is effectively induced by Il-1β, TNF-α and Il-6 through NF-κB signaling. Interestingly, these cytokines as well as the NFκB pathway were found to be significantly upregulated in our CAF dataset.

5.2.1 Complete elimination of Saa3 did not affect overall PDAC development

Germline elimination of *Saa3* had no effect of PDAC development as reflected by the similar number of lesions observed in *Saa3 null* mice as well as by the lack of benefit in survival. However, *Saa3 null* tumors exhibit stroma remodeling including reduced fibrosis and ECM, infiltrating macrophages and increased vessel density (Fig 38). Indeed, *Saa3 null* CAFs had an elevated Angiogenesis signature as revealed by GSEA pathway analysis. It has been suggested that increased vessel density along with a reduction in fibrosis may improve the efficacy of chemotherapy treatments (124, 151, 163). However, we did not observe a significant increase in the therapeutic benefit of tumor-bearing *Saa3 null* mice treated either with Gemcitabine alone.

Since PDAC is inherently poorly vascularized antiangiogenic therapies might not be beneficial. However, in preclinical trials VEGF inhibition reduced tumorigenicity (236). On the other hand, Phase III clinical trials resulted in questionable improvement of overall survival probably due to lack of patient classification (237). Therefore, we speculated whether there would be increased therapeutic benefit in *Saa3* knockout mice, where angiogenesis is highly induced, when treating mice with Gemcitabine and anti-VEGF monoclonal antibody. Indeed, *Saa3* null mice responded slightly better to this combination than Saa3 competent KPeCY mice. Of note, mice in both cohorts lived longer upon this combination treatment. However, the low number of mice in the study could be the reason for the non-significant differences. The other possible explanation is the effect of the infiltrating pro-tumorigenic M2 macrophages that may have provoked therapy resistance. Reduction of gemcitabine induced apoptosis by TAMs in PDAC have been reported earlier (153).

To investigate whether TAMs are the source of the more aggressive Saa3 null tumors and of the resistance to treatment we depleted macrophages with Clodronate and, at the same time, treated the mice with Gemcitabine. However, while tumor volume change was diminished mice died at similar time compared to the control arm, probably due the toxicity of the treatment.

In conclusion, increasing the number of treated mice and further analysis of these tumor samples could help to understand the mechanism of therapy resistance induced by the tumor stroma in PDAC.

5.2.2 Saa3 null tumor cells have increased migratory but not homing properties

Saa3 null tumors were also less differentiated and more invasive, as suggested by a higher proliferation index and increased numbers of pancreatic CD133+ cancer stem cells (239). In addition, *Saa3 null* tumor cells showed an enhanced migratory phenotype (Fig 38). We observed an unexpected abundance of *Saa3 null* tumor cells in the liver during the early stages of pancreatic tumor development, constituting as much as 15% of all liver cells. We also identified a group of PDGFRα expressing tumor cells in the pancreas of the same mice. PDGFRα+ expression on tumor cells was recently demonstrated to drive invasive and migratory phenotypic changes in papillary thyroid cancer (241). However, these migrating tumor cells did not elicit metastatic outgrowths (Fig 38), possibly due to their observed lack of proliferative capacity within the *Saa3 null* liver microenvironment. Whether this migratory phenomenon is due to an intrinsic property of the *Saa3 null* tumor cells or it is a consequence of the absence of this protein in liver tissue and/or in pro-metastatic macrophages, remains to be determined. Interestingly, we observed that the absence of *Saa3* in liver tissue of tumor bearing mice inhibits expression of the *Saa1* and *Saa2* isoforms. Since SAA1 has been described as a potent inducer of liver metastasis (7, 26), the reduce levels of expression of *Saa1/Saa2* in *Saa3 null* livers could explain why the abundant disseminated pancreatic tumor cells cannot form metastatic foci. Conditional ablation of *Saa3* expression in specific cell populations including tumor cells, CAFs, macrophages and possibly other immune cells should help to better define the role of Saa3 during the various stages of tumor development.

5.2.3 Saa3 is required for the pro-tumorigenic properties of CAFs but not for tumor cells

Orthotopic co-injection of *Saa3 null* CAFs with *Saa3* competent tumor cells in the pancreas of *nude* mice significantly reduced tumor size (Fig 38). The inhibitory effect of *Saa3 null* CAFs was even more pronounced than that induced by NPFs. However, this inhibitory effect was not observed when we used *Saa3 null* tumor cells. Since loss of *Saa3* expression had no significant effect on the tumorigenic properties of pancreatic tumor cells, the observed lack of anti-tumorigenic effect of *Saa3 null* CAFs on *Saa3 null* tumor cells must be due to a defective cross-talk between *Saa3 null* tumor cells and *Saa3 null* CAFs. These results were also observed *in vitro* using tumor organoids, ruling out a putative role of a third cellular partner in this cross-talk. These reconstruction experiments

recapitulate the results obtained with *Saa3 null* mice in which both CAFs and tumor cells are devoid of *Saa3*. Thus, explaining why PDAC development is unaffected in *Saa3 null* mice. Taken together, these results underscore the critical role for Saa3 in mediating the interaction between CAFs and tumor cells and predict that selective elimination of *Saa3* in CAFs might provide significant therapeutic benefit. Future studies using conditional ablation of *Saa3* should help to better define the pro-tumorigenic role of Saa3 in CAFs. Besides, inhibition of Saa3 by monoclonal blocking antibody in established tumors could also shed light on whether Saa3 has a role in epithelial cells in early stages of tumor development.

Comparative transcriptional profiling of tumor cells and CAFs expressing or lacking *Saa3* revealed that *Saa3 null* cells display an increased proliferative signature, metabolic reprogramming and could suggest altered heterotypic cell-to-cell contact. Moreover, *Saa3* deficient CAFs show reduced overall cytokine secretion with the exception of the TNF-α and IL-6 pathways. This result was unexpected since acute-phase SAA apolipoproteins have been reported to enhance the expression of inflammatory cytokines including IL-1β, IL-6, TNF-α, IL-8 and G-CSF. Likewise, pro-inflammatory cytokines such as IL-1β, IL-6, and TNFα induce the synthesis of these SAA proteins (253). Therefore, upregulation of TNF-α, NF-κB and IL-6 pathways may result from an effort by the *Saa3 null* cells to induce expression of Saa3 thereby generating an inflammatory loop. Finally, the reduction of glycolysis and the downregulation of cholesterol homeostasis in *Saa3 null* CAFs, shown by GSEA pathway analysis, could contribute to their inhibitory activity on tumor cells observed in orthotopic co-injection experiments, by reducing nutrient transport. Similarly, recent results showed metabolic reprograming of PDGF induced CAFs by switching from oxidative phosphorylation to glycolysis and to support tumor cells with nutrients (148).

Comparative analysis of *Saa3* competent and *Saa3 null* CAFs revealed minor changes in their transcriptome. Yet, we identified three overexpressed genes in *Saa3* deficient CAFs. Of particular interest was *Mpp6*, a member of the peripheral MAGUK family of proteins primarily involved in controlling epithelial cell polarity (254). Mpps also function in tumor suppression and receptor clustering by forming multiprotein complexes containing distinct sets of transmembrane, cytoskeletal, and cytoplasmic signaling proteins (255).

Interestingly, *Mpp6* overexpression appears to be responsible for the loss of pro-tumorigenic effect of *Saa3 null* CAFs (Fig 38). Indeed, knock down of *Mpp6* expression

in these mutant CAFs restored their pro-tumorigenic properties as determined in co-injection studies with *Saa3* proficient pancreatic tumor cells in *nude* mice. Interestingly, the expression levels of *Mpp6* were unaffected by the presence or absence of Saa3 in tumor cells, suggesting that the functional relationship between Saa3 and Mpp6 might be limited to CAFs. Understanding the molecular pathways implicated in the inhibitory role of Mpp6 on the pro-tumorigenic effect of CAFs should unveil novel therapeutic opportunities (Fig 38).

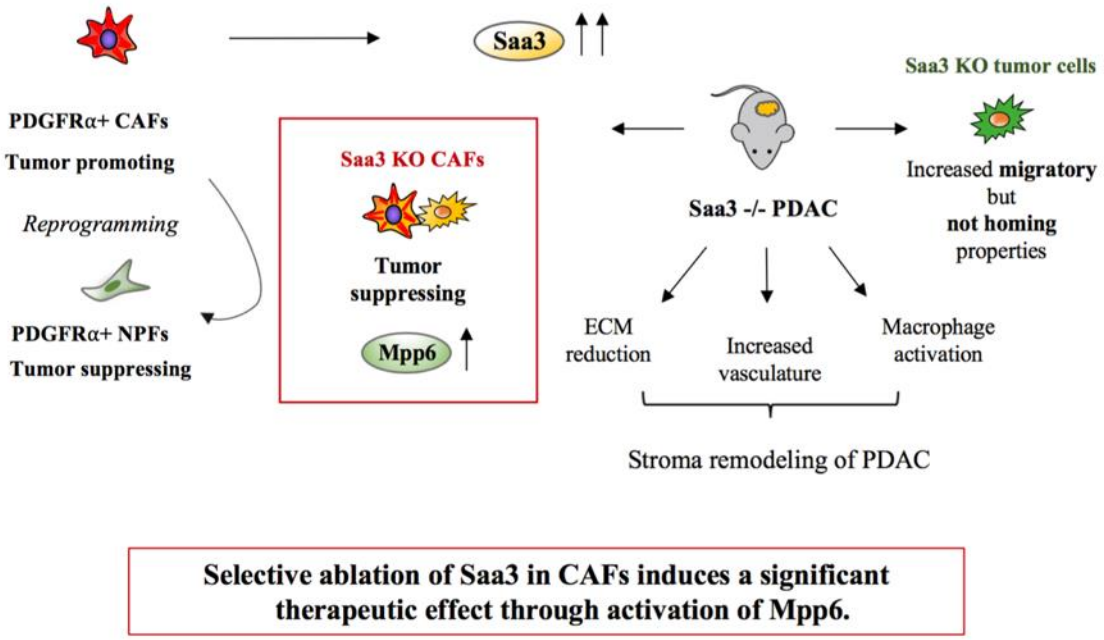

Figure 38. Summary of CAFs and Saa3 characterization in PDAC mouse model. The scheme depicts our hypothesis: to reprogram tumor promoting CAFs into a more protective phenotype, similar to tumor suppressing NPFs. CAFs overexpress Saa3. *Saa3 null* PDAC mice display stroma remodeling, migratory but not proliferative tumor cells and more importantly, tumor suppressing phenotype of CAFs mediated by Mpp6 activation. Vertical arrows indicate upregulation of genes (Saa3, Mpp6).

5.3 SAA1 in human PDAC

Finally, we have interrogated whether our observations in GEM PDAC tumor models could be translated to the human scenario. As indicated above, the *SAA3* locus is a non-expressed pseudogene (183, 184). On the other hand, the acute-phase SAA1 protein

has structural and functional characteristics that closely resemble those of murine Saa3, suggesting that SAA1 and Saa3 could be orthologue proteins.

Indeed, *SAA1* is overexpressed in human CAFs compared to NPFs. Moreover, high levels of *SAA1* expression in the stromal component of human PDAC tumors correlate with significantly worse survival regardless of whether the tumor samples contain "normal" or "activated" stroma. However, high *SAA1* expression in tumor samples with low stroma content also correlate with slightly increased survival, suggesting that SAA1 may have a pro-tumorigenic effect when is highly expressed in stroma, but a possible anti-tumorigenic effect when overexpressed in tumor cells. A dual role for SAA proteins depending on cellular context has already been reported by other investigators (180, 198). In addition, it was described in a recent study that polymorphic variants of SAA1 could be the responsible for the different tumor promoting and suppressing functions. Out of the five SAA1 polymorphic allele, SAA1.1 and SAA1.3 possessed anti-angiogenic properties, whereas SAA1.5 lacked tumor suppressive effect (196). Of note, these polymorphic variants were not identified in mice (197), suggesting distinct regulatory processes of SAA levels in human and mice. Studying the functional relevance of the SAA1 variants in different cell populations of the tumor could shed light on the dual properties of this protein.

Finally, *MPP6* levels inversely correlated with *SAA1* expression in human PDAC samples. Therefore, our results support the concept that murine Saa3 may serve as a model to study the role of the human acute-phase SAA1 protein in pancreatic cancer and to develop novel therapeutic strategies against this potential target. Since SAA1 is a secreted protein, it is conceivable that its pro-tumorigenic properties could be dwarfed with specific monoclonal antibodies providing that they are primarily delivered to the desmoplastic stroma, trying to avoid as much as possible their interaction with the tumor cells. In addition, a better understanding of the signaling pathways driven by SAA1 should provide clues about differential signaling mechanisms in stromal versus tumor cells.

Despite all the efforts invested in preclinical and clinical studies to find efficient treatment PDAC remains an incurable disease with slowly progressing therapeutic advances. Therefore, it is very important to search for novel strategies based on studies focusing on PDAC pathobiology that could help to design therapeutic approaches and could also be considered for the process of precision medicine.

6 Conclusions

1. Cancer Associated Fibroblasts (CAFs) represent a heterogeneous population of fibroblasts in PDAC. PDGFRα+ subpopulation of CAFs display strong inflammatory signature with particular emphasis on innate immune response, cytokine and competent cascade signaling compared to PDGFRα+ normal pancreatic fibroblasts (NPFs).
2. PDGFRα+ CAFs are pro-tumorigenic, while PDGFRα+ NPFs are tumor inhibitory when co-injected subcutaneously with mouse pancreatic tumor cells into nude mice and in co-culture *in vitro* studies with organoids.
3. Comparative transcriptional profiling of PDGFRα+ CAFs identified *Saa3* as the top upregulated gene and shRNA mediated functional validation qualified it as a potential target in CAFs.
4. Other candidate genes, like *Haptoglobin, Lumican, Has1* and *Mesothelin* were chosen for *in vivo* studies since they fulfill our criteria of target selection: overexpression in CAFs, low expression in NPFs, functional and human relevance in PDAC. Knock-out alleles of these gene have been incorporated in the therapeutic PDAC strain by CRISPR/Cas9 gene editing strategy: single *Has1* knockout and the triple combination of *Haptoglobin*, *Lumican* and *Mesothelin*.
5. Germline elimination of *Saa3* in a PDAC mouse strain does not seem to affect tumor development, as reflected by the same number and type of PanIN lesions present induced by the *K-Ras* oncogene in the context of *p53* activity and by the lack of significant survival difference in mice that develop PDAC in a *p53* deficient background. However, tumors lacking *Saa3* exhibit an undifferentiated phenotype.
6. *Saa3* elimination induces stroma remodeling, namely: extracellular matrix reorganization, vessel density increase and macrophage infiltration. These stromal changes do not result in a significant therapeutic benefit when tumor-bearing mice are treated with the standard of care Gemcitabine alone or in combination with the macrophage depleting agent Clodronate, or VEGF blocking antibody.
7. Saa3 is a mediator of the pro-tumorigenic properties of PDGFRα+ CAFs as shown by significant decrease in tumor growth when *Saa3 null* CAFs and *Saa3* expressing tumor cells are co-injected orthotopically in the pancreas of nude mice.

Same results were observed in co-culture with organoids *in vitro*. However, anti-tumorigenic effect of *Saa3 null* CAFs is lost when tumor cells also lack *Saa3* expression.

8. Anti-tumorigenic properties of *Saa3 null* CAFs are mediated by the upregulation of the tight junction protein membrane-associated guanylate kinases family member 6 (Mpp6) as revealed by the transcriptional profiling of *Saa3 null* and competent CAFs and validated by orthotopic tumor reconstruction experiments. Mpp6 silencing in *Saa3 null* CAFs restored their tumor growth supporting properties.
9. *Saa3 null* tumor cells displayed migratory phenotype *in vitro* and *in vivo*, as illustrated by the high number of disseminated tumor cells in the liver of the PDAC mouse strain. Nonetheless, these tumor cells were unable to proliferate and form metastatic outgrowth.
10. SAA1, the human orthologue of mouse Saa3, is overexpressed in PDAC samples and in human CAFs. Moreover, this overexpression correlates with significantly worse survival when pancreatic stroma signatures are transcriptionally separated. SAA1-MPP6 expression negatively correlates in human CAFs. Therefore, our PDAC mouse model can help to study therapeutic opportunities that could be translated to patients.

7 Summary

Pancreatic ductal adenocarcinoma (PDAC) is characterized by the presence of abundant desmoplastic stroma primarily composed of cancer associated fibroblasts (CAFs). It is generally accepted that CAFs stimulate tumor progression and might be implicated in drug resistance and immunosuppression. However, CAFs represent a heterogeneous population in the tumor microenvironment. Distinct subpopulations of CAFs could possess different pro- and anti-tumorigenic properties. Indeed, our results show that PDGFRα+ CAFs isolated from genetically engineered mouse PDAC tumors support tumor growth, whereas normal pancreatic fibroblasts (NPFs) have tumor inhibitory effect in an orthotopic model. Thus, we have compared the transcriptional profile of CAF subpopulations with that of NPFs to identify genes potentially implicated in their pro-tumorigenic properties. We describe several differentially expressed candidate genes for targeting CAFs, as well as their *in vivo* functional validation by RNAi silencing and by generation of distinct stromal knockout mouse models. We report, that the top upregulated gene, *Saa3*, a member of the Serum Amyloid A (SAA) family, is a key mediator of the pro-tumorigenic activity of PDGFRα+ subpopulation of CAFs. Whereas *Saa3* competent CAFs stimulate the growth of tumor cells in an orthotopic model, *Saa3 null* CAFs inhibit tumor growth. Saa3 also plays a role in the cross-talk between CAFs and tumor cells. Ablation of *Saa3* in pancreatic tumor cells makes them insensitive to the inhibitory effect of *Saa3 null* CAFs. As a consequence, germline ablation of *Saa3* does not prevent PDAC development in mice. The pro-tumorigenic activity of Saa3 in CAFs is mediated by Mpp6, a member of the palmitoylated membrane protein subfamily of the peripheral membrane-associated guanylate kinases (MAGUK). Finally, we interrogated whether these observations could be translated to a human scenario. Indeed, *SAA1*, the orthologue of murine Saa3, is overexpressed in human CAFs. Moreover, high levels of *SAA1* in the stromal component correlate with worse survival. These findings support the concept that selective inhibition of SAA1 in CAFs may provide potential therapeutic benefit to PDAC patients. In addition, further stroma-knockout PDAC mouse models generated in this study could help to better understand the complex pathobiology of pancreatic cancer and to design novel therapeutic approaches.

Összefoglalás

A pancreas tumorok legnagyobb részét a ductalis adenocarcinoma (PDAC) alkotja, melyet hatalmas mennyiségű desmoplasticus stróma jellemez. A pancreas tumorok strómáját nagyrészt tumor-asszociált fibroblasztok (TAF) formálják. Általánosan elfogadott, hogy a strómális TAF-ok fontos szerepet játszanak a daganatok képződésében, a terápiás rezisztenciában és az immunszuppresszióban. Azonban a TAF-ok a tumor mikrokörnyezet egy heterogén populációja, ahol különböző pro – és antitumorális tulajdonságokkal rendelkezhetnek. Erdeményeink is ezt indokolják, mivel transzgénikus PDAC egérmodellből izolált TAF-ok tumor serkentő, míg normál pancreas fibroblasztok (NPF) tumor gátló hatásúnak bizonyultak. Ennek tükrében, TAF és NPF populációk transzkripciós összehasonlító analízisével olyan terápiás célpontokat vizsgáltunk, melyek fontos szerepet játszhatnak a TAF-ok protumorális tulajdonságainak kialakulásában. Több olyan overexpresszált gént azonosítottunk, melyek potenciális TAF targetként szolgálhatnak, valamint ezeket *in vivo* funkcionálisan is validáltuk különböző egérmodellek segítségével. A legjelentősebben upregulált génnek az Saa3, a Serum Amyloid A (SAA) család tagja mutatkozott, amely eredményeink alapján kulcsszerepet játszik a PDGFRα+ TAF-ok szubpopulációjának pro-tumorális aktivitásában. Míg az Saa3-at expresszáló TAF-ok serkentik, az Saa3 null TAF-ok gátolják a tumor növekedését ortotopikus modellben. Ugyanakkor, az Saa3 fehérje, tumor sejt – fibroblaszt interakció mechanizmusában betöltött szerepét az is mutatja, hogy az Saa3 null tumor sejtek érzéketlenné válnak az Saa3 null TAF-ok növekedés gátló hatásával szemben. Ennek következtében az Saa3 null állatokban nem gátolt a pancreas tumorok progressziója. TAF-okban viszont, az Saa3 protumorális aktivitását az Mpp6, a perifériás membránhoz kapcsolódó guanilát-kinázok (MAGUK) tagja közvetíti. Végül megfigyeléseink felhasználhatóságát humán pancreas daganatokban is vizsgáltuk, ahol az Saa3 humán ortológja, az SAA1 valóban overexpresszált tumor és TAF mintákban. Ezen felül, az SAA1 emelkedett szintje a PDAC strómában rosszabb túléléssel korrelál. Ez alapján elképzelhető, hogy az SAA1 szelektív gátlása TAF-okban potencialis terápiás előnyökkel járhat pancreas tumoros betegek számára. Emellett, a további TAF célpontokra létrehozott knockout egérmodelljeink tanulmányozása nagymértékben hozzájárulhat új, hatékonyabb terápiák kifejlesztéséhez.

8 References

1. Siegel RL, Miller KD, Jemal A (2017) Cancer statistics, 2017. *CA Cancer J Clin* 67(1):7–30.
2. Ying H, Kimmelman AC, Lyssiotis CA, Hua S, Chu GC, Fletcher-Sananikone E, Locasale JW, Son J, Zhang H, Coloff JL, Yan H, Wang W, Chen S, Viale A, Zheng H, Paik JH, Lim C, Guimaraes AR, Martin ES, Chang J, Hezel AF, Perry SR, Hu J, Gan B, Xiao Y, Asara JM, Weissleder R, Wang YA, Chin L, Cantley LC, Depinho RA (2012) Oncogenic kras maintains pancreatic tumors through regulation of anabolic glucose metabolism. *Cell* 149(3):656–670.
3. Kamisawa T, Wood LD, Itoi T, Takaori K (2016) Pancreatic cancer. *Lancet (London, England)* 388(10039):73–85.
4. Hidalgo M (2010) Pancreatic cancer. *N Engl J Med* 362(17):1605–1617.
5. Hruban RH, Goggins M, Parsons J, Kern SE (2000) Progression Model for Pancreatic Cancer. *Clin Cancer Res* 6(8):2969–2972.
6. Maitra A, H.Hruban R (2008) Pancreatic Cancer. *Annu Rev Pathol* 4(3):157–188.
7. Sipos B, Frank S, Gress T, Hahn S, Klöppel G (2009) Pancreatic intraepithelial neoplasia revisited and updated. *Pancreatology* 9(1–2):45–54.
8. Hruban RH, Fukushima N (2007) Pancreatic adenocarcinoma: Update on the surgical pathology of carcinomas of ductal origin and panins. *Mod Pathol* 20(1):61–70.
9. Raphael BJ, Hruban RH, Aguirre AJ, Moffitt RA, Yeh JJ, Stewart C, Robertson AG, Zenklusen JC, et al. (2017) Integrated Genomic Characterization of Pancreatic Ductal Adenocarcinoma. *Cancer Cell* 32(2):185–203.e13.
10. Malumbres M, Barbacid M (2003) RAS oncogenes: The first 30 years. *Nat Rev Cancer* 3(6):459–465.
11. Hoover KB, Liao SY, Bryant PJ (1998) Loss of the tight junction MAGUK ZO-1 in breast cancer: relationship to glandular differentiation and loss of heterozygosity. *Am J Pathol* 153(6):1767–1773.
12. Bryant KL, Mancias JD, Kimmelman AC, Der CJ (2014) KRAS: feeding pancreatic cancer proliferation. *Trends Biochem Sci* 39(2):91–100.
13. Scheffzek K (1997) The Ras-RasGAP Complex: Structural Basis for GTPase Activation and Its Loss in Oncogenic Ras Mutants. *Science* 277(5324):333–338.

14. Calhoun ES, Jones JB, Ashfaq R, Adsay V, Baker SJ, Valentine V, Hempen PM, Hilgers W, Yeo CJ, Hruban RH, Kern SE (2003) BRAF and FBXW7 (CDC4, FBW7, AGO, SEL10) mutations in distinct subsets of pancreatic cancer: potential therapeutic targets. *Am J Pathol* 163(4):1255–1260.
15. Witkiewicz AK, McMillan EA, Balaji U, Baek GH, Lin WC, Mansour J, Mollaee M, Wagner KU, Koduru P, Yopp A, Choti MA, Yeo CJ, McCue P, White MA, Knudsen ES (2015) Whole-exome sequencing of pancreatic cancer defines genetic diversity and therapeutic targets. *Nat Commun* 6:1–11.
16. Caldas C, Hahn SA, Da-Costa LT, Redston MS, Schutte M, Seymour AB, Weinstein CL, Hruban RH, Yeo CJ, Kern SE (1994) Frequent somatic mutations and homozygous deletions of the p16 (MTS1) gene in pancreatic adenocarcinoma. *Nat Genet* 8(1):27–32.
17. Rozenbium E, Mieke Schutte, Goggins M, Hahn SA, Panzer S, Zahurak M, Goodman SN, Sohn TA, Hruban RH, Yeo CJ, Kern SE (1997) Tumor-suppresive pathways in pancreatic carcinoma. *Cancer Res* 57(410):1731–1734.
18. Hustinx SR, Leoni LM, Yeo CJ, Brown PN, Goggins M, Kern SE, Hruban RH, Maitra A (2005) Concordant loss of MTAP and p16/CDKN2A expression in pancreatic intraepithelial neoplasia: Evidence of homozygous deletion in a noninvasive precursor lesion. *Mod Pathol* 18(7):959–963.
19. Sherr CJ, Bertwistle D, Den Besten W, Kuo ML, Sugimoto M, Tago K, Williams RT, Zindy F, Roussel MF (2005) p53-dependent and -independent functions of the Arf tumor suppressor. *Cold Spring Harb Symp Quant Biol* 70(4):129–137.
20. Hezel AF, Kimmelman AC, Stanger BZ, Bardeesy N, Depinho RA (2006) Genetics and biology of pancreatic ductal adenocarcinoma Genetics and biology of pancreatic ductal adenocarcinoma. *Genes Dev* 1(30):355–385.
21. Hahn SA, Schutte M, Hoque AT, Moskaluk CA, da Costa LT, Rozenblum E, Weinstein CL, Fischer A, Yeo CJ, Hruban RH, Kern SE (1996) DPC4, a candidate tumor suppressor gene at human chromosome 18q21.1. *Science* 271(3):350–353.
22. Maitra A, Adsay NV, Argani P, Iacobuzio-Donahue C, De Marzo A, Cameron JL, Yeo CJ, Hruban RH (2003) Multicomponent analysis of the pancreatic adenocarcinoma progression model using a pancreatic intraepithelial neoplasia tissue microarray. *Mod Pathol* 16(9):902–912.
23. Fleming JB, Shen G-L, Holloway SE, Davis M, Brekken R a. (2005) Molecular consequences of silencing mutant K-ras in pancreatic cancer cells: justification for

K-ras-directed therapy. *Mol Cancer Res* 3(7):413–23.

24. Cox AD, Der CJ (2010) Ras history: The saga continues. *Small GTPases* 1(1):2–27.
25. Stephen AG, Esposito D, Bagni RG, McCormick F (2014) Dragging ras back in the ring. *Cancer Cell* 25(3):272–281.
26. Baccarini M (2005) Second nature: Biological functions of the Raf-1 "kinase." *FEBS Lett* 579(15):3271–3277.
27. Marais R, Light Y, Fpaterson H, Marshall CJ (1995) Ras recruits Raf-1 to the plasma membrane for activation by tyrosine phosphorylation. *EMBO J* 1413(13):3136–3145.
28. Rodriguez-Viciana P, Warne PH, Vanhaesebroeck1 B, Waterfield1l2 MD, Downward3 J (1996) Activation of phosphoinositide 3-kinase by interaction with Ras and by point mutation. *EMBO J* 15(10):2442–2451.
29. Vivanco I, Sawyers CL (2002) The phosphatidylinositol 3-Kinase–AKT pathway in human cancer. *Nat Rev Cancer* 2(7):489–501.
30. Baer R, Cintas C, Dufresne M, Cassant-Sourdy S, Schönhuber N, Planque L, Lulka H, Couderc B, Bousquet C, Garmy-Susini B, Vanhaesebroeck B, Pyronnet S, Saur D, Guillermet-Guibert J (2014) Pancreatic cell plasticity and cancer initiation induced by oncogenic Kras is completely dependent on wild-type PI 3-kinase p110α. *Genes Dev* 28(23):2621–2635.
31. Eser S, Reiff N, Messer M, Seidler B, Gottschalk K, Dobler M, Hieber M, Arbeiter A, Klein S, Kong B, Michalski CW, Schlitter AM, Esposito I, Kind AJ, Rad L, Schnieke AE, Baccarini M, Alessi DR, Rad R, Schmid RM, Schneider G, Saur D (2013) Selective requirement of PI3K/PDK1 signaling for kras oncogene-driven pancreatic cell plasticity and cancer. *Cancer Cell* 23(3):406–420.
32. Korc M, Chandrasekar B, Yamanaka Y, Friess H, Buchier M, Beger HG (1992) Overexpression of the epidermal growth factor receptor in human pancreatic cancer is associated with concomitant increases in the levels of epidermal growth factor and transforming growth factor alpha. *J Clin Invest* 90(4):1352–1360.
33. Li J, Kleeff J, Giese N, Buchler MW, Korc M, Friess H (2004) Gefitinib ('Iressa', ZD1839), a selective epidermal growth factor receptor tyrosine kinase inhibitor, inhibits pancreatic cancer cell growth, invasion, and colony formation. *Int J Oncol* 25(1):203–210.
34. Bruns CJ, Solorzano CC, Harbison MT, Ozawa S, Tsan R, Fan D, Abbruzzese J,

Traxler P, Buchdunger E, Radinsky R, Fidler IJ (2000) Blockade of the epidermal growth factor receptor signaling by a novel tyrosine kinase inhibitor leads to apoptosis of endothelial cells and therapy of human pancreatic carcinoma. *Cancer Res* 60(11):2926–2935.

35. Moore MJ, Goldstein D, Hamm J, Figer A, Hecht JR, Gallinger S, Au HJ, Murawa P, Walde D, Wolff RA, Campos D, Lim R, Ding K, Clark G, Voskoglou-Nomikos T, Ptasynski M, Parulekar W (2007) Erlotinib plus gemcitabine compared with gemcitabine alone in patients with advanced pancreatic cancer: A phase III trial of the National Cancer Institute of Canada Clinical Trials Group. *J Clin Oncol* 25(15):1960–1966.
36. Bergmann U, Funatomi H, Yokoyama M, Beger HG, Korc M (1995) Insulin-like growth factor I overexpression in human pancreatic cancer: evidence for autocrine and paracrine roles. *Cancer Res* 55(10):2007–2011.
37. Valsecchi ME, McDonald M, Brody JR, Hyslop T, Freydin B, Yeo CJ, Solomides C, Peiper SC, Witkiewicz AK (2012) Epidermal growth factor receptor and insulinlike growth factor 1 receptor expression predict poor survival in pancreatic ductal adenocarcinoma. *Cancer* 118(14):3484–3493.
38. Dong X, Javle M, Hess KR, Shroff R, Abbruzzese JL, Li D (2010) Insulin-like growth factor axis gene polymorphisms and clinical outcomes in pancreatic cancer. *Gastroenterology* 139(2):464–473.e3.
39. Hirakawa T, Yashiro M, Murata A, Hirata K, Kimura K, Amano R, Yamada N, Nakata B, Hirakawa K (2013) IGF-1 receptor and IGF binding protein-3 might predict prognosis of patients with resectable pancreatic cancer. *BMC Cancer* 13(1):392.
40. Baxter RC (2014) IGF binding proteins in cancer: Mechanistic and clinical insights. *Nat Rev Cancer* 14(5):329–341.
41. Cross MJ, Claesson-Welsh L (2001) FGF and VEGF function in angiogenesis: Signalling pathways, biological responses and therapeutic inhibition. *Trends Pharmacol Sci* 22(4):201–207.
42. Yamanaka Y, Friess H, Buchler M, Beger HG, Uchida E, Onda M, Kobrin MS, Korc M (1993) Overexpression of acidic and basic fibroblast growth factors in human pancreatic cancer correlates with advanced tumor stage. *Cancer Res* 53(21):5289–5296.
43. Gnatenko DA, Kopantsev EP, Sverdlov ED (2016) The Role of the Signaling

Pathway FGF/FGFR in Pancreatic Cancer. *ISSN Biochem (Moscow), Suppl Ser B Biomed Chem Orig Russ Text © Biomeditsinskaya Khimiya* 11(2):101–110.

44. Ferrara N, Gerber HP, LeCouter J (2003) The biology of VEGF and its receptors. *Nat Med* 9(6):669–676.
45. Seo Y, Baba H, Fukuda T, Takashima M, Sugimachi K (2000) High expression of vascular endothelial growth factor is associated with liver metastasis and a poor prognosis for patients with ductal pancreatic adenocarcinoma. *Cancer* 88(10):2239–2245.
46. Marschall Z Von, Cramer T, Höcker M, Burde R, Plath T, Schirner M, Heidenreich R, Breier G, Riecken E, Wiedenmann B, Rosewicz S (2000) De novo expression of vascular endothelial growth factor in human pancreatic cancer: Evidence for an autocrine mitogenic loop. *Gastroenterology* 119(5):1358–1372.
47. Ingham PW, McMahon AP (2001) Hedgehog signaling in animal development : paradigms and principles Hedgehog signaling in animal development : paradigms and principles. *Genes Dev* 15(23):3059–3087.
48. Thayer SP, Di Magliano MP, Heiser PW, Nielsen CM, Roberts DJ, Lauwers GY, Qi YP, Gysin S, Fernández-del Castillo C, Yajnik V, Antoniu B, McMahon M, Warshaw AL, Hebrok M (2003) Hedgehog is an early and late mediator of pancreatic cancer tumorigenesis. *Nature* 425(6960):851–856.
49. Tian H, Callahan CA, DuPree KJ, Darbonne WC, Ahn CP, Scales SJ, de Sauvage FJ (2009) Hedgehog signaling is restricted to the stromal compartment during pancreatic carcinogenesis. *Proc Natl Acad Sci* 106(11):4254–4259.
50. Olive KP, Jacobetz MA, Davidson CJ, Gopinathan A, McIntyre D, Honess D, Madhu B, Goldgraben MA, Caldwell ME, Allard D, Frese KK, DeNicola G, Feig C, Combs C, Winter SP, Ireland-Zecchini H, Reichelt S, Howat WJ, Chang A, Dhara M, Wang L, Ruckert F, Grutzmann R, Pilarsky C, Izeradjene K, Hingorani SR, Huang P, Davies SE, Plunkett W, Egorin M, Hruban RH, Whitebread N, McGovern K, Adams J, Iacobuzio-Donahue C, Griffiths J, Tuveson DA (2009) Inhibition of Hedgehog Signaling Enhances Delivery of Chemotherapy in a Mouse Model of Pancreatic Cancer. *Science (80-)* 324(5933):1457–1461.
51. Rhim AD, Oberstein PE, Thomas DH, Mirek ET, Palermo CF, Sastra SA, Dekleva EN, Saunders T, Becerra CP, Tattersall IW, Westphalen CB, Kitajewski J, Fernandez-Barrena MG, Fernandez-Zapico ME, Iacobuzio-Donahue C, Olive KP, Stanger BZ (2014) Stromal elements act to restrain, rather than support, pancreatic

ductal adenocarcinoma. *Cancer Cell* 25(6):735–747.

52. Lee JJ, Perera RM, Wang H, Wu D-C, Liu XS, Han S, Fitamant J, Jones PD, Ghanta KS, Kawano S, Nagle JM, Deshpande V, Boucher Y, Kato T, Chen JK, Willmann JK, Bardeesy N, Beachy PA (2014) Stromal response to Hedgehog signaling restrains pancreatic cancer progression. *Proc Natl Acad Sci* 111(30):E3091–E3100.
53. Zavadil J, Böttinger EP (2005) TGF-β and epithelial-to-mesenchymal transitions. *Oncogene* 24(37):5764–5774.
54. Krantz SB, Shields MA, Dangi-Garimella S, Munshi HG, Bentrem DJ (2012) Contribution of epithelial-to-mesenchymal transition and cancer stem cells to pancreatic cancer progression. *J Surg Res* 173(1):105–112.
55. Korc M (2007) Pancreatic cancer associated stroma production. *Am J Surg* 194(4 Supplement 1):s84–s86.
56. Sánchez-Elsner T, Botella LM, Velasco B, Corbí A, Attisano L, Bernabéu C (2001) Synergistic Cooperation between Hypoxia and Transforming Growth Factor-β Pathways on Human Vascular Endothelial Growth Factor Gene Expression. *J Biol Chem* 276(42):38527–38535.
57. Darnell J, Kerr I, Stark G (1994) Jak-STAT pathways and transcriptional activation in response to IFNs and other extracellular signaling proteins. *Science (80-)* 264(5164):1415–1421.
58. Zhong Z, Wen Z, Darnell JE (1994) Stat3: a STAT family member activated by tyrosine phosphorylation in response to epidermal growth factor and interleukin-6. *Science* 264(5155):95–98.
59. Bao S, Tang F, Li X, Hayashi K, Gillich A, Lao K, Surani MA (2009) Epigenetic reversion of post-implantation epiblast to pluripotent embryonic stem cells. *Nature* 461(7268):1292–1295.
60. Scholz A, Heinze S, Detjen KM, Peters M, Welzel M, Hauff P, Schirner M, Wiedenmann B, Rosewicz S (2003) Activated signal transducer and activator of transcription 3 (STAT3) supports the malignant phenotype of human pancreatic cancer. *Gastroenterology* 125(3):891–905.
61. Nagathihalli NS, Castellanos JA, Shi C, Beesetty Y, Reyzer ML, Caprioli R, Chen X, Walsh AJ, Skala MC, Moses HL, Merchant NB (2015) Signal Transducer and Activator of Transcription 3, Mediated Remodeling of the Tumor Microenvironment Results in Enhanced Tumor Drug Delivery in a Mouse Model

of Pancreatic Cancer. *Gastroenterology* 149(7):1932–1943.

62. Lee J-Y, Hennighausen L (2005) The transcription factor Stat3 is dispensable for pancreatic β-cell development and function. *Biochem Biophys Res Commun* 334(3):764–768.
63. Wei D, Le X, Zheng L, Wang L, Frey JA, Gao AC, Peng Z, Huang S, Xiong HQ, Abbruzzese JL, Xie K (2003) Stat3 activation regulates the expression of vascular endothelial growth factor and human pancreatic cancer angiogenesis and metastasis. *Oncogene* 22(3):319–329.
64. Corcoran RB, Contino G, Deshpande V, Tzatsos A, Conrad C, Benes CH, Settleman J, Engelman JA (2013) STAT3 plays a critical role in KRAS-induced pancreatic tumorigenesis. *Cancer Res* 71(14):5020–5029.
65. Mace TA, Ameen Z, Collins A, Wojcik S, Mair M, Young GS, Fuchs JR, Eubank TD, Frankel WL, Bekaii-Saab T, Bloomston M, Lesinski GB (2013) Pancreatic cancer-associated stellate cells promote differentiation of myeloid-derived suppressor cells in a StAT3-dependent manner. *Cancer Res* 73(10):3007–3018.
66. Lesina M, Kurkowski MU, Ludes K, Rose-John S, Treiber M, Klöppel G, Yoshimura A, Reindl W, Sipos B, Akira S, Schmid RM, Algül H (2011) Stat3/Socs3 Activation by IL-6 Transsignaling Promotes Progression of Pancreatic Intraepithelial Neoplasia and Development of Pancreatic Cancer. *Cancer Cell* 19(4):456–469.
67. Grivennikov SI, Greten FR, Karin M (2010) Immunity, inflammation, and cancer. *Cell* 140(6):883–899.
68. Kopper L, Zalatnai A, Timar J (2005) Genomics of pancreatic cancer: does it make any improvement in diagnosis, prognosis and therapy? *Pathol Oncol Res* 11(2):69–73.
69. Ling J, Kang Y, Zhao R, Xia Q, Lee DF, Chang Z, Li J, Peng B, Fleming JB, Wang H, Liu J, Lemischka IR, Hung MC, Chiao PJ (2012) KrasG12D-Induced IKK2/β/NF-κB Activation by IL-1α and p62 Feedforward Loops Is Required for Development of Pancreatic Ductal Adenocarcinoma. *Cancer Cell* 21(1):105–120.
70. Chow JYC, Ban M, Wu HL, Nguyen F, Huang M, Chung H, Dong H, Carethers JM (2010) TGF-ß downregulates PTEN via activation of NF-κB in pancreatic cancer cells. *Am J Physiol Gastrointest Liver Physiol* 298(11):275–282.
71. Collisson EA, Sadanandam A, Olson P, Gibb WJ, Truitt M, Gu S, Cooc J, Weinkle J, Kim GE, Jakkula L, Feiler HS, Ko AH, Olshen AB, Danenberg KL, Tempero

MA, Spellman PT, Hanahan D, Gray JW (2011) Subtypes of pancreatic ductal adenocarcinoma and their differing responses to therapy. *Nat Med* 17(4):500–503.

72. Moffitt RA, Marayati R, Flate EL, Volmar KE, Loeza SGH, Hoadley KA, Rashid NU, Williams LA, Eaton SC, Chung AH, Smyla JK, Anderson JM, Kim HJ, Bentrem DJ, Talamonti MS, Iacobuzio-Donahue CA, Hollingsworth MA, Yeh JJ (2015) Virtual microdissection identifies distinct tumor- and stroma-specific subtypes of pancreatic ductal adenocarcinoma. *Nat Genet* 47(10):1168–1178.
73. Bailey P, Chang DK, Nones K, Johns AL, Patch AM, Gingras MC, Miller DK, Grimmond SM, et al. (2016) Genomic analyses identify molecular subtypes of pancreatic cancer. *Nature* 531(7592):47–52.
74. David P. Ryan, M.D., Theodore S. Hong, M.D., and Nabeel Bardeesy P., Ryan DP, Hong TS, Bardeesy N (2014) Pancreatic Adenocarcinoma. *N Engl J Med* 371(11):1039–1049.
75. Passero FC, Saif MW (2017) *Second line treatment options for pancreatic cancer* doi:10.1080/14656566.2017.1369955.
76. Burris Iii HA, Moore MJ, Andersen J, Green MR, Rothenberg ML, Modiano MR, Cripps MC, Portenoy RK, Storniolo AM, Tarassoff P, Nelson R, Dorr FA, Stephens CD, Von Hoff DD (1997) Improvements in survival and clinical benefit with gemcitabine as first- line therapy for patients with advanced pancreas cancer: A randomized trial. *J Clin Oncol* 15(6):2403–2413.
77. Conroy T, Desseigne F, Ychou M, Bouché O, Guimbaud R, Bécouarn Y, Adenis A, Raoul J-L, Gourgou-Bourgade S, de la Fouchardière C, Bennouna J, Bachet J-B, Khemissa-Akouz F, Péré-Vergé D, Delbaldo C, Assenat E, Chauffert B, Michel P, Montoto-Grillot C, Ducreux M (2011) FOLFIRINOX versus Gemcitabine for Metastatic Pancreatic Cancer. *N Engl J Med* 364(19):1817–1825.
78. Zeitouni D, Pylayeva-Gupta Y, Der CJ, Bryant KL (2016) KRAS mutant pancreatic cancer: No lone path to an effective treatment. *Cancers (Basel)* 8(4):1–22.
79. Mirzoeva OK, Collisson EA, Schaefer PM, Hann B, Hom YK, Ko AH, Korn WM (2013) Subtype-Specific MEK-PI3 Kinase Feedback as a Therapeutic Target in Pancreatic Adenocarcinoma. *Mol Cancer Ther* 12(10):2213–2225.
80. Fuchs CS, Azevedo S, Okusaka T, Van Laethem J-L, Lipton LR, Riess H, Szczylik C, Moore MJ, Peeters M, Bodoky G, Ikeda M, Melichar B, Nemecek R, Ohkawa S, Świeboda-Sadlej A, Tjulandin SA, Van Cutsem E, Loberg R, Haddad V,

Gansert JL, Bach BA, Carrato A (2015) A phase 3 randomized, double-blind, placebo-controlled trial of ganitumab or placebo in combination with gemcitabine as first-line therapy for metastatic adenocarcinoma of the pancreas: the GAMMA trial†. *Ann Oncol* 26(5):921–927.

81. Hurwitz HI, Uppal N, Wagner SA, Bendell JC, Beck JT, Wade SM, Nemunaitis JJ, Stella PJ, Pipas JM, Wainberg ZA, Manges R, Garrett WM, Hunter DS, Clark J, Leopold L, Sandor V, Levy RS (2015) Randomized, double-blind, phase II study of ruxolitinib or placebo in combination with capecitabine in patients with metastatic pancreatic cancer for whom therapy with gemcitabine has failed. *J Clin Oncol* 33(34):4039–4047.
82. Narayanan V, Weekes CD (2016) Molecular therapeutics in pancreas cancer. *World J Gastrointest Oncol* 8(4):366–379.
83. Thomas AM, Santarsiero LM, Lutz ER, Armstrong TD, Chen Y-C, Huang L-Q, Laheru DA, Goggins M, Hruban RH, Jaffee EM (2004) Mesothelin-specific CD8 $^{+}$ T Cell Responses Provide Evidence of In Vivo Cross-Priming by Antigen-Presenting Cells in Vaccinated Pancreatic Cancer Patients. *J Exp Med* 200(3):297–306.
84. Royal RE, Levy C, Turner K, Mathur A, Hughes M, Kammula US, Sherry RM, Topalian SL, Yang JC, Lowy I, Rosenberg SA (2010) Phase 2 trial of single agent ipilimumab (Anti-CTLA-4) for locally advanced or metastatic pancreatic adenocarcinoma. *J Immunother* 33(8):828–833.
85. Zheng L, Jr LAD, Donehower RC, Jaffee EM (2014) Previously Treated Pancreatic Cancer. 36(7):382–389.
86. Brahmer JR, Tykodi SS, Chow LQ, Hwu WJ, Topalian SL, Hwu P, Drake CG, Camacho LH, Kauh J, Odunsi K, Pitot HC, Hamid O, Bhatia S, Martins R, Eaton K, Chen S, Salay TM, Alaparthy S, Grosso JF, Korman AJ, Parker SM, Agrawal S, Goldberg SM, Pardoll DM, Gupta A, Wigginton JM (2012) Safety and activity of anti-PD-L1 antibody in patients with advanced cancer. *N Engl J Med* 366(1533–4406 (Electronic)):2455–2465.
87. Feig C, Jones JO, Kraman M, Wells RJB, Deonarine A, Chan DS, Connell CM, Roberts EW, Zhao Q, Caballero OL, Teichmann SA, Janowitz T (2013) Targeting CXCL12 from FAP-expressing carcinoma- associated fibroblasts synergizes with anti – PD-L1 immunotherapy in pancreatic cancer. *Proc Natl Acad Sci U S A* 110(50):20212–20217.

88. Kiss K, Baghy K, Spisák S, Szanyi S, Tulassay Z, Zalatnai A, Löhr JM, Jesenofsky R, Kovalszky I, Firneisz G (2015) Chronic hyperglycemia induces trans-differentiation of human pancreatic stellate cells and enhances the malignant molecular communication with human pancreatic cancer cells. *PLoS One* 10(5):1–18.

89. Pérez-Mancera P a, Guerra C, Barbacid M, Tuveson D a (2012) What we have learned about pancreatic cancer from mouse models. *Gastroenterology* 142(5):1079–1092.

90. Hingorani SR, Petricoin EF, Maitra A, Rajapakse V, King C, Jacobetz MA, Ross S, Conrads TP, Veenstra TD, Hitt BA, Kawaguchi Y, Johann D, Liotta LA, Crawford HC, Putt ME, Jacks T, Wright CVE, Hruban RH, Lowy AM, Tuveson DA (2003) Preinvasive and invasive ductal pancreatic cancer and its early detection in the mouse. *Cancer Cell* 4(6):437–450.

91. Guerra C, Mijimolle N, Dhawahir A, Dubus P, Barradas M, Serrano M, Campuzano V, Barbacid M (2003) Tumor induction by an endogenous K-ras oncogene is highly dependent on cellular context. *Cancer Cell* 4(2):111–120.

92. Guerra C, Schuhmacher AJ, Cañamero M, Grippo PJ, Verdaguer L, Pérez-Gallego L, Dubus P, Sandgren EP, Barbacid M (2007) Chronic Pancreatitis Is Essential for Induction of Pancreatic Ductal Adenocarcinoma by K-Ras Oncogenes in Adult Mice. *Cancer Cell* 11(3):291–302.

93. Guerra C. BM (2012) Genetically engineered mouse models of pancreatic cancer. *Cancer J* 18(6):502–510.

94. Hingorani SR, Wang L, Multani AS, Combs C, Deramaudt TB, Hruban RH, Rustgi AK, Chang S, Tuveson DA (2005) Trp53R172H and KrasG12D cooperate to promote chromosomal instability and widely metastatic pancreatic ductal adenocarcinoma in mice. *Cancer Cell* 7(5):469–483.

95. Navas C, Hernández-Porras I, Schuhmacher AJ, Sibilia M, Guerra C, Barbacid M (2012) EGF Receptor Signaling Is Essential for K-Ras Oncogene-Driven Pancreatic Ductal Adenocarcinoma. *Cancer Cell* 22(3):318–330.

96. Ardito CM, Grüner BM, Takeuchi KK, Lubeseder-Martellato C, Teichmann N, Mazur PK, DelGiorno KE, Carpenter ES, Halbrook CJ, Hall JC, Pal D, Briel T, Herner A, Trajkovic-Arsic M, Sipos B, Liou GY, Storz P, Murray NR, Threadgill DW, Sibilia M, Washington MK, Wilson CL, Schmid RM, Raines EW, Crawford HC, Siveke JT (2012) EGF Receptor Is Required for KRAS-Induced Pancreatic

Tumorigenesis. *Cancer Cell* 22(3):304–317.

97. Schönhuber N, Seidler B, Schuck K, Veltkamp C, Schachtler C, Zukowska M, Eser S, Feyerabend TB, Paul MC, Eser P, Klein S, Lowy AM, Banerjee R, Yang F, Lee CL, Moding EJ, Kirsch DG, Scheideler A, Alessi DR, Varela I, Bradley A, Kind A, Schnieke AE, Rodewald HR, Rad R, Schmid RM, Schneider G, Saur D (2014) A next-generation dual-recombinase system for time- and host-specific targeting of pancreatic cancer. *Nat Med* 20(11):1340–1347.
98. Tlsty TD, Coussens LM (2006) Tumor stroma and regulation of cancer development. *Annu Rev Pathol* 1:119–150.
99. Hanahan D, Coussens LM (2012) Accessories to the crime: functions of cells recruited to the tumor microenvironment. *Cancer Cell* 21(3):309–322.
100. De Visser KE, Eichten A, Coussens LM (2006) Paradoxical roles of the immune system during cancer development. *Nat Rev Cancer* 6(1):24–37.
101. Pollard JW (2004) Opinion: Tumour-educated macrophages promote tumour progression and metastasis. *Nat Rev Cancer* 4(1):71–78.
102. Condeelis J, Pollard JW (2006) Macrophages: Obligate partners for tumor cell migration, invasion, and metastasis. *Cell* 124(2):263–266.
103. Nielsen SR, Quaranta V, Linford A, Emeagi P, Rainer C, Santos A, Ireland L, Sakai T, Sakai K, Kim Y-S, Engle D, Campbell F, Palmer D, Ko JH, Tuveson D a, Hirsch E, Mielgo A, Schmid MC (2016) Macrophage-secreted granulin supports pancreatic cancer metastasis by inducing liver fibrosis. *Nat Cell Biol* 18(5):549–560.
104. Mantovani A, Marchesi F, Malesci A, Laghi L, Allavena P (2017) Tumour-associated macrophages as treatment targets in oncology. *Nat Rev Clin Oncol* 14(7):399–416.
105. Bandyopadhyay K, Marrero I, Kumar V (2016) NKT cell subsets as key participants in liver physiology and pathology. *Cell Mol Immunol* 13(3):337–346.
106. Ali HR, Chlon L, Pharoah PDP, Markowetz F, Caldas C, Breast H, Invasion C, Infiltration IC, DeNardo DG, Coussens LM, Dushyanthen S, Beavis PA, Savas P, Teo ZL, Zhou C, Mansour M, Darcy PK, Loi S, Gajewski TF, Schreiber H, Fu Y-X, Hamby ME, Hoyt MA, Martin JL, Robles TF, Sloan K, Thomas KS, Irwin MR, Man Y, Stojadinovic A, Mason J, Avital I, Bilchik A, Bruecher B (2015) Innate and adaptive immune cells in the tumor microenvironment. *Nat Immunol* 13(10):1014–1022.

107. Spurrell EL, Lockley M (2014) Adaptive immunity in cancer immunology and therapeutics. *Ecancermedicalscience* 8(1):1–10.
108. Swann JB, Smyth MJ (2007) Review series Immune surveillance of tumors. *J Clin Invest* 117(5):1137–1146.
109. Vesely MD, Kershaw MH, Schreiber RD, Smyth MJ (2011) Natural Innate and Adaptive Immunity to Cancer. *Annu Rev Immunol* 29(1):235–271.
110. Gallimore A, Godkin A (2008) Regulatory T cells and tumour immunity - Observations in mice and men. *Immunology* 123(2):157–163.
111. Martin-orozco N, Muranski P, Chung Y, Yang XO, Lu S, Hwu P, Restifo NP, Overwijk WW, Dong C (2010) Th17 cells promote cytotoxic T cell activation in tumor immunity. *Immunity* 31(5):787–798.
112. Michot JM, Bigenwald C, Champiat S, Collins M, Carbonnel F, Postel-Vinay S, Berdelou A, Varga A, Bahleda R, Hollebecque A, Massard C, Fuerea A, Ribrag V, Gazzah A, Armand JP, Amellal N, Angevin E, Noel N, Boutros C, Mateus C, Robert C, Soria JC, Marabelle A, Lambotte O (2016) Immune-related adverse events with immune checkpoint blockade: A comprehensive review. *Eur J Cancer* 54:139–148.
113. Folkman J (2003) Fundamental concepts of the angiogenic process. *Curr Mol Med* 3(7):643–651.
114. De Bock K, Cauwenberghs S, Carmeliet P (2011) Vessel abnormalization: another hallmark of cancer?Molecular mechanisms and therapeutic implications. *Curr Opin Genet Dev* 21(1):73–79.
115. Palma M De, Coussens LM (2008) Immune Cells and Inflammatory Mediators as Regulators of Tumor Angiogenesis. *Angiogenesis*:225–237.
116. Stockmann C, Schadendorf D, Klose R, Helfrich I (2014) The Impact of the Immune System on Tumor: Angiogenesis and Vascular Remodeling. *Front Oncol* 4(April):1–13.
117. Bergers G, Brekken R, Mcmahon G, Vu TH, Itoh T, Tamaki K, Tanzawa K, Thorpe P, Itohara S, Hanahan D (2010) Matrix metalloproteinase-9 triggers the angiogenic switch during carcinogenesis. *Nat Cell Biol* 2(10):737–744.
118. Rolny C, Mazzone M, Tugues S, Laoui D, Johansson I, Coulon C, Squadrito ML, Segura I, Li X, Knevels E, Costa S, Vinckier S, Dresselaer T, Åkerud P, De Mol M, Salomäki H, Phillipson M, Wyns S, Larsson E, Buysschaert I, Botling J, Himmelreich U, Van Ginderachter JA, De Palma M, Dewerchin M, Claesson-

Welsh L, Carmeliet P (2011) HRG inhibits tumor growth and metastasis by inducing macrophage polarization and vessel normalization through downregulation of PlGF. *Cancer Cell* 19(1):31–44.

119. Nozawa H, Chiu C, Hanahan D (2006) Infiltrating neutrophils mediate the initial angiogenic switch in a mouse model of multistage carcinogenesis. *Proc Natl Acad Sci* 103(33):12493–12498.
120. Crawford Y, Kasman I, Yu L, Zhong C, Wu X, Modrusan Z, Kaminker J, Ferrara N (2009) PDGF-C Mediates the Angiogenic and Tumorigenic Properties of Fibroblasts Associated with Tumors Refractory to Anti-VEGF Treatment. *Cancer Cell* 15(1):21–34.
121. Bosman FT, Stamenkovic I (2003) Functional structure and composition of the extracellular matrix. *J Pathol* 200(4):423–428.
122. Hynes RO (2009) Extracellular matrix: not just prety fibrils. *Science* 326(5957):1216–1219.
123. Wozniak MA, Desai R, Solski PA, Der CJ, Keely PJ (2003) ROCK-generated contractility regulates breast epithelial cell differentiation in response to the physical properties of a three-dimensional collagen matrix. *J Cell Biol* 163(3):583–595.
124. Provenzano PP, Cuevas C, Chang AE, Goel VK, Von Hoff DD, Hingorani SR (2012) Enzymatic Targeting of the Stroma Ablates Physical Barriers to Treatment of Pancreatic Ductal Adenocarcinoma. *Cancer Cell* 21(3):418–429.
125. Lu P, Weaver VM, Werb Z (2012) The extracellular matrix: A dynamic niche in cancer progression. *J Cell Biol* 196(4):395–406.
126. Ruiter D, Bogenrieder T, Elder D, Herlyn M (2002) Melanoma-stroma interactions: structural and functional aspects. *Lancet Oncol* 3(1):35–43.
127. Kalluri R (2016) The biology and function of fibroblasts in cancer. *Nat Rev Cancer* 16(9):582–598.
128. Dvorak HF (1986) Tumors: wounds that do not heal. Similarities between tumor stroma generation and wound healing. *N Engl J Med* 315(26):1650–9.
129. Tomasek JJ, Gabbiani G, Hinz B, Chaponnier C, Brown RA (2002) Myofibroblasts and mechano: Regulation of connective tissue remodelling. *Nat Rev Mol Cell Biol* 3(5):349–363.
130. Öhlund D, Elyada E, Tuveson D (2014) Fibroblast heterogeneity in the cancer wound. *J Exp Med* 211(8):1503–1523.

131. Neesse A, Michl P, Frese KK, Feig C, Cook N, Jacobetz M a, Lolkema MP, Buchholz M, Olive KP, Gress TM, Tuveson D a (2011) Stromal biology and therapy in pancreatic cancer. *Gut* 60(6):861–868.
132. Desmoulière A, Chaponnier C, Gabbiani G (2005) Tissue repair, contraction, and the myofibroblast. *Wound Repair Regen* 13(1):7–12.
133. Hawinkels LJAC, Paauwe M, Verspaget HW, Wiercinska E, Van Der Zon JM, Van Der Ploeg K, Koelink PJ, Lindeman JHN, Mesker W, Ten Dijke P, Sier CFM (2014) Interaction with colon cancer cells hyperactivates TGF-β signaling in cancer-associated fibroblasts. *Oncogene* 33(1):97–107.
134. Paland N, Kamer I, Kogan-Sakin I, Madar S, Goldfinger N, Rotter V (2009) Differential Influence of Normal and Cancer-Associated Fibroblasts on the Growth of Human Epithelial Cells in an In vitro Cocultivation Model of Prostate Cancer. *Mol Cancer Res* 7(8):1212–1223.
135. Berdiel-Acer M, Sanz-Pamplona R, Calon A, Cuadras D, Berenguer A, Sanjuan X, Paules MJ, Salazar R, Moreno V, Batlle E, Villanueva A, Molleví DG (2014) Differences between CAFs and their paired NCF from adjacent colonic mucosa reveal functional heterogeneity of CAFs, providing prognostic information. *Mol Oncol* 8(7):1290–1305.
136. Zhang J, Chen L, Liu X, Kammertoens T, Blankenstein T, Qin Z (2013) Fibroblast-specific protein 1/S100A4-positive cells prevent carcinoma through collagen production and encapsulation of carcinogens. *Cancer Res* 73(9):2770–2781.
137. Feig C, Jones JO, Kraman M, Wells RJB, Deonarine A, Chan DS, Connell CM, Roberts EW, Zhao Q, Caballero OL, Teichmann S a, Janowitz T, Jodrell DI, Tuveson DA, Fearon DT (2013) Targeting CXCL12 from FAP-expressing carcinoma-associated fibroblasts synergizes with anti-PD-L1 immunotherapy in pancreatic cancer. *Proc Natl Acad Sci U S A* 110(50):20212–20217.
138. Cuttler AS, Leclair RJ, Stohn JP, Wang Q, Sorenson CM, Liaw L, Lindner V (2011) Characterization of Pdgfrb-Cre transgenic mice reveals reduction of ROSA26 reporter activity in remodeling arteries. *Genesis* 49(8):673–680.
139. Weissmueller S, Manchado E, Saborowski M, Iv JPM, Wagenblast E, Davis CA, Moon S, Pfister NT, Darjus F, Kitzing T, Aust D, Markert EK, Wu J, Sean M, Pilarsky C, Prives C, Biankin A V, Scott W (2014) Mutant p53 drives pancreatic cancer metastasis through cell- autonomous PDGF receptor beta signaling. *Cell* 157(2):382–394.

140. Erez N, Truitt M, Olson P, Hanahan D (2010) Cancer-Associated Fibroblasts Are Activated in Incipient Neoplasia to Orchestrate Tumor-Promoting Inflammation in an NF-κB-Dependent Manner. *Cancer Cell* 17(2):135–147.
141. Demoulin J-B, Montano-Almendras CP (2012) Platelet-derived growth factors and their receptors in normal and malignant hematopoiesis. *Am J Blood Res* 2(1):44–56.
142. Farahani RM, Xaymardan M (2015) Platelet-Derived Growth Factor Receptor Alpha as a Marker of Mesenchymal Stem Cells in Development and Stem Cell Biology. *Stem Cells Int* 2015:1–8.
143. Jechlinger M, Sommer A, Moriggl R, Seither P, Kraut N, Capodiecci P, Donovan M, Cordon-Cardo C, Beug H, Grünert S (2006) Autocrine PDGFR signaling promotes mammary cancer metastasis. *J Clin Invest* 116(6):1561–1570.
144. Spaeth EL, Dembinski JL, Sasser AK, Watson K, Klopp A, Hall B, Andreeff M, Marini F (2009) Mesenchymal stem cell transition to tumor-associated fibroblasts contributes to fibrovascular network expansion and tumor progression. *PLoS One* 4(4).e4992.
145. Fullár A, Dudás J, Oláh L, Hollósi P, Papp Z, Sobel G, Karászi K, Paku S, Baghy K, Kovalszky I (2015) Remodeling of extracellular matrix by normal and tumor-associated fibroblasts promotes cervical cancer progression. *BMC Cancer* 15(1):256.
146. Chaffer CL, Weinberg RA (2011) A Perspective on Cancer Cell Metastasis. *Science (80-)* 331(6024):1559–1564.
147. Dirat B, Bochet L, Dabek M, Daviaud D, Dauvillier S, Majed B, Wang YY, Meulle A, Salles B, Le Gonidec S, Garrido I, Escourrou G, Valet P, Muller C (2011) Cancer-associated adipocytes exhibit an activated phenotype and contribute to breast cancer invasion. *Cancer Res* 71(7):2455–2465.
148. Zhang D, Wang Y, Shi Z, Liu J, Sun P, Hou X, Zhang J, Zhao S, Zhou BP, Mi J (2015) Metabolic Reprogramming of Cancer-Associated Fibroblasts by IDH3α Downregulation. *Cell Rep* 10(8):1335–1348.
149. Bissell MJ, Hines WC (2011) Why don't we get more cancer? A proposed role of the microenvironment in restraining cancer progression. *Nat Med* 17(3):320–329.
150. Flaberg E, Markasz L, Petranyi G, Stuber G, Dicså F, Alchihabi N, Oláh É, Csízy I, Józsa T, Andrén O, Johansson JE, Andersson SO, Klein G, Szekely L (2011) High-throughput live-cell imaging reveals differential inhibition of tumor cell

proliferation by human fibroblasts. *Int J Cancer* 128(12):2793–2802.

151. Olive KP, Jacobetz M a, Davidson CJ, Gopinathan A, McIntyre D, Honess D, Madhu B, Goldgraben M a, Caldwell ME, Allard D, Frese KK, DeNicola G, Feig C, Combs C, Winter SP, Ireland-Zecchini H, Reichelt S, Howat WJ, Chang A, Dhara M, Wang L, Rückert F, Grützmann R, Pilarsky C, Izeradjene K, Hingorani SR, Huang P, Davies SE, Plunkett W, Egorin M, Hruban RH, Whitebread, N, McGovern K, Adams J, Iacobuzio-Donahue C, Griffiths J, Tuveson D a (2009) Inhibition of Hedgehog Signaling. *Science (80-)* 324(5933):1457–1461.
152. Neesse A, Algül H, Tuveson DA, Gress TM (2015) Stromal biology and therapy in pancreatic cancer: a changing paradigm. *Gut* 64(9):1476–1484.
153. Weizman N, Krelin Y, Shabtay-Orbach a, Amit M, Binenbaum Y, Wong RJ, Gil Z (2014) Macrophages mediate gemcitabine resistance of pancreatic adenocarcinoma by upregulating cytidine deaminase. *Oncogene* 33(29):3812–3819.
154. Zhu Y, Herndon JM, Sojka DK, Kim KW, Knolhoff BL, Zuo C, Cullinan DR, Luo J, Bearden AR, Lavine KJ, Yokoyama WM, Hawkins WG, Fields RC, Randolph GJ, DeNardo DG (2017) Tissue-Resident Macrophages in Pancreatic Ductal Adenocarcinoma Originate from Embryonic Hematopoiesis and Promote Tumor Progression. *Immunity* 47(2):323–338.e6.
155. Bachem MG, Schneider E, Groß H, Weidenbach H, Schmid RM, Menke A, Siech M, Beger H, Grünert A, Adler G (1998) Identification, culture, and characterization of pancreatic stellate cells in rats and humans. *Gastroenterology* 115(2):421–432.
156. Kordes C, Sawitza I, Häussinger D (2009) Hepatic and pancreatic stellate cells in focus. *Biol Chem* 390(10):1003–1012.
157. Apte M V, Haber PS, Applegate TL, Norton ID, Mccaughan GW, Korsten MA, Pirola RC, Wilson JS (1998) Periacinar stellate shaped cells in rat pancreas: identification, isolation, and culture. *Gut* 43:128–133.
158. Erkan M, Adler G, Apte M V., Bachem MG, Buchholz M, Detlefsen S, Esposito I, Friess H, Gress TM, Habisch HJ, Hwang RF, Jaster R, Kleeff J, Klöppel G, Kordes C, Logsdon CD, Masamune A, Michalski CW, Oh J, Phillips PA, Pinzani M, Reiser-Erkan C, Tsukamoto H, Wilson J (2012) StellaTUM: Current consensus and discussion on pancreatic stellate cell research. *Gut* 61(2):172–178.
159. Haber PS, Keogh GW, Apte M V., Moran CS, Stewart NL, Crawford DHG, Pirola

RC, McCaughan GW, Ramm GA, Wilson JS (1999) Activation of Pancreatic Stellate Cells in Human and Experimental Pancreatic Fibrosis. *Am J Pathol* 155(4):1087–1095.

160. Froeling FEM, Feig C, Chelala C, Dobson R, Mein CE, Tuveson DA, Clevers H, Hart IR, Kocher HM (2011) Retinoic acid-induced pancreatic stellate cell quiescence reduces paracrine Wntβ-catenin signaling to slow tumor progression. *Gastroenterology* 141(4):1486–1497.e14.
161. Ikenaga N, Ohuchida K, Mizumoto K, Cui L, Kayashima T, Morimatsu K, Moriyama T, Nakata K, Fujita H, Tanaka M (2010) CD10+ pancreatic stellate cells enhance the progression of pancreatic cancer. *Gastroenterology* 139(3):1041–1051.e8.
162. Öhlund D, Handly-Santana A, Biffi G, Elyada E, Almeida AS, Ponz-Sarvise M, Corbo V, Oni TE, Hearn SA, Lee EJ, Chio IIC, Hwang C-I, Tiriac H, Baker LA, Engle DD, Feig C, Kultti A, Egeblad M, Fearon DT, Crawford JM, Clevers H, Park Y, Tuveson DA (2017) Distinct populations of inflammatory fibroblasts and myofibroblasts in pancreatic cancer. *J Exp Med* 214(3):579–596.
163. Jacobetz MA, Chan DS, Neesse A, Bapiro TE, Cook N, Frese KK, Feig C, Nakagawa T, Caldwell ME, Zecchini HI, Lolkema MP, Jiang P, Kultti A, Thompson CB, Maneval DC, Jodrell DI, Frost GI, Shepard HM, Skepper JN, Tuveson DA (2013) Hyaluronan impairs vascular function and drug delivery in a mouse model of pancreatic cancer. *Gut* 62(1):112–120.
164. Von Hoff DD, Ramanathan RK, Borad MJ, Laheru DA, Smith LS, Wood TE, Korn RL, Desai N, Trieu V, Iglesias JL, Zhang H, Soon-Shiong P, Shi T, Rajeshkumar N V., Maitra A, Hidalgo M (2011) Gemcitabine plus nab-paclitaxel is an active regimen in patients with advanced pancreatic cancer: A phase I/II trial. *J Clin Oncol* 29(34):4548–4554.
165. Frese KK, Neesse A, Cook N, Bapiro TE, Lolkema MP, Jodrell DI, Tuveson DA (2012) Nab-paclitaxel potentiates gemcitabine activity by reducing cytidine deaminase levels in a mouse model of pancreatic cancer. *Cancer Discov* 2(3):260–269.
166. Neesse A, Frese KK, Chan DS, Bapiro TE, Howat WJ, Richards FM, Ellenrieder V, Jodrell DI, Tuveson DA (2014) SPARC independent drug delivery and antitumour effects of nab-paclitaxel in genetically engineered mice. *Gut* 63(6):974–983.

167. Hessmann E, Patzak MS, Klein L, Chen N, Kari V, Ramu I, Bapiro TE, Frese KK, Gopinathan A, Richards FM, Jodrell DI, Verbeke C, Li X, Heuchel R, Löhr JM, Johnsen SA, Gress TM, Ellenrieder V, Neesse A (2017) Fibroblast drug scavenging increases intratumoural gemcitabine accumulation in murine pancreas cancer. *Gut* 67(3):497–507.

168. Neesse A, Frese KK, Bapiro TE, Nakagawa T, Sternlicht MD, Seeley TW, Pilarsky C, Jodrell DI, Spong SM, Tuveson DA (2013) CTGF antagonism with mAb FG-3019 enhances chemotherapy response without increasing drug delivery in murine ductal pancreas cancer. *Proc Natl Acad Sci* 110(30):12325–12330.

169. Steele CW, Karim SA, Leach JDG, Bailey P, Upstill-Goddard R, Rishi L, Foth M, Bryson S, McDaid K, Wilson Z, Eberlein C, Candido JB, Clarke M, Nixon C, Connelly J, Jamieson N, Carter CR, Balkwill F, Chang DK, Evans TRJ, Strathdee D, Biankin A V., Nibbs RJB, Barry ST, Sansom OJ, Morton JP (2016) CXCR2 Inhibition Profoundly Suppresses Metastases and Augments Immunotherapy in Pancreatic Ductal Adenocarcinoma. *Cancer Cell* 29(6):832–845.

170. Özdemir BC, Pentcheva-Hoang T, Carstens JL, Zheng X, Wu CC, Simpson TR, Laklai H, Sugimoto H, Kahlert C, Novitskiy S V., DeJesus-Acosta A, Sharma P, Heidari P, Mahmood U, Chin L, Moses HL, Weaver VM, Maitra A, Allison JP, LeBleu VS, Kalluri R (2014) Depletion of carcinoma-associated fibroblasts and fibrosis induces immunosuppression and accelerates pancreas cancer with reduced survival. *Cancer Cell* 25(6):719–734.

171. Doherty J, Cleveland J (2013) Targeting lactate metabolism for cancer therapeutics. *J Clin Invest* 123(9):3685–3692.

172. Larriba MJ, Ordóñez-Morán P, Chicote I, Martín-Fernández G, Puig I, Muñoz A, Pálmer HG (2011) Vitamin D receptor deficiency enhances Wnt/β-catenin signaling and tumor burden in colon cancer. *PLoS One* 6(8):e23524.

173. Sherman MH, Yu RT, Engle DD, Ding N, Atkins AR, Tiriac H, Collisson EA, Connor F, Van Dyke T, Kozlov S, Martin P, Tseng TW, Dawson DW, Donahue TR, Masamune A, Shimosegawa T, Apte M V., Wilson JS, Ng B, Lau SL, Gunton JE, Wahl GM, Hunter T, Drebin JA, O'Dwyer PJ, Liddle C, Tuveson DA, Downes M, Evans RM (2014) Vitamin D receptor-mediated stromal reprogramming suppresses pancreatitis and enhances pancreatic cancer therapy. *Cell* 159(1):80–93.

174. Haubeiss S, Schmid JO, Mürdter TE, Sonnenberg M, Friedel G, van der Kuip H,

Aulitzky WE (2010) Dasatinib reverses Cancer-associated Fibroblasts (CAFs) from primary Lung Carcinomas to a Phenotype comparable to that of normal Fibroblasts. *Mol Cancer* 9(168):1–8.

175. Malle E, Sodin-Semrl S, Kovacevic A (2009) Serum amyloid A: An acute-phase protein involved in tumour pathogenesis. *Cell Mol Life Sci* 66(1):9–26.
176. Uhlar CM, Whitehead AS (1999) Serum amyloid A, the major vertebrate acute-phase reactant. *Eur J Biochem* 265(2):501–523.
177. Manley PN, Ancsin JB, Kisilevsky R (2006) Rapid recycling of cholesterol: The joint biologic role of C-reactive protein and serum amyloid A. *Med Hypotheses* 66(4):784–792.
178. Malle E, Steinmetz A, Raynes JG (1993) Serum amyloid A (SAA): an acute phase protein and apolipoprotein. *Atherosclerosis* 102(2):131–146.
179. Strachans AF, Brandtb W, Wooll P, Westhuyzen DR Van Der, Coetzee GA, Beer MC De, Shephards EG, Beersjj FC De (1989) Human Serum Amyloid A Protein. 264(31):18368–18373.
180. Malle E, Sodin-Semrl S, Kovacevic A (2009) Serum amyloid A: An acute-phase protein involved in tumour pathogenesis. *Cell Mol Life Sci* 66(1):9–26.
181. Derebe MG, Zlatkov CM, Gattu S, Ruhn KA, Vaishnava S, Diehl GE, MacMillan JB, Williams NS, Hooper L V. (2014) Serum amyloid A is a retinol binding protein that transports retinol during bacterial infection. *Elife* 3:e03206.
182. Meek RL, Benditt EP (1986) Amyloid A gene family expression in different mouse tissues. *J Exp Med* 164(6):2006–2017.
183. Kluve-Beckerman B (1991) Nonexpression of the Human Serum Amyloid A Three SAA3 Genes. *DNA Cell Biol* 10(9):651–662.
184. Larson M (2003) Induction of human mammary-associated serum amyloid A3 expression by prolactin or lipopolysaccharide. *Biochem Biophys Res Commun* 301(4):1030–1037.
185. de Beer MC, Yuan T, Kindy MS, Asztalos BF, Roheim PS, de Beer FC (1995) Characterization of constitutive human serum amyloid A protein (SAA4) as an apolipoprotein. *J Lipid Res* 36(3):526–534.
186. Meek RL, Eriksen N, Benditt EP (1989) Serum amyloid A in the mouse. Sites of uptake and mRNA expression. *Am J Pathol* 135(2):411–419.
187. de Seny D, Cobraiville G, Charlier E, Neuville S, Esser N, Malaise D, Malaise O, Calvo FQ, Relic B, Malaise MG (2013) Acute-Phase Serum Amyloid A in

Osteoarthritis: Regulatory Mechanism and Proinflammatory Properties. *PLoS One* 8(6):e66769.

188. O'Hara R, Murphy EP, Whitehead AS, FitzGerald O, Bresnihan B (2000) Acute-phase serum amyloid A production by rheumatoid arthritis synovial tissue. *Arthritis Res* 2(2):142–144.
189. Meek RL, Eriksen N, Benditt EP (1992) Murine serum amyloid A3 is a high density apolipoprotein and is secreted by macrophages. *Proc Natl Acad Sci U S A* 89(17):7949–7952.
190. Kumon Y, Hosokawa T, Suehiro T, Ikeda Y, Sipe JD, Hashimoto K (2002) Acute-phase, but not constitutive serum amyloid A (SAA) is chemotactic for cultured human aortic smooth muscle cells. *Amyloid* 9(4):237–241.
191. Hansen MT, Forst B, Cremers N, Quagliata L, Ambartsumian N, Grum-Schwensen B, Klingelhöfer J, Abdul-Al a, Herrmann P, Osterland M, Stein U, Nielsen GH, Scherer PE, Lukanidin E, Sleeman JP, Grigorian M (2015) A link between inflammation and metastasis: serum amyloid A1 and A3 induce metastasis, and are targets of metastasis-inducing S100A4. *Oncogene* 34(4):425-435
192. Villapol S, Kryndushkin D, Balarezo MG, Campbell AM, Saavedra JM, Shewmaker FP, Symes AJ (2015) Hepatic Expression of Serum Amyloid A1 Is Induced by Traumatic Brain Injury and Modulated by Telmisartan. *Am J Pathol* 185(10):2641–2652.
193. De Buck M, Gouwy M, Wang JM, Van Snick J, Proost P, Struyf S, Van Damme J (2016) The cytokine-serum amyloid A-chemokine network. *Cytokine Growth Factor Rev* 30(8):55–69.
194. De Buck M, Gouwy M, Wang JM, Van Snick J, Opdenakker G, Struyf S, Van Damme J (2016) Structure and Expression of Different Serum Amyloid A (SAA) Variants and their Concentration-Dependent Functions During Host Insults. *Curr Med Chem* 23(17):1725–55.
195. Ren Y, Wang H, Lu D, Xie X, Chen X, Peng J, Hu Q, Shi G, Liu S (2014) Expression of serum amyloid A in uterine cervical cancer. *Diagn Pathol* 9(1):1–9.
196. Lung HL, Man OY, Yeung MC, Ko JMY, Cheung AKL, Law EWL, Yu Z, Shuen WH, Tung E, Chan SHK, Bangarusamy DK, Cheng Y, Yang X, Kan R, Phoon Y, Chan KC, Chua D, Kwong DL, Lee AWM, Ji MF, Lung ML (2015) SAA1 polymorphisms are associated with variation in antiangiogenic and tumor-

suppressive activities in nasopharyngeal carcinoma. *Oncogene* 34(7):878–889.

197. Sun L, Ye RD (2016) Serum amyloid A1: Structure, function and gene polymorphism. *Gene* 583(1):48–57.
198. Siegmund S V., Schlosser M, Schildberg FA, Seki E, De Minicis S, Uchinami H, Kuntzen C, Knolle PA, Strassburg CP, Schwabe RF (2016) Serum amyloid a induces inflammation, proliferation and cell death in activated hepatic stellate cells. *PLoS One* 11(3):1–17.
199. Zhang L (1997) Gene Expression Profiles in Normal and Cancer Cells. *Science (80-)* 276(5316):1268–1272.
200. Yokoi K, Shih LC, Kobayashi R, Koomen J, Hawke D, Li D, Hamilton SR, Abbruzzese JL, Coombes KR, Fidler IJ (2005) Serum amyloid A as a tumor marker in sera of nude mice with orthotopic human pancreatic cancer and in plasma of patients with pancreatic cancer. *Int J Oncol* 27(5):1361–1369.
201. Firpo MA, Gay DZ, Granger SR, Scaife CL, City SL, Disario JA, City SL, Boucher KM, City SL, Mulvihill SJ (2010) Improved Diagnosis of Pancreatic Adenocarcinoma using Haptoglobin and Serum Amyloid A in a Panel Screen. *World J Surg* 33(4):716–722.
202. Han CY, Subramanian S, Chan CK, Omer M, Chiba T, Wight TN, Chait A (2007) Adipocyte-Derived Serum Amyloid A3 and Hyaluronan Play a Role in Monocyte Recruitment and Adhesion. *Diabetes* 56(9):2260–2273.
203. Chiba T, Han CY, Vaisar T, Shimokado K, Kargi A, Chen M-H, Wang S, McDonald TO, O'Brien KD, Heinecke JW, Chait A (2009) Serum amyloid A3 does not contribute to circulating SAA levels. *J Lipid Res* 50(7):1353–1362.
204. Lee JM, Kim EK, Seo H, Jeon I, Chae MJ, Park YJ, Song B, Kim YS, Kim YJ, Ko HJ, Kang CY (2014) Serum amyloid A3 exacerbates cancer by enhancing the suppressive capacity of myeloid-derived suppressor cells via TLR2-dependent STAT3 activation. *Eur J Immunol* 44(6):1672–1684.
205. Deguchi A, Tomita T, Omori T, Komatsu A, Ohto U, Takahashi S, Tanimura N, Akashi-Takamura S, Miyake K, Maru Y (2013) Serum Amyloid A3 Binds MD-2 To Activate p38 and NF- B Pathways in a MyD88-Dependent Manner. *J Immunol* 191(4):1856–1864.
206. Khoa D. Nguyen, Claudia Macaubas, Phi Truong, Nan Wang, Tieying Hou, Taejin Yoon and EDM (2010) Serum amyloid A induces mitogenic signals in regulatory T cells via monocyte activation. *Hum Dev* 45(6):1654–1668.

207. Hiratsuka S, Watanabe A, Sakurai Y, Akashi-Takamura S, Ishibashi S, Miyake K, Shibuya M, Akira S, Aburatani H, Maru Y (2008) The S100A8-serum amyloid A3-TLR4 paracrine cascade establishes a pre-metastatic phase. *Nat Cell Biol* 10(11):1349–1355.
208. Mack GS, Marshall A (2010) Lost in migration. *Nat Biotechnol* 28(3):214–29.
209. Den Hartigh LJ, Wang S, Goodspeed L, Ding Y, Averill M, Subramanian S, Wietecha T, O'Brien KD, Chait A (2014) Deletion of serum amyloid A3 improves high fat high sucrose diet-induced adipose tissue inflammation and hyperlipidemia in female mice. *PLoS One* 9(9):1–13.
210. Urieli-Shoval S, Finci-Yeheskel Z, Dishon S, Galinsky D, Linke RP, Ariel I, Levin M, Ben-Shachar I, Prus D (2010) Expression of serum amyloid a in human ovarian epithelial tumors: implication for a role in ovarian tumorigenesis. *J Histochem Cytochem* 58(11):1015–1023.
211. Wendling O, Bornert J-M, Chambon P, Metzger D (2009) Efficient temporally-controlled targeted mutagenesis in smooth muscle cells of the adult mouse. *Genesis* 47(1):14–18.
212. Ruzankina Y, Pinzon-Guzman C, Asare A, Ong T, Pontano L, Cotsarelis G, Zediak VP, Velez M, Bhandoola A, Brown EJ (2007) Deletion of the Developmentally Essential Gene ATR in Adult Mice Leads to Age-Related Phenotypes and Stem Cell Loss. *Cell Stem Cell* 1(1):113–126.
213. Natarajan A, Wagner B, Sibilia M (2007) The EGF receptor is required for efficient liver regeneration. *Proc Natl Acad Sci* 104(43):17081–17086.
214. Jesenberger V, Procyk KJ, Rüth J, Schreiber M, Theussl HC, Wagner EF, Baccarini M (2001) Protective role of Raf-1 in Salmonella-induced macrophage apoptosis. *J Exp Med* 193(3):353–364.
215. Moreno-Mateos MA, Vejnar CE, Beaudoin JD, Fernandez JP, Mis EK, Khokha MK, Giraldez AJ (2015) CRISPRscan: Designing highly efficient sgRNAs for CRISPR-Cas9 targeting in vivo. *Nat Methods* 12(10):982–988.
216. Boj SF, Hwang C Il, Baker LA, Chio IIC, Engle DD, Corbo V, Jager M, Ponz-Sarvise M, Tiriac H, Spector MS, Gracanin A, Oni T, Yu KH, Van Boxtel R, Huch M, Rivera KD, Wilson JP, Feigin ME, Öhlund D, Handly-Santana A, Ardito-Abraham CM, Ludwig M, Elyada E, Alagesan B, Biffi G, Yordanov GN, Delcuze B, Creighton B, Wright K, Park Y, Morsink FHM, Molenaar IQ, Borel Rinkes IH, Cuppen E, Hao Y, Jin Y, Nijman IJ, Iacobuzio-Donahue C, Leach SD, Pappin DJ,

Hammell M, Klimstra DS, Basturk O, Hruban RH, Offerhaus GJ, Vries RGJ, Clevers H, Tuveson DA (2015) Organoid models of human and mouse ductal pancreatic cancer. *Cell* 160(1–2):324–338.

217. Liang C-C, Park AY, Guan J-L (2007) In vitro scratch assay: a convenient and inexpensive method for analysis of cell migration in vitro. *Nat Protoc* 2(2):329–333.
218. Graña O, Rubio-Camarillo M, Fernandez-Riverola F, Pisano DG, Glez-Peña D (2017) Nextpresso: Next Generation Sequencing Expression Analysis Pipeline. *Curr Bioinform* 12 (DOI : 10.2174/1574893612666170810153850).
219. Langmead B, Trapnell C, Pop M, Salzberg SL (2009) Ultrafast and memory-efficient alignment of short DNA sequences to the human genome. *Genome Biol* 10(3):R25.
220. Li H, Handsaker B, Wysoker A, Fennell T, Ruan J, Homer N, Marth G, Abecasis G, Durbin R (2009) The Sequence Alignment/Map format and SAMtools. *Bioinformatics* 25(16):2078–2079.
221. Subramanian A, Tamayo P, Mootha VK, Mukherjee S, Ebert BL, Gillette MA, Paulovich A, Pomeroy SL, Golub TR, Lander ES, Mesirov JP (2005) Gene set enrichment analysis: A knowledge-based approach for interpreting genome-wide expression profiles. *Proc Natl Acad Sci* 102(43):15545–15550.
222. von Ahrens D, Bhagat TD, Nagrath D, Maitra A, Verma A (2017) The role of stromal cancer-associated fibroblasts in pancreatic cancer. *J Hematol Oncol* 10(1):76.
223. Sharon Y, Alon L, Glanz S, Servais C, Erez N (2013) Isolation of Normal and Cancer-associated Fibroblasts from Fresh Tissues by Fluorescence Activated Cell Sorting (FACS). *J Vis Exp* (71):1–6.
224. Labernadie A, Kato T, Brugués A, Serra-Picamal X, Derzsi S, Arwert E, Weston A, González-Tarragó V, Elosegui-Artola A, Albertazzi L, Alcaraz J, Roca-Cusachs P, Sahai E, Trepat X (2017) A mechanically active heterotypic E-cadherin/N-cadherin adhesion enables fibroblasts to drive cancer cell invasion. *Nat Cell Biol* 19(3):224–237.
225. Lujambio A, Akkari L, Simon J, Grace D, Tschaharganeh DF, Bolden JE, Zhao Z, Thapar V, Joyce JA, Krizhanovsky V, Lowe SW (2013) Non-cell-autonomous tumor suppression by p53. *Cell* 153(2):449–460.
226. Barbour KW, Davis T, White A, Baumann H, Berger FG (2001) Haptoglobin,

inflammation, and tumorigenesis in the MIN mouse. *Redox Rep* 6(6):366–368.

227. Ishiwata T, Cho K, Kawahara K, Yamamoto T, Fujiwara Y, Uchida E, Tajiri T, Naito Z (2007) Role of lumican in cancer cells and adjacent stromal tissues in human pancreatic cancer. *Oncol Rep* 18(3):537–543.
228. Siiskonen H, Oikari S, Pasonen-Seppänen S, Rilla K (2015) Hyaluronan synthase 1: A mysterious enzyme with unexpected functions. *Front Immunol* 6(2):1–11.
229. Miyoshi E, Shinzaki S, Moriwaki K, Matsumoto H (2010) Identification of fucosylated haptoglobin as a novel tumor marker for pancreatic cancer and its possible application for a clinical diagnostic test. *Methods Enzymol.*478:153-164
230. Lim SK, Kim H, Lim SK, bin Ali a, Lim YK, Wang Y, Chong SM, Costantini F, Baumman H (1998) Increased susceptibility in Hp knockout mice during acute hemolysis. *Blood* 92(6):1870–1877.
231. Bera TK, Pastan I (2000) Mesothelin is not required for normal mouse development or reproduction. *Mol Cell Biol* 20(8):2902–2906.
232. Chakravarti S, Magnuson T, Lass JH, Jepsen KJ, LaMantia C, Carroll H (1998) Lumican regulates collagen fibril assembly: Skin fragility and corneal opacity in the absence of lumican. *J Cell Biol* 141(5):1277–1286.
233. Kobayashi N, Miyoshi S, Mikami T, Koyama H, Kitazawa M, Takeoka M, Sano K, Amano J, Isogai Z, Niida S, Oguri K, Okayama M, McDonald JA, Kimata K, Taniguchi S, Itano N (2010) Hyaluronan deficiency in tumor stroma impairs macrophage trafficking and tumor neovascularization. *Cancer Res* 70(18):7073–7083.
234. Hu Y, He M-Y, Zhu L-F, Yang C-C, Zhou M-L, Wang Q, Zhang W, Zheng Y-Y, Wang D-M, Xu Z-Q, Wu Y-N, Liu L-K (2016) Tumor-associated macrophages correlate with the clinicopathological features and poor outcomes via inducing epithelial to mesenchymal transition in oral squamous cell carcinoma. *J Exp Clin Cancer Res* 35(1):12.
235. Riabov V, Gudima A, Wang N, Mickley A, Orekhov A, Kzhyshkowska J (2014) Role of tumor associated macrophages in tumor angiogenesis and lymphangiogenesis. *Front Physiol* 5(3):1–13.
236. Lorusso V, Ribatti D, Silvestris N (2016) Angiogenesis in pancreatic ductal adenocarcinoma: A controversial issue. *Oncotarget* 7(36):58649–58658.
237. Kindler HL, Niedzwiecki D, Hollis D, Sutherland S, Schrag D, Hurwitz H, Innocenti F, Mulcahy MF, O'Reilly E, Wozniak TF, Picus J, Bhargava P, Mayer

RJ, Schilsky RL, Goldberg RM (2010) Gemcitabine plus bevacizumab compared with gemcitabine plus placebo in patients with advanced pancreatic cancer: Phase III trial of the Cancer and Leukemia Group B (CALGB 80303). *J Clin Oncol* 28(22):3617–3622.

238. Zagorac S, Alcala S, Bayon GF, Kheir TB, Schoenhals M, González-Neira A, Fraga MF, Aicher A, Heeschen C, Sainz B (2016) DNMT1 inhibition reprograms pancreatic cancer stem cells via upregulation of the miR-17-92 cluster. *Cancer Res* 76(15):4546–4558.
239. Hermann PC, Huber SL, Herrler T, Aicher A, Ellwart JW, Guba M, Bruns CJ, Heeschen C (2007) Distinct Populations of Cancer Stem Cells Determine Tumor Growth and Metastatic Activity in Human Pancreatic Cancer. *Cell Stem Cell* 1(3):313–323.
240. Steller EJA, Raats DA, Koster J, Rutten B, Govaert KM, Emmink BL, Snoeren N, Van Hooff SR, Holstege FCP, Maas C, Borel Rinkes IHM, Kranenburg O (2013) PDGFRB promotes liver metastasis formation of mesenchymal-like colorectal tumor cells. *Neoplasia* 15(2):204–17.
241. Ekpe-Adewuyi E Lopez-Campistrous A Tang X Brindley D McMullen T (2016) Platelet derived growth factor receptor alpha mediates nodal metastases in papillary thyroid cancer by driving the epithelial-mesenchymal transition. *Oncotarget* 7(50):83684–83700.
242. Baulida J (2017) Epithelial-to-mesenchymal transition transcription factors in cancer-associated fibroblasts. *Mol Oncol* 11(2017):847–859.
243. Reigstad CSC, Lundén GOG, Felin J, Bäckhed F (2009) Regulation of serum amyloid A3 (SAA3) in mouse colonic epithelium and adipose tissue by the intestinal microbiota. *PLoS One* 4(6):2–10.
244. O'Brien KD, Chait A (2006) Serum amyloid A: the "other" inflammatory protein. *Curr Atheroscler Rep* 8(1):62–68.
245. De Santo C, Arscott R, Booth S, Karydis I, Jones M, Asher R, Salio M, Middleton M, Cerundolo V (2010) Invariant NKT cells modulate the suppressive activity of IL-10-secreting neutrophils differentiated with serum amyloid A. *Nat Immunol* 11(11):1039–1046.
246. Apte M V., Wilson JS, Lugea A, Pandol SJ (2013) A starring role for stellate cells in the pancreatic cancer microenvironment. *Gastroenterology* 144(6):1210–1219.
247. Bhowmick NA, Chytil A, Plieth D, Gorska AE, Dumont N, Shappell S,

Washington MK, Neilson EG, Moses HL (2004) TGF- Signaling in Fibroblasts Modulates the Oncogenic Potential of Adjacent Epithelia. *Science (80-)* 303(5659):848–851.

248. Trimboli AJ, Cantemir-Stone CZ, Li F, Wallace JA, Merchant A, Creasap N, Thompson JC, Caserta E, Wang H, Chong J-L, Naidu S, Wei G, Sharma SM, Stephens JA, Fernandez SA, Gurcan MN, Weinstein MB, Barsky SH, Yee L, Rosol TJ, Stromberg PC, Robinson ML, Pepin F, Hallett M, Park M, Ostrowski MC, Leone G (2009) Pten in stromal fibroblasts suppresses mammary epithelial tumours. *Nature* 461(7267):1084–1091.
249. Tang Z, Qian M, Ho M (2013) The Role of Mesothelin in Tumor Progression and Targeted Therapy. *Anticancer Agents Med Chem* 13(2):276–280.
250. Mitchell TI, Coon CI, Brinckerhoff CE (1991) Serum Amyloid A (SAA3) produced by rabbit synovial fibroblasts treated with phorbol esters or interleukin 1 induces synthesis of collagenase and is neutralized with specific antiserum. *J Clin Invest* 87(4):1177–1185.
251. Ather JL, Ckless K, Martin R, Foley KL, Suratt BT, Boyson JE, Fitzgerald K a, Flavell R a, Eisenbarth SC, Poynter ME (2011) Serum amyloid A activates the NLRP3 inflammasome and promotes Th17 allergic asthma in mice. *J Immunol* 187(1):64–73.
252. Sommer G, Weise S (2008) The adipokine SAA3 is induced by interleukin-1β in mouse adipocytes. *J Cell Biochem* 2247:2241–2247.
253. Jensen LE, Whitehead a S (1998) Regulation of serum amyloid A protein expression during the acute-phase response. *Biochem J* 334 (3):489–503.
254. Gosens I, van Wijk E, Kersten FFJ, Krieger E, van der Zwaag B, Märker T, Letteboer SJF, Dusseljee S, Peters T, Spierenburg HA, Punte IM, Wolfrum U, Cremers FPM, Kremer H, Roepman R (2007) MPP1 links the Usher protein network and the Crumbs protein complex in the retina. *Hum Mol Genet* 16(16):1993–2003.
255. Tseng T-C, Marfatia SM, Bryant PJ, Pack S, Zhuang Z, O'Brien JE, Lin L, Hanada T, Chishti AH (2001) VAM-1: a new member of the MAGUK family binds to human Veli-1 through a conserved domain. *Biochim Biophys Acta - Gene Struct Expr* 1518(3):249–259.

Publications

Publications related to this work:

Djurec M, Graña O, Lee A, Troulé K, Espinet E, Cabras L, Navas C, Blasco MT, Martín-Díaz L, Burdiel M, Li J, Liu Z, Vallespinós M, Sanchez-Bueno F, Sprick MR, Trumpp A, Sainz Jr B, Al-Shahrour F, Rabadan R, Guerra C, Barbacid M. (2018) Saa3 is a key mediator of the protumorigenic properties of cancer-associated fibroblasts in pancreatic tumors. *Proc Natl Acad Sci* 115(6):E1147–E1156.

Publications not related to this work:

Sanclemente M, Francoz S, Esteban-Burgos L, Bousquet-Mur E, **Djurec M**, Lopez-Casa P, Hidalgo M, Guerra C, Drosten M, Musteanu M, Barbacid M. (2018) c-RAF Ablation Induces Regression of Advanced Kras/Trp53 Mutant Lung Adenocarcinomas by a Mechanism Independent of MAPK Signaling. *Cancer Cell* 33(2):217–228.e4.

Acknowledgements

First of all, I would like to thank to Mariano Barbacid for giving me the opportunity to do my PhD work in his excellent laboratory with such strong expertise and background in genetics and mouse models, as well as exceptional research tools. I learned how to be precise and persistent on perfect data presentation and to generate independent research projects, as well as how to ask important and relevant questions.

I am grateful to Carmen Guerra for her constant attention, scientific advices and supervision, and for her energy to believe in this difficult project. I am also thankful for her support and availability whenever I needed help.

I would like to express my gratitude to my consultant at Semmelweis University, Professor Kopper László for his scientific feedback and inspiration, as well as for his support and motivation since the moment I decided to dedicate myself to cancer research.

To Experimental Oncology lab: I appreciate the tremendous amount of help I got from you and the professional working environment you created. I am truly happy I could spend these important years together with the OE laboratory and I cannot be thankful enough for the hopefully lifelong friendships I was gifted.

I am especially grateful to all the CNIO Units, without their input we wouldn't have such a great and productive working environment. Kevin, Osvaldo, Ultan, Manu and Diego, you are fantastic professional help, I can only hope I will be working with you again sometime in the future.

To my dear Phd friends: Vero and Karolina, I have no words to express what your friendship, support and care meant to me during these years. The sentence (together with my love) is yours: without you it would have been impossible.

Lastly, I want to thank to my family for their constant support during these years. I know it was difficult for you being apart from each other and listening to the infinite procrastinating answer for the question: when are you coming home? Especially to my Mother, who is my inspiration, my professional exemplar and my eternal support, who was always there whatever happened, even in the most difficult moments. Because that is mother's job, the hardest one in life.

I am enormously thankful to János and Ildi for their tremendous help and for giving me such strong background at home so I was able to pursue this career.

I am very proud to have such great siblings: Laura, Andi and Imi I do not know what I would do without you in life. Your strength and love inspired me to achieve this goal and even though we could only share moments the past years, you made them all special. Erika, you are such a nice sister-in-law and made me feel good whenever I needed. And last but not least…Lotti. You closed me in your heart in the most crucial moment.

Finally, and most importantly, I would like to dedicate this thesis work to the memory of my beloved Father, Dr. Djurec István.